Investigating Polarisation–Sensitive Optical Coherence Tomography as a Measure of Biomarkers in Systemic Sclerosis

A thesis submitted to the University of

Manchester for the degree of Master of Philosophy of Photon Physics in the

Faculty of Science and Engineering

2023

Lewis E Smith

School of Natural Sciences

Department of Physics and Astronomy

Word Count: 22717

Tables

Figures

Publications

Published:

1. Marjanovic, E.J., Sharma, V., Smith, L. *et al.* Polarisation-sensitive optical coherence tomography measurement of retardance in fibrosis, a non-invasive biomarker in patients with systemic sclerosis. *Sci. Rep.* **12**, 2893 (2022). https://doi.org/10.1038/s41598-022-06783-7

Draft Journal Article:

1. Smith, L. *et al.* A comparative study of epidermal thickness measurements taken with polarisation-sensitive optical coherence tomography and high frequency ultrasound, for skin thickness assessment in systemic sclerosis (for submission to Annals of the Rheumatic Diseases)

Draft Letter:

1. Smith, L. *et al*. Structural assessment of ulcers and digital pitting in patients with systemic sclerosis through the use of 3D polarisation-sensitive optical coherence tomography (for submission to Annals of the Rheumatic Diseases)

Abstract

Polarisation-sensitive optical coherence tomography (PS-OCT) is an enhancement of OCT, utilising circularly-polarised light for structural analysis. Polarised light imaging is an established assessment method for biological tissues and PS-OCT has been used in clinical assessment across a wide range of medical specialities since its inception. Systemic sclerosis is a debilitating rheumatic auto-immune disease in which connective tissues experience fibrosis (scarring) and lesions. Collagen, which is known to be birefringent, is a key component in these changes.

This thesis reports on three clinical studies that were undertaken to investigate physical metrics by statistical assessment. These were focused on: the correlation of structural measurements, retardation as a biomarker, system reliability, and the feasibility of 3D lesion assessment. The first study's primary aim was the assessment of retardation as a biomarker comparing a cohort of healthy controls and patients. The second study's main objective was to validate PS-OCT's structural depth measurements by comparison to a gold standard, high-frequency ultrasound (HFUS). The third study aimed to assess the feasibility of imaging lesions in 3D. Ulcers and pitting in patients were scanned with polarisation sensitivity.

Study one found an indicative relation between tissue retardation and grouped modified Rodnan skin score, the gold standard for skin thickness assessment. In the second study validation of epidermal thickness measurements with HFUS was not possible due to low reliability of ultrasound measurements (HFUS Intra/Inter-Class Correlations (ICCs) between 0.1-0.6). The PS-OCT system was able to achieve a penetration depth in skin of up to 800 μm. In study three, 3D imaging was performed on two pitting lesions, tissue adjacent to pitting, and five ulcerations. Surface and subsurface structure, and retardation, were clearly visible establishing the usefulness of this technique for longitudinal response to treatment studies.

Declaration

No portion of the work referred to in the thesis has been submitted in support of an application for another degree or qualification of this or any other university or other institute of learning

Copyright statement

i. The author of this thesis (including any appendices and/or schedules to this thesis) owns certain copyright or related rights in it (the "Copyright") and s/he has given the University of Manchester certain rights to use such Copyright, including for administrative purposes.

ii. Copies of this thesis, either in full or in extracts and whether in hard or electronic copy, may be made only in accordance with the Copyright, Designs and Patents Act 1988 (as amended) and regulations issued under it or, where appropriate, in accordance with licensing agreements which the University has from time to time. This page must form part of any such copies made.

iii. The ownership of certain Copyright, patents, designs, trademarks and other intellectual property (the "Intellectual Property") and any reproductions of copyright works in the thesis, for example graphs and tables ("Reproductions"), which may be described in this thesis, may not be owned by the author and may be owned by third parties. Such Intellectual Property and Reproductions cannot and must not be made available for use without the prior written permission of the owner(s) of the relevant Intellectual Property and/or Reproductions.

iv. Further information on the conditions under which disclosure, publication and commercialisation of this thesis, the Copyright and any Intellectual Property and/or Reproductions described in it may take place is available in the University IP Policy (see http://documents.manchester.ac.uk/DocuInfo.aspx?DocID=2442 0), in any relevant Thesis restriction declarations deposited in the University Library, the University Library's regulations (see http://www.library.manchester.ac.uk/about/regulations/) and in the University's policy on Presentation of Theses.

Acknowledgements

I would like to thank everyone who has supported me throughout this research, both emotionally and professionally. You have all been invaluable and I could not have done it without your guidance.

My partner, Dr Laura Weatherburn, especially, you have been my rock. You have always been there and I cannot thank you enough.

I would also like to thank my family, Jon, Jackie, and soon-to-be Dr Alicia Smith. Your support and backing over the last couple of years has been incredible and I am extremely grateful for everything you have done.

Special thanks also to Dr Andrea Murray, Dr Graham Dinsdale, Prof Mark Dickinson, Jo Manning, and everyone from the Scleroderma research group. Your oversight, guidance, and expertise have been unparalleled. Thank you for everything.

None of this would have been possible without the backing and support of soon-to-be Dr Alex Crombie. Thank you, and everyone at Sheffield Hallam University.

Last but certainly not least, I would like to thank soon-to-be Dr Rosie Barnes and the whole PSI PGR community.

1. Introduction

1.1 Interferometry and Optical Coherence Tomography

Interferometry is an optical measurement technique that utilises the interference of electromagnetic waves. Configurations look to compare a beam that is split and directed along different paths. Measurements and observations are then made at a point of recombination where the resulting interference pattern is directly related to the paths taken. Early devices were designed to test the aether theory by Michelson and Morley, but continued developments have led to broad applications. These include spectroscopy, heterodyne techniques, and high resolution length measurements [1], which significantly has been used in the detection of gravitational waves [2].

One common configuration is the Michelson Interferometer, as shown in Figure 1.1. The setup utilises a single beam splitter *B*, and two mirrors M_1 and M_2, and can include a compensating plate *C* to account for path differences caused by the beam splitter. Incoming light, from a source *S*, is directed onto the beam splitter, with semi-reflective surface *A*, where it is separated into two beams of approximately equal intensity. Each beam is then directed normally onto its corresponding mirror. The returning rays are recombined at the beam splitter and the interference pattern is observed at *O*. M_2' marks where the image of M_2 appears in the alternate path.

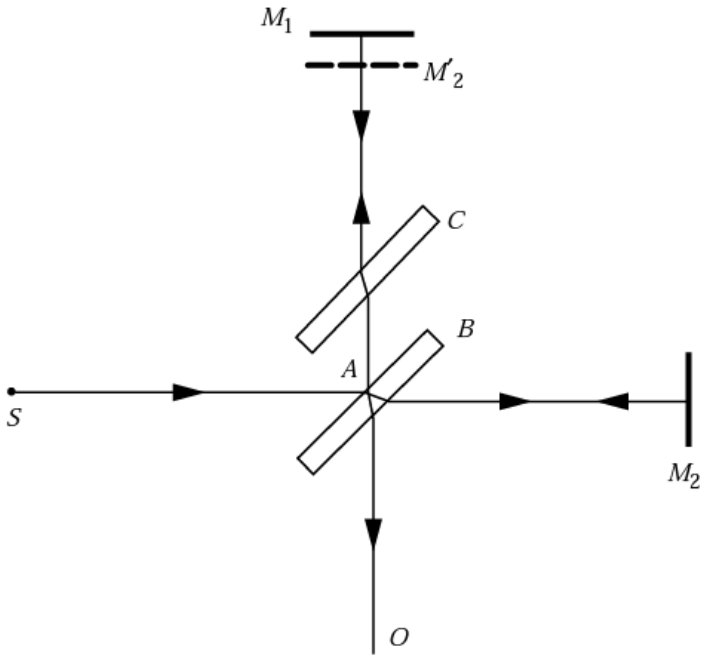

Figure 1.1: Ray diagram of a Michelson Interferometer: single beam splitter *B* with semi-reflective surface *A*, two mirrors M_1 and M_2 where M_2' marks where the image of M_2 appears in the alternate path, compensating plate *C*, source *S*, and observation at *O*. [1]

This optical arrangement is designed to measure differences between the two paths. When a coherent monochromatic source with wavelength λ is used, peak intensity at *O* is only observed at positions where the difference in path length Δp is given by,

$$\Delta p = m\lambda, \tag{1.1.1}$$

where m is an integer [1].

Optical Coherence Tomography, OCT, is an application that utilises the Michelson interferometer for structural depth measurements in turbid media, such as biological tissues. This is achieved by removing one of the mirrors and replacing it with the medium being investigated. This optical path in the OCT system is referred to as the sample arm. The other path, known has the reference arm, has a configuration which is dependent on the system's measurement process. Early systems required the reference mirror to move

over a distance, which equates to the scan depth within the sample, in the normal direction to the plain of the mirror, with measurements recorded with respect to time. Hence, these systems are termed time domain (TD) [3]. This configuration can be seen in Figure 1.2.

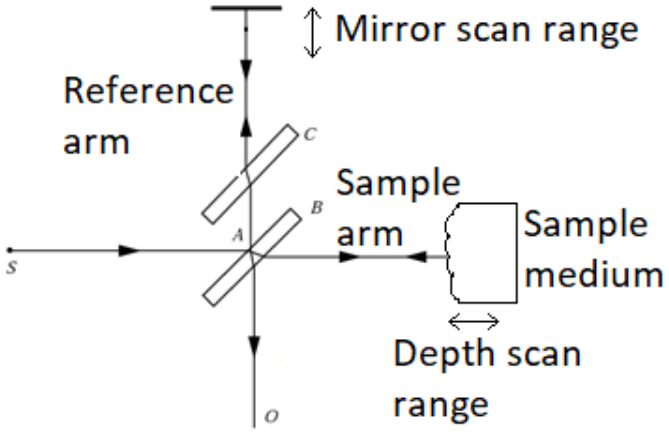

Figure 1.2: Simplified TD-OCT ray diagram, modified from Optical Interferometry *[1]*.

Alternatively, the mirror is kept in a fixed location corresponding to the maximum scan depth in the sample and measurements are analysed with a Fourier transform. This approach is referred to as Fourier domain (FD) OCT. The two main FD techniques used are spectral domain (SD) and swept source (SS) OCT (also known as optical frequency domain imaging, OFDI, in some specific applications [4]). The former uses a spectrometer and the latter a swept laser source in order to determine wavenumber dependent intensity profile [3].

OCT systems use a low-coherence, and hence broadband, light source. This is because when imaging semi-transparent media, after the initial beam has traversed the scan depth, reflections from multiple scatters in the sample will occur simultaneously, and hence will be received by the detector at once. As a result it is necessary to distinguish between these reflection peaks and a broadband source facilitates this to a high

resolution [3]. The complex electric field, E, of a broadband light source can be described by,

$$E = s(k,\omega)e^{i(kz-\omega t)}, \tag{1.1.2}$$

where $s(k,\omega)$ is the wavenumber, k, and angular frequency, ω, dependent amplitude function, z is distance and t is time. Hence, it can be shown that the resulting intensity profile measured by a detector at the exit of the system is the squared sum of the electric field of the reference and sample beams, given by,

$$I(k,\omega) = \frac{\rho}{2}\left\langle \left| \frac{s(k,\omega)}{\sqrt{2}} r_R e^{i(2kz_R-\omega t)} + \frac{s(k,\omega)}{\sqrt{2}} \sum_{n=1}^{N} r_{S_n} e^{i(2kz_n-\omega t)} \right|^2 \right\rangle, \tag{1.1.3}$$

where $I(k,\omega)$ is the intensity profile, ρ is the responsivity of the detector where the factor of two accounts for the double pass of the field through the beam splitter, the angular brackets denote integration over the detector's response time, the root two acting on the amplitude function is a result of the half power split produced by the beam splitter, r_R and r_{S_n} are the reflectivities of the reference mirror and the n^{th} sample boundary respectively, and z_R and z_n are the distances from the beam splitter to the reference mirror and n^{th} sample boundary respectively and the factor of two acting on them is to account for the double pass of each arm [5].

Expanding this produces three terms that relate to the contribution from direct, cross, and auto-correlation. The resulting intensity profile is given by,

$$I(k) = \frac{\rho S(k)}{4}\left[\left(R_R + \sum_{n=1}^{N} R_n\right)\right.$$

$$+\left(\sum_{n=1}^{N}\sqrt{R_R R_n}\left(e^{i2k(z_R-z_n)} + e^{-i2k(z_R-z_n)}\right)\right)$$

$$\left.+\left(\sum_{n\neq m=1}^{N}\sqrt{R_n R_m}\left(e^{i2k(z_n-z_m)} + e^{-i2k(z_n-z_m)}\right)\right)\right], \qquad (1.1.4)$$

where $S(k)$ is the time integral of the squared amplitude function, and R_R, R_n and R_m are the power reflectivities of the reference mirror, and the *n*th and *m*th sample boundaries respectively. The first bracketed section describes the direct-correlation (DC) term, the second line is the cross-correlation (CC) term, and the final section is the auto-correlation (AC) term. The DC term will dominate a system in which the R_R is greater than the sum of the R_n. It is not related to the path length difference between the two arms and is only affected by the reflectivities of the reference mirror and the sample layers. The CC term is the direct result of the reference and sample beam interference, and hence the desired functional term. It has both a wavenumber and path length dependence allowing for both TD and FD analysis. The AC term is the result of interference between in-sample reflections [5].

The Fourier analysis of the CC term allows for a relationship between intensity at a given wavenumber and the sample reflector depth, to be found. The resulting intensity dependence is given by,

$$i(z) \propto \gamma(z) \otimes \sum_{n=1}^{N} \sqrt{R_R R_n}\,\delta(z \pm 2(z_R - z_n)), \qquad (1.1.5)$$

where $i(z)$ is the intensity profile and $\gamma(z)$ is the coherence function of the light source [5].

Figure 1.3 shows a typical spectrometer-based SD-OCT system. The light source, as previously discussed, is broadband to maximise axial resolution, producing typical values between 1 – 10 µm. This is due to its inverse proportionality with bandwidth, the only other determining variable being central wavelength [5]. This is important in the applications of OCT as it allows for distinction between small, separate sample boundaries. Light exiting the system is directed onto a grating which in turn diffracts the beam onto a one-dimensional CCD. This allows for spectral analysis of the intensity profile [3].

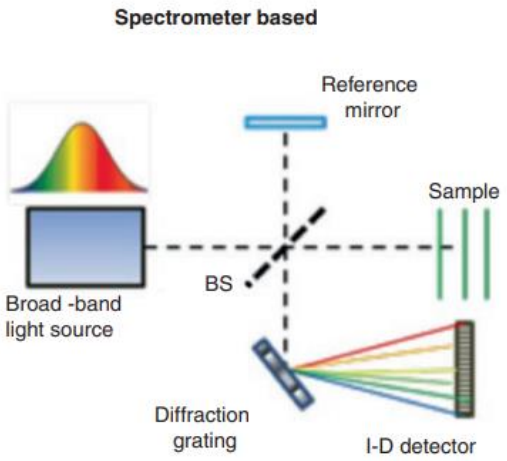

Figure 1.3: Ray diagram of SD-OCT system. Light from a broadband source is directed into a beam-splitter, BS. This separates equal proportions of the light intensity onto the reference mirror and sample. Rays reflected from these surfaces recombine at the BS and are directed onto a diffraction grating. The light from the grating is spectrally dispersed onto a one-dimensional CCD allowing for spectral analysis *[6]*.

1.2 Polarised Nature of Light and Birefringence

The electric field component of an electromagnetic plane wave propagating in a direction z at a time t can be written as,

$$\boldsymbol{E} = \boldsymbol{E_o} e^{i(kz-\omega t)}, \tag{1.2.1}$$

where $\boldsymbol{E_o}$ is the electric field amplitude vector. The magnetic field component oscillates perpendicularly to the electric field and generally manipulation of both components is assumed to be equivalent, allowing for just the electric field to be represented.

Polarisation describes the amplitude and phase relation between the vector components of the amplitude of the wave. This can be represented in the form,

$$\boldsymbol{E_o} = A\hat{\boldsymbol{\imath}} + Be^{i\varphi}\hat{\boldsymbol{\jmath}}, \tag{1.2.2}$$

where A and B are the electric field magnitudes in the $\hat{\boldsymbol{\imath}}$ and $\hat{\boldsymbol{\jmath}}$ directions respectively, and are perpendicular to the direction of propagation, and φ is the phase difference between the components. For ease of manipulation this is typically written in the vector form,

$$\boldsymbol{E_o} = \begin{pmatrix} Ae^{i\varphi_x} \\ Be^{i\varphi_y} \end{pmatrix} = \begin{pmatrix} E_x \\ E_y \end{pmatrix}, \tag{1.2.3}$$

where,

$$\varphi_x + \varphi_y = \varphi. \tag{1.2.4}$$

This is known as Jones vector notation and can only represent coherent light of constant polarisation state. This is known as complete polarisation. When used with Jones matrices, which represent the effects of polarising components, they can predict the resultant polarisation of a beam leaving an optical setup. These operations are known as Jones calculus and have the form,

$$\begin{pmatrix} E_x' \\ E_y' \end{pmatrix} = \begin{pmatrix} m_{11} & m_{12} \\ m_{21} & m_{22} \end{pmatrix} \begin{pmatrix} E_x \\ E_y \end{pmatrix}, \tag{1.2.5}$$

where the prime amplitude components in combination form the resultant Jones vector, and the m_{ij} values make up the Jones matrix of a polarising component interacting with polarised light described by the non-prime vector [7].

There are two special cases of polarisation, linear and circular. Linear is defined when the whole electric field is in a single orientation, and hence there is zero or π phase delay between perpendicular components. Circular polarisation is defined as an equal ratio of vertical and horizontal field components with a $\frac{\pi}{2}$ or $\frac{3\pi}{2}$ phase difference. All other combinations of completely polarised light are termed elliptically polarised. The Jones vectors for these special cases are conventionally normalised such that,

$$I = \boldsymbol{E_o}^{\dagger} \cdot \boldsymbol{E_o} = 1, \tag{1.2.6}$$

where † denotes the complex transpose.

This produces the following,

$$\boldsymbol{E_H} = \begin{pmatrix} 1 \\ 0 \end{pmatrix}, \qquad \boldsymbol{E_V} = \begin{pmatrix} 0 \\ 1 \end{pmatrix}, \tag{1.2.7}$$

$$\boldsymbol{E_{H+45}} = \frac{1}{\sqrt{2}}\begin{pmatrix}1\\1\end{pmatrix}, \qquad \boldsymbol{E_{H-45}} = \frac{1}{\sqrt{2}}\begin{pmatrix}1\\-1\end{pmatrix}, \tag{1.2.8}$$

$$\boldsymbol{E_{LHP}} = \frac{1}{\sqrt{2}}\begin{pmatrix}1\\i\end{pmatrix}, \qquad \boldsymbol{E_{RHP}} = \frac{1}{\sqrt{2}}\begin{pmatrix}1\\-i\end{pmatrix}, \tag{1.2.9}$$

where $\boldsymbol{E_H}$ and $\boldsymbol{E_V}$ are horizontally and vertically polarised, $\boldsymbol{E_{H\pm 45}}$ are linearly polarised plus or minus 45° from the horizontal, and $\boldsymbol{E_{LHP}}$ and $\boldsymbol{E_{RHP}}$ are left and right hand circular polarised [8].

As previously discussed, optical components that change the polarisation state of light can be represented by Jones Matrices. Two common types are polarisers and retarders. Polarisers produce a predetermined polarised output. This can be achieved by a number of methods and can be used to filter unpolarised light for optical applications. Retarders change a polarised beam from one state to another. This occurs due to birefringence, which is an optical property resulting from the lattice structure of a material which causes two differing refractive indices depending of polarisation state [9]. Commercial retarders that are cut to produce exact wavelength dependent polarisation phase delay are known as wave plates. They are designed to be used in optical setups where polarised light needs to be changed to an alternate state of pure polarisation. Additionally, some retarders change refractive indices when under stress or applied voltage, allowing for variable control [10].

Materials where the optical properties differ depending on orientation are termed anisotropic. The phenomena is generally the result of a consistent lattice structure where bond strengths between molecules are different for different parts of the unit cell. The

consistent structure allows for the effect of these individual bond structures to be observed on a macroscopic scale. The refractive index n in any given spatial dimension i is given by,

$$n_i = \sqrt{\frac{\varepsilon_i}{\varepsilon_o}}, \tag{1.2.10}$$

where ε_i is the relative permittivity in the $\underline{\hat{\imath}}$ direction, and ε_o is the permittivity of free space. Most passive retarders use uniaxial crystals. These materials have structures in which two of their three refractive indices are equal. The equal indices are referred to as the ordinary index n_o, and the differing index, the extraordinary index n_e. The extraordinary axis defines the optic axis, OA, as light propagating in that direction will always have electric field oscillations in the ordinary plane and hence the polarisation of the light will not affect the resultant beam.

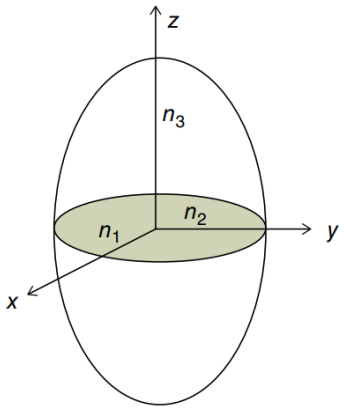

Figure 1.4: Indicatrix of a positive uniaxial crystal. The three refractive indices, n_1, n_2 and n_3, of a crystal are represented as lengths on a 3D axis and are depicted as the dimensions of an oval. The X and Y components, n_1 and n_2, in this case are equal, which is indicated by the shaded circle in that plane. *[10]*.

Figure 1.4 shows a representation of a situation where the extraordinary index, n_3, is larger than ordinary indices, n_1 and n_2, through the use of an indicatrix diagram. A

material with this characteristic is termed a positive uniaxial crystal. It can be seen that the ordinary axes create a plane. If the extraordinary index was smaller than the ordinary, it would be a negative uniaxial crystal. Where all three refractive indices are equal the material is isotropic. If all indices differ the material is biaxial [10].

Uniaxial materials have an absolute birefringence, Δn, given by,

$$\Delta n = n_e - n_o \text{ [11]}. \tag{1.2.11}$$

Measurements of this quantity can provide insight into the structure of a material and are used for this purpose in material science, through the use of polarimetry. As previously discussed, some materials' birefringence alters with applied stress, this is called photoelasticity. Measurement of a material in different states of applied stress allows for structural analysis and determination of potential failure points [10]. Birefringence measurements can also be applied to bulk materials with an unknown concentration of birefringent material, such as biological tissues. In both measurement processes it is important that circular polarisation is used so that equal electric field is applied to both vertical and horizontal axes, without knowledge of the orientation of the material axis being required. This is known as optic axis insensitivity. Given an applied monochromatic beam of wavenumber, k, and material thickness, d, material birefringent is given by,

$$\Delta n = \frac{\varphi}{kd}. \tag{1.2.12}$$

In biological tissue measurements, a factor of two is required in order to account for a double pass as measurements can only be made on reflection as transmission is not normally possible [5].

1.3 Polarisation-Sensitive Optical Coherence Tomography

Polarisation-sensitive optical coherence tomography, PS-OCT, was originally developed from a method for making fibre-based optical reflectometers, used for diagnosis of optical components, polarisation-insensitive. Early fibre systems had to use linearly polarised light to characterise optical devices, due to the fibre components available at the time. As a result they could only be used with polarisation maintaining samples. In this configuration a sample reflection that has experienced some change in polarisation will not necessarily match the polarisation state of the reference beam, resulting in a misrepresentation of the intensity of the reflection. Kobayashi et al. developed a system by which the reference beam would be polarised at 45° at the point of recombination and the resulting interference signal would be split by a polarising beam splitter and directed onto two photodetectors. This means that reference intensity is equal in horizontal and vertical components, and resultant intensities of each would be represented when combined [12].

Hee et al. further developed this configuration for the measurement of polarisation properties. Significantly, circularly polarised light was used which allowed for insensitivity to the sample's OA orientation, which was achieved using a quarter wave plate, QWP. This is necessary when imaging samples of unknown polarisation properties in order to ensure measurements are representative. Light entering the system is linearly polarised and is then split into the sample and reference arms. The sample arm contains a QWP oriented at 45° in order to produce circularly polarised light which is then incident on the sample. In the reference arm, in order to produce linear polarisation at 45°, a QWP is used at 22.5° so a double pass produces the required state. As before, the recombined beam is split into vertical and horizontal components in a polarisation beam splitter and directed onto two detectors [13]. A standard configuration is shown in Figure 1.5.

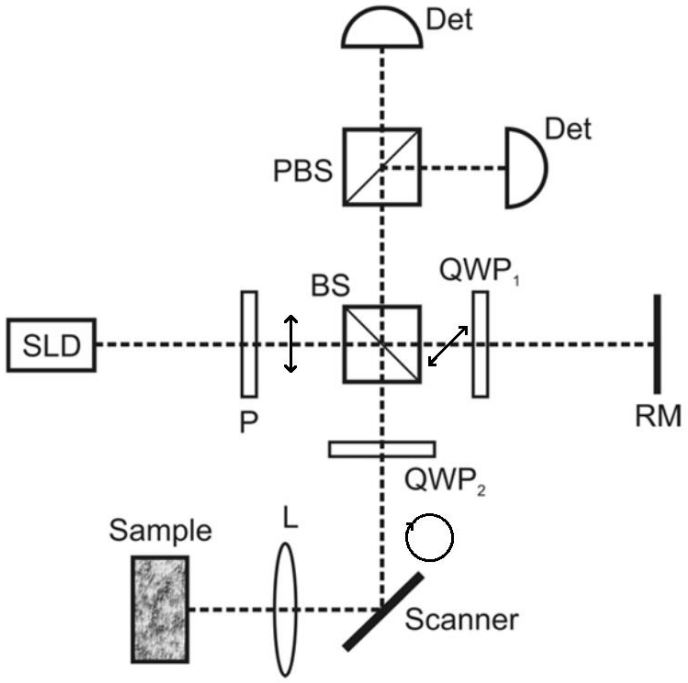

Figure 1.5: Simplified ray diagram of a PS-OCT system *[14]*: SLD, super luminescent diode; P, polariser; BS, beam splitter; L, lens; RM, reference mirror; PBS, polarising beam splitter; Det, detector; $QWP_{1/2}$ are orientated at 22.5 ° and 45 ° to the vertical respectively. The polarisation state at key stages is shown using arrows. ↕ denotes vertical polarisation after incoming light passes P. ⤢ denotes 45 ° polarisation resulting from the double pass of, initially, linearly polarised light through QWP_1. ⥁ denotes left-hand polarised light produced by the transmission of vertically polarised light through QWP_2.

The rotation of a generic polarising component with Jones matrix $\boldsymbol{J}_x$ to an angle θ can be described by the Jones calculus operation,

$$\boldsymbol{J}_x(\theta) = \boldsymbol{J}_{Rot}(-\theta)\boldsymbol{J}_x\boldsymbol{J}_{Rot}(\theta), \tag{1.3.1}$$

where $\boldsymbol{J}_x(\theta)$ is the resultant rotated Jones matrix and $\boldsymbol{J}_{Rot}(\theta)$ is the Jones rotation matrix, which is given by,

$$\boldsymbol{J}_{Rot}(\theta) = \begin{pmatrix} \cos\theta & \sin\theta \\ -\sin\theta & \cos\theta \end{pmatrix}. \tag{1.3.2}$$

Hence given that the Jones matrix for a QWP, $\boldsymbol{J}_{QWP}$, is given by,

$$\boldsymbol{J}_{QWP} = \begin{pmatrix} 1 & 0 \\ 0 & -i \end{pmatrix}, \tag{1.3.3}$$

it can be shown that vertically polarised light $\boldsymbol{E_V}$, as defined in (1.2.7), when passed through a QWP rotated to 45° from the vertical is changed to $\boldsymbol{E_{LHP}}$, as defined in (1.2.9).

A generic retarder rotated by an angle θ can be described by the Jones matrix, $\boldsymbol{J_{Ret}}(\varphi, \theta)$,

$$\boldsymbol{J}_{Ret}(\varphi, \theta) = \begin{pmatrix} \cos\frac{\varphi}{2} + i\sin\frac{\varphi}{2}\cos 2\theta & i\sin\frac{\varphi}{2}\sin 2\theta \\ i\sin\frac{\varphi}{2}\sin 2\theta & \cos\frac{\varphi}{2} - i\sin\frac{\varphi}{2}\cos 2\theta \end{pmatrix}, \tag{1.3.4}$$

where θ is angle of rotation [8]. Hence the state change that occurs within the sample arm of a PS-OCT system, containing a sample that produces a phase delay φ with its OA at an angle θ to the vertical, can be described by,

$$\boldsymbol{E}_S = \boldsymbol{J}_{Rot}(45°)\boldsymbol{J}_{QWP}\boldsymbol{J}_{Rot}(-45°)\boldsymbol{J}_{Ret}(\varphi, -\theta)\boldsymbol{J}_M\boldsymbol{J}_{Ret}(\varphi, \theta)\boldsymbol{E_{LHP}}, \tag{1.3.5}$$

where $\boldsymbol{E}_S$ is the resultant Jones vector and $\boldsymbol{J}_M$ is the Jones mirror matrix and represents handedness change resulting from a reflection. As a result this operation can be used to prove the OA insensitivity of circularly polarised light. The resultant intensity of each component can be shown to be given by,

$$I_x = 8\sin^2\frac{\varphi}{2}\cos^2\frac{\varphi}{2}, \tag{1.3.6}$$

$$I_y = 2\left(\sin^2\frac{\varphi}{2} - \cos^2\frac{\varphi}{2}\right)^2, \tag{1.3.7}$$

and hence independent of sample OA orientation.

Due to the circularity of polarisation, it can be shown that, having measured an intensity for both components of the interferogram, that polarisation phase angle, commonly termed retardation, can be defined as,

$$\varphi = \arctan\left(\sqrt{\frac{I_x}{I_y}}\right) [14]. \tag{1.3.8}$$

Hence a quantitative measure of birefringence can be made given (1.2.12), where d is the total path length of the beam within the sample and k is the central wavenumber of the broadband light source.

However, Jones vectors and matrices can only represent complete polarisation and non-depolarising samples respectively. This can undermine certain specific applications, such as imaging biological tissue for more detailed optical property analysis. Schmitt showed that non-spherical scatterers are effective depolarisers and can be abundant in biological tissue [15]. Hence, some analysis techniques employ the use of Stokes vector and Mueller matrices in order to represent these depolarising effects [14].

Like Jones vectors and matrices, Stokes vector relates to Mueller matrices as,

$$\boldsymbol{S}' = \boldsymbol{M}\boldsymbol{S}, \tag{1.3.9}$$

where $\boldsymbol{S}'$ is the resultant Stokes vector due to the interaction of an incident beam described by Stoke vector $\boldsymbol{S}$ with an object given by the Mueller matrix $\boldsymbol{M}$. Stokes vectors have four real components with values between −1 and 1, termed Stokes parameters. They represent, the total intensity I, the *x*-*y* polarisation component Q, the ±45 ° polarisation component U, and the left-right circular polarisation component V. Mueller matrices consists of sixteen components in a 4x4 arrangement.

Stokes parameters can be defined such that they are given by,

$$\boldsymbol{S} = \begin{bmatrix} I \\ Q \\ U \\ V \end{bmatrix} = \begin{bmatrix} {E_x}^2 + {E_y}^2 \\ {E_x}^2 - {E_y}^2 \\ 2{E_x}^2{E_y}^2 \cos\varphi \\ 2{E_x}^2{E_y}^2 \sin\varphi \end{bmatrix}. \tag{1.3.10}$$

Given that the interferogram within a PS-OCT system will contain Jones vectors representing the two orthogonal polarisation components, it's possible to calculate these parameters using only the photodetectors' intensity outputs. This method is described in detail by de Boer [16]. Additionally, Stokes parameters allow for the calculation of the degree of polarisation (DOP), which is given by,

$$DOP = \sqrt{\frac{Q^2 + U^2 + V^2}{I^2}}. \tag{1.3.11}$$

This gives a proportional representation of polarised light intensity relative to total intensity of a beam, from unity for complete polarisation, where DOP is equal to 1, to DOP equalling zero for non-polarised light [14].

1.4 Polarisation-Sensitive Clinical Imaging Techniques

Polarisation-sensitive microscopy has been used in cell biology since the 1800s, although early instruments were described as 'crude' by Allen et al. Refinement did not come until the 1950s with improved contrast and sensitivity [17], and development of bulk biological tissue imaging systems, such as PS-OCT, did not make significant progress until the 1990s [18].

Early polarisation-sensitive microscopy enabled cellular substructure analysis, not possible in conventional imaging, allowing for significant developments in cell biology. Development continued despite advancements in alternative imaging modalities, such as electron microscopy as pre-treatments required caused cell damage until the mid-1970s [19]. Early development towards biological tissue imaging used devices similar to forward scattering polarimeters [20] seen in material science, developing into backwards scattering polarimeters [21] and in turn inspiring the enhancement of OCT for polarisation measurements [13].

As with polarisation imaging in other fields, biomedical research focuses on two key characteristics of samples; depolarisation and birefringence. High scattering events are the main cause of depolarisation [21] and are dependent on numerous factors including refractive index, and size and shape of particles [14]. Whereas birefringence is observed in biological tissues with consistent repeating structure and is often associated with the presence of ordered collagen fibres [22]. Deviation of these quantities from literature values, in a given biological tissue type, can be the result of biochemical changes resulting from disease [23].

In Ramella-Roman et al.'s review of polarisation imaging in clinical applications, devices are grouped into two distinct subsections defined by the form of light source used, incoherent and coherent. This groups devices such as, forwards and backwards scattering polarimeters, and microscopes as incoherent systems, and interferometer based systems, such as PS-OCT, and speckle imaging as coherent. Incoherent systems generally can only measure bulk properties of samples, whereas coherence allows for PS-OCT to take depth dependent measurements and speckle to measure high resolution surface structure [18].

Conventional (forwards scattering) polarimeters use analysis of a polarisation gated source transmitted through a sample to determine polarising properties. Their fundamental form, as in Figure 1.6, consists of; a light source, an initial polariser, referred to as the polarisation state generator PSG, the sample, a second polariser, referred to as the polarisation state analyser PSA, and a light intensity measure, often photodetectors, but user observation via an objective is also used. The simplicity of the system is a key benefit to this approach. This paired with its ability to measure the Stokes parameters of the light or the Muller matrix of a given sample, by manipulation of the polarisers and the use of photodetectors, makes it a viable choice for clinical applications [24]. However, it is limited by its use of transmission, making bulk biological tissue and *in vivo* measurements impractical.

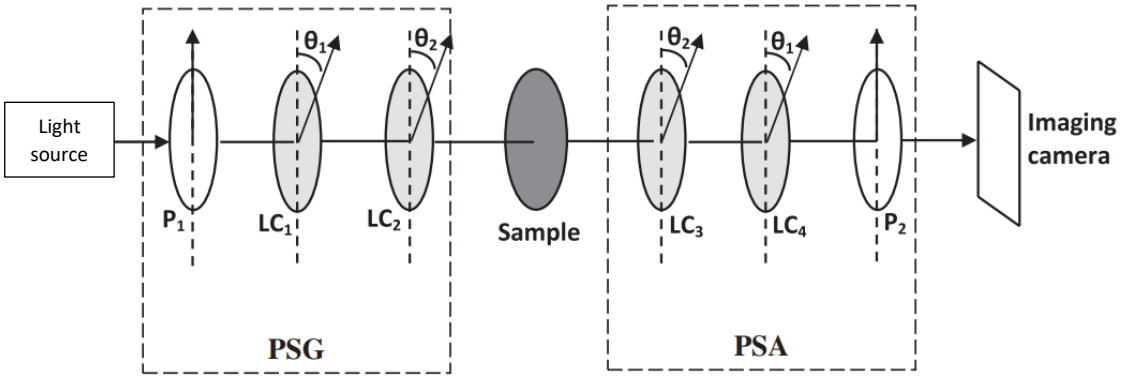

Figure 1.6: Typical polarimeter, with PSG and PSA containing fixed polarisers, P, and liquid crystal variable retarders, LC, for the variable control of gated and analysed states *[26]*.

In order to allow for polarimeters to measure in samples where transmission is not convenient, devices were developed that resemble reflectometers. These are sometimes termed backscattering polarimeters, or polarimeters with backwards geometry [25]. These devices use the same gating and analyser arrangements, but light being analysed is reflected rather than transmitted. In order to achieve this two different arrangements can be used, the light source can be oriented to direct light normal to the sample surface with the detector at an angle to the normal [20, 26], or the opposite, with the source at an angle and the detector at the normal [17], as shown in Figure 1.7. The normal is used as a method of reducing surface glare [17]. As previously discussed, the main advantage of backscattering geometry is to increase feasibility of *in vivo* and bulk biological tissue measurements, which are important for clinical research. However, larger numbers of high scattering events can cause fine details to be masked resulting in misrepresentation of sample qualities. This can be partly reduced by large detector arm path lengths [25] and beam width filtering [20].

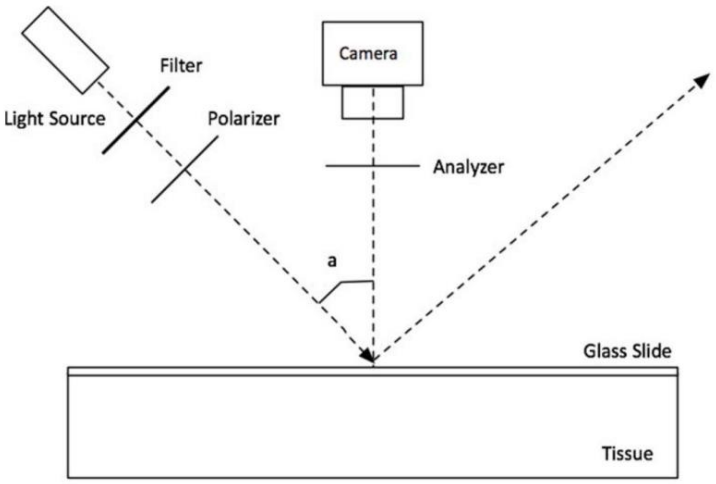

Figure 1.7: Backscattering polarimeter, with detector at normal to surface *[18]*.

A further development of this approach is confocal microscopy. This additionally adds a lens between the source and the sample, which allows for light to be focused on substructures. A lens and pinhole before the detector allow for unfocused light to be excluded [17]. A typical arrangement is shown in Figure 1.8. An adjustable focus allows for measurements to be made as a function of depth. However, this still requires repeated measurements by physically moving the lens to focus it on sequential substructures [17]. Additionally, the spatial resolution is diffraction limited by the pinhole, creating a physical restriction on continued development [27].

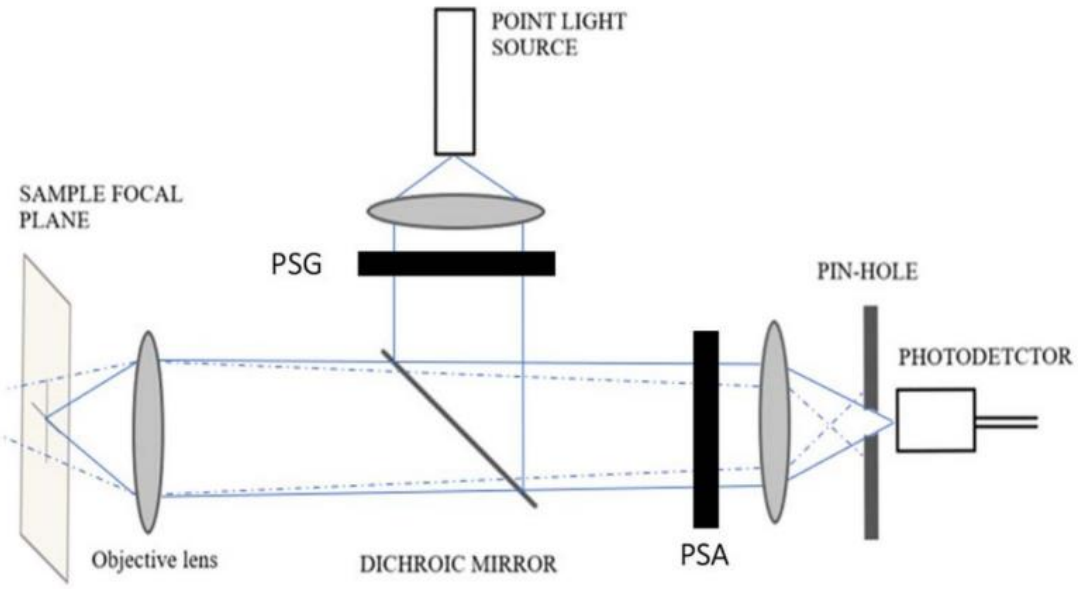

Figure 1.8: Typical configuration of a confocal polarisation sensitive microscope. The dichroic mirror filters out wavelengths reflected back from the sample that are used to cause fluorescent excitation in contrast agents typically employed in confocal microscopy *[18]*.

PS-OCT, as previously described, uses the coherence relation between two independent beam paths to create a depth scan, a significant advantage over other techniques. This allows for an axial resolution only limited by the point spread function of the source, which is defined as,

$$\delta z = l_c = \frac{2 \ln 2 \, {\lambda_0}^2}{\pi \Delta\lambda}, \tag{1.4.1}$$

where δz is axial resolution, l_c is coherence length, λ_0 is the central wavelength and $\Delta\lambda$ is the spectral bandwidth [5]. Additionally, spectral domain systems can complete a full depth scan without the need for physical movement of optical components, allowing for significantly faster scan times. However, the width of the sample is still imaged by physically scanning a mirror over it [6].

Speckle imaging uses a high coherence laser source to measure fine surface imperfections and perfusion using the autocorrelation interference between multiple points in the diffusely reflected beam. The resulting interferogram, called a speckle pattern, is measured by a detector [28], similar to a backscattering polarimeter. Light from the source is directed through a polariser and the backscattered beam passes through a polarising beam splitter. This allows for perpendicular components to be measured simultaneously [29], as in PS-OCT. A typical system is shown in Figure 1.9. This technique is mainly used for perfusion measurements [17], but has also been applied to imaging of skin lesions [29]. Tchvialeva et al. describe the main advantage of the technique in skin imaging to be the high speed imaging, allowing it to avoid movement artefacts [29]. However, the images produced can be complex and difficult to interpret [30].

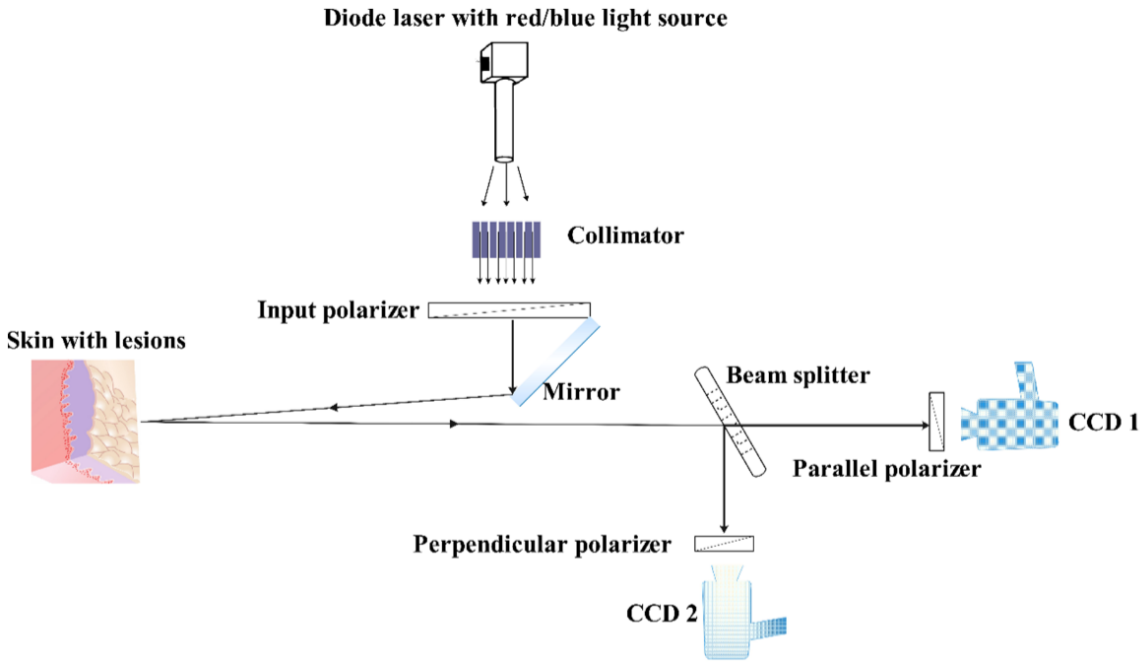

Figure 1.9: Polarisation speckle system *[31]*.

1.5 Clinical Applications of Conventional and Polarisation-Sensitive OCT

OCT's predecessor, optical coherence domain reflectometry, OCDR, [32] had been investigated as a possible ophthalmological, eye disorder focused, measurement method since the late 1980s [33] [34]. Hence, the application of OCT for biomedical imaging in the early 1990s was a natural progression. The study by Huang et al. into the feasibility of the system was one of the initial investigations and compared results from two contrasting tissue types; *ex vivo* samples of retina and coronary artery [35]. Ocular tissue has been an area of continuous investigation since early biological tissue imaging [20] [21] [33] [34], and its morphology is well documented. Additionally, the retinal tissue is transparent and therefore notably different to the high-scattering turbid artery tissue. Crucially, both are of clinical importance due to the difficulty to differentiating between healthy and diseased tissues using other techniques [35].

Similarly, Hee et al.'s development of polarisation-sensitive OCDR a year later, which directly lead to PS-OCT, was undertaken with clinical applications in mind. As well as using commercial optical components to characterise the system and test functionality, calf artery samples were imaged *ex vivo* as a direct precursor for human tissue studies [13]. One of the first descriptions of PS-OCT was made by de Boer et al. in a demonstration of the technique's ability to produce images that could distinguish altered birefringence in biological tissue caused by thermal denaturing. As with early OCT biomedical applications this tested an established principle as a baseline reference [36].

The continued development of these OCT techniques have led to clinical, surgical and routine medical applications across wide ranging specialties. The review by Zysk et al. of the development of OCT in clinical settings identifies the areas that have seen the most significant implementation as ophthalmology and cardiology, cardiology being the medical specialty relating to the heart and circulatory system. These areas particularly have implemented the use of OCT due to its high resolution and imaging functionality not possible with alternative methods in the specialties [37]. Additionally, gastroenterology,

which investigates disorders of the digestive system, is the medical specialty with the third most annual publications as of 2018 [38]. However, rheumatology, relating to connective tissue, pulmonology, relating to the respiratory system, and dentistry are also notable for their application of OCT techniques [37].

Ophthalmic Application - Since the first commercialisation of OCT for ophthalmic imaging, systems have become common in clinics [6] and as of the late 2000s have been considered the superior technique for evaluation of multiple retinal conditions. Significantly, they have the resolution to measure symptomatic features of conditions that were beyond the functional range of previous methods and have only been reported since the commercialisation of OCT [37].

OCT's high resolution (1 – 15 µm), relative to other ophthalmic imaging modalities (magnetic resonance imaging: 100 x 200 µm² [39]), has allowed for its application in retinal thickness measurements [37] (220 µm), which has been a focus of clinical investigation since the first OCT studies [35]. Importantly, it enables not only total thickness measurements, but also identification and measurement of structural layers and hence subtle abnormalities within these structures. Additionally, the resolution has also facilitated the diagnosis and evaluation of conditions relating to the interface of the retinal surface and fluid within the eye, termed the vitreous. Zysk et al. emphasise OCT's contribution in this area particularly, stating that it has '*greatly expanded the general understanding*' [37].

The first studies to apply PS-OCT to ophthalmic research, in the early 2000s, looked to apply the established imaging capabilities of OCT with the well documented polarising properties of ocular tissue [40]. Significantly, previous imaging techniques in this area had only measured bulk biological tissue properties such as total birefringence, making PS-OCT's depth resolved measurements valuable to diagnosis. In conditions where ocular tissue layers have been distorted or displaced, the identification of biological tissue types

within structures can be difficult to differentiate using OCT intensity scans, here PS-OCT brought a notable advantage. Additionally, imaging of the cornea's OA orientation in some conditions has indicated that early observation may be possible before visible structural changes occur, as shown in Figure 1.10, making PS-OCT an invaluable diagnostic tool. Depolarisation occurs in compounds key for metabolic processes in photoreceptors and can be used as a diagnostic tool for the identification of age-related macular degeneration [41].

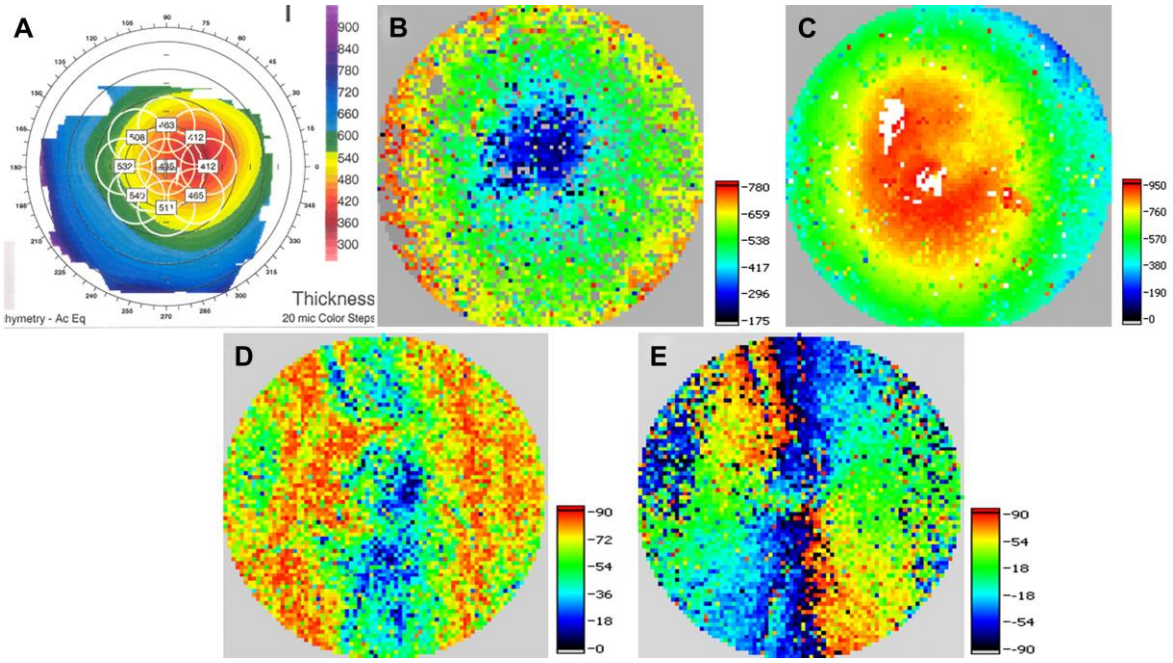

Figure 1.10: Images of the cornea from a patient with a disease that causes thinning of the cornea, keratoconus. (A) is a multimodal thickness scan in µm, (B) PS-OCT thickness scan in µm, (C) is the surface height map, (D) is retardation, and (E) is OA orientation [42].

Cardiologic Application

- As previously described, the application of OCT to cardiovascular tissue imaging has been a focus since the first feasibility studies. However, the publication of the first clinical intravascular *in vivo* imaging was not until 2001, with the release of the first commercially available system following three years later. FD systems were not commercially available until 2009. This combined with the need to engineer novel catheter imaging systems and develop methods to reduce the impact of high scattering events observed in blood [38], are likely causes for this differential in implementation in comparison to ophthalmology.

A major area of interest in the application of OCT in cardiology is the imaging of materials built up in the linings of arteries, these masses are termed plaques. The disease associated with this, atherosclerosis, makes up 75% of cardiovascular diseases. Vulnerability of plaques to rupture is an indication of disease progression, and failure can result in death and long term disability. Hence this is an important area of research. Zysk et al. described the application of OCT to imaging of vulnerable plaques '*an ideal clinical application*'. This is in part due to its high resolution, which is an order of magnitude higher than the current clinical standard, intravascular ultrasound, IVUS. However, it is limited by its low penetration depth of up to 3 mm and hence requires the use of alternative imaging modalities to locate areas of interest. Additionally, as previously discussed, the attenuation due to scattering in blood is also a limiting factor and supplementary steps, such as a saline flush, are necessary to reduce this effect [37].

PS-OCT's application in cardiology is still in its early stages due to the polarising effects of stressed optical fibres used in catheters. As previously discussed, some materials exhibit a change in birefringence when stress is applied, when this occurs within an imaging system the light incident on the sample will no longer have a known polarisation. This means that OA insensitive imaging is no longer possible and so measurements cannot be reliably compared to reference values [38]. However, *ex vivo* imaging has shown unique birefringence properties of vulnerable plaques that would make PS-OCT potentially a valuable diagnostic tool [37].

Gastric Application - Studies of possible applications of OCT in gastroenterology initially focused on identifying indicators associated with disease and assessing imaging quality. The first commercial endoscope was released in 2013 spurring multiple clinical studies and resulting in the creation of a one thousand patient registry collected across eighteen sites throughout the USA. However, OCT's application in routine clinical practice has been held back due to standardisation issues primarily caused by the complexity of image

interpretation. Machine learning and algorithmic analysis are aiding progress in this area [4].

The initial feasibility studies showed success in differentiating between multiple conditions defined by the presence of nonstandard cells within tissues, termed dysplasia. This was further improved after the commercial release of specialty specific imaging systems, achieving 87% diagnostic accuracy for one condition, Barrett's oesophagus dysplasia. As with the other medical specialities discussed, OCT's high resolution is a major benefit in diagnostics [4]. However in addition to this, probes specifically for the application of OCT in gastroenterology have been developed that consist of a 12 mm probe head within a tethered capsule, as shown in Figure 1.11. This is a significant development as standard endoscopy techniques typically require sedation and can only be administered by specialists, neither of which are required with this probe type. Additionally, standard endoscopy only records surface images and hence misses key substructure abnormalities which can be crucial for diagnostics [43].

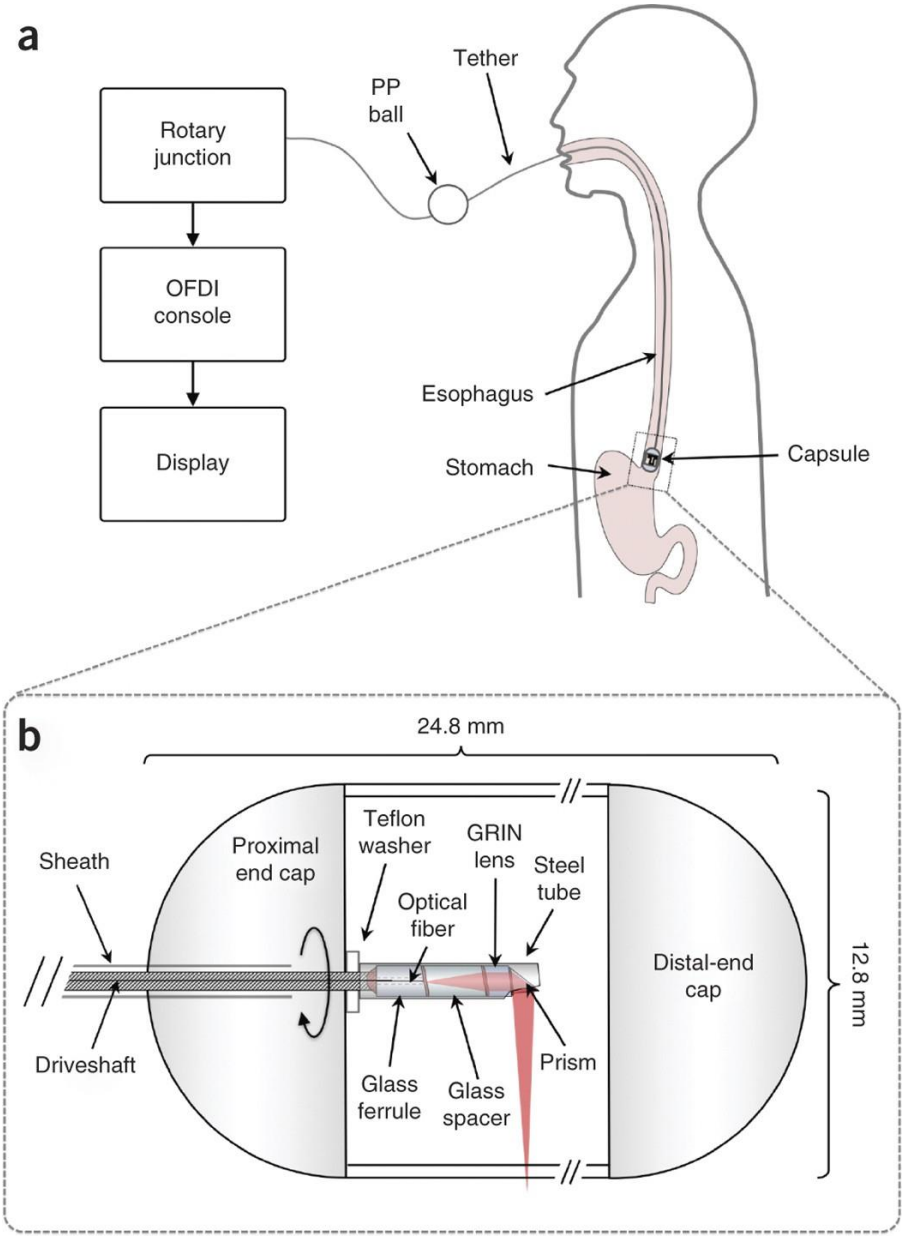

Figure 1.11: (A) Reference diagram of application of capsule (B) Schematic of capsule [43].

The application of PS-OCT in gastroenterology has had very little development, however it is hoped that it will produce improved tissue layer differentiation where intensity differences are subtle in conventional OCT. However, it is likely that it would suffer from the same fibre issues as previously discussed in reference to cardiovascular applications of PS-OCT. Tsai et al. claim that an unpublished study has shown differing birefringence between substructures in swine oesophagus imaged *in vivo* [4], which would be an important result for the basis of further studies in this area.

Rheumatic Application - Unlike the other medical specialties discussed, rheumatic conditions can affect tissues from multiple organ systems including; vascular, gastrointestinal, and nervous systems. This is in addition to the areas commonly connected with the specialty, namely joints and associated surrounding tissues [44]. As a result, an OCT system that can make representative measurements for a particular condition may not be appropriate for another. The first application of OCT in a rheumatology relevant tissue was a PS-OCT feasibility study in 1997. This is unlike other specialties discussed, that had initial investigations conducted using conventional OCT, which is due to established literature results of birefringent properties of tendons [36]. The first conventional OCT publication specifically focused on a rheumatic condition was two years later and was an *in vivo* clinical study comparing the cartilage of healthy and osteoarthritic specimens [45].

The diversity of conventional OCT techniques in rheumatology is evident from the approximately even ratio of publications in the specialty for; imaging of cartilage, angiography, and macular imaging, as found by Web of Science [46]. The review by Chu et al. of imaging of biomarkers for characterisation of pre-osteoarthritic joints identifies OCT's substructure analysis in cartilage as capable of identifying abnormalities not visible in conventional techniques. Notably, it also correlates to both magnetic resonance imaging, MRI, and arthroscopy, which do not directly correlate to each other. This is believed to be due to OCT's quantitative cross-section imaging, as seen in MRI, and its high resolution, as seen in conventional arthroscopy [47].

As previously discussed, the first imaging of tendons in OCT was completed by a PS-OCT system. The publication identifies that the collagen is the birefringent constituent of the tissue, and hence reasons that other tissues containing it may also exhibit birefringence [36]. The vast majority of rheumatology publications, identified by Web of Science, investigating the application of PS-OCT are focused on the imaging of cartilage and developing *in vivo* imaging techniques [46]. However, research is starting to review its use in conditions such as systemic sclerosis (SSc) [48], due to established symptomatic

skin fibrosis, as a quantitative measure of disease progression, as will be discussed in Chapters 2 and 3.

1.6 Systemic Sclerosis

SSc is a multi-system connective tissue disease defined by fibrosis of soft tissues and microvascular dysfunction. Fibrosis, termed sclerosis (thickening or hardening), affects multiple organ systems [49], (including the heart, lungs, kidneys and skin). It is commonly referred to as scleroderma, which refers only to the fibrosis of skin, which is a characteristic manifestation for the majority of, but not all, patients [50]. PubMed, a medical publication search engine run by the US National Library of Medicine, shows scleroderma publications starting from the early 1900s, with distinction of SSc within publications from 1950 [51].

The primer on SSc by Allanore et al. describes the pathophysiology of the disease. They note that although the condition is not well understood it is believed that a genetic vulnerability can cause it to be triggered by an environmental event. In addition to scleroderma, the two other non-organ specific symptoms are microvascular damage and dysfunction of immune response. Hypoxia, the insufficient supply of oxygen to tissue, is commonly one of the first results of the condition and is caused by capillary damage [49]. This can result in Raynaud's phenomenon, which is often the earliest symptom of SSc [52]. Alterations in the immune response are seen as modified function and number of immune cells, and inflammatory signatures in lung and skin tissues [49].

The 2020 review by Herrick et al. describes Raynaud's phenomena as, '*symmetrical transient vascular events in the fingers and toes triggered by cold or emotional stress and manifest by skin color changes'*. This is shown in Figure 1.12. It is categorised into two sub-definitions depending on cause, primary and secondary. Primary Raynaud's is caused by thermoregulation dysfunction, whereas secondary Raynaud's results from damage

caused to the vascular system by secondary disease, such as SSc [53]. It is seen in 95% of SSc patients [52].

Figure 1.12: Example of Raynaud's phenomena [53].

SSc is notable in the variability of symptoms seen between patients [49]. As a result in 2013 the American college of rheumatology, ACR, and the European league against rheumatism, ELAR, created a score based classicisation criteria in order to aid clinical research. Notably scleroderma has the highest weighting, with more than double the score of any other criteria. Other higher scoring criteria are Raynaud's, immune cell prevalence, and fingertip lesions. This can be seen in ACR and ELAR's table shown below, table 1.1 [50].

Item	Sub-item(s)	Weight/score†
Skin thickening of the fingers of both hands extending proximal to the metacarpophalangeal joints *(sufficient criterion)*	–	9
Skin thickening of the fingers *(only count the higher score)*	Puffy fingers	2
	Sclerodactyly of the fingers (distal to the metacarpophalangeal joints but proximal to the proximal interphalangeal joints)	4
Fingertip lesions *(only count the higher score)*	Digital tip ulcers	2
	Fingertip pitting scars	3
Telangiectasia	–	2
Abnormal nailfold capillaries	–	2
Pulmonary arterial hypertension and/or interstitial lung disease *(maximum score is 2)*	Pulmonary arterial hypertension	2
	Interstitial lung disease	2
Raynaud's phenomenon	–	3
SSc-related autoantibodies (anticentromere, anti–topoisomerase I [anti–Scl-70], anti–RNA polymerase III) *(maximum score is 3)*	Anticentromere	3
	Anti–topoisomerase I	
	Anti–RNA polymerase III	

Table 1.1: 'The American College of Rheumatology/European League Against Rheumatism criteria for the classification of systemic sclerosis. …†The total score is determined by adding the maximum weight (score) in each category. Patients with a total score of ≥9 are classified as having definite systemic sclerosis.' as defined by van den Hoogen et al. [50].

For patients with skin involvement, the condition is sub-defined into limited cutaneous, lcSSc, and diffuse cutaneous, dcSSc. LcSSc is defined as scleroderma only in distal extremities, such as fingers, and face, whereas dcSSc additionally presents in proximal extremities, such as upper arms, and the trunk. DcSSc is often associated with rapid

disease progression and earlier onset of organ complications, although patients can change between subgroups [49].

Fingertip lesions, also known as digital lesions or digital tip lesions, are another high scoring criteria. In this context they are sub-defined as ulcerations and pitting. There is disagreement on the definition of ulcers, but a systematic review by Suliman et al. proposed a definition as, '*Loss of epidermal covering with a break in the basement membrane (which separates dermis from epidermis). It appears clinically as visible blood vessels, fibrin, granulation tissue and/or underlying deeper structures (e.g., muscle, ligament, fat) or as it would appear on debridement'.* This has been found to have excellent intra-rater and moderate inter-rater reliability [54]. Pitting can be defined as '*small-sized hyperkeratosis'* [55]. Both have been found to have a significant impact on patient quality of life and hand function [56] [57]. Images of these can be seen in Figure 1.13.

Figure 1.13: (A) Digital ulcers on all fingers (B) Digital pitting on right index finger. Images provided courtesy of Graham Dinsdale (Salford Royal, NHS)

Strimbu defined biomarkers as a '*broad subcategory of medical signs, that is, objective indications of medical state observed from outside the patient, which can be measured accurately and reproducibly*' [58]. In the context of SSc, determination of these markers is

hoped to aid sub-classification and monitoring disease progression. Although some measurable indicators have been identified, variability of these between clinical outcomes means that improved prognostic markers are still required [59].

The main biomarkers used in the diagnosis and prognosis of SSc are quantitative measures of antibody and biochemical indicators. Significantly, some autoantibodies are specific to the condition and are included in the disease classification criteria. Growth factors, protein groups that stimulate tissue growth, are also strongly associated with fibrosis. However, the reliability of measurements of these structures is still under investigation, with some studies showing inconsistent results. Compounds associated with immune system regulation are also used as indicators [60]. Measurements of these compounds requires samples to be taken from patients, which is invasive and time is required to process results in clinical laboratories.

In contrast a technique that can provide an immediate measure of disease is the modified Rodnan skin score, mRSS. This is a classification technique, carried out by trained clinicians, that uses relative palpation of skin as a quantitative estimator of skin thickness. The system assigns an integer value between 0 and 3, with 0 being no detectable skin involvement and 3 being severe skin involvement [61]. The ability of this technique to make immediate assessment of skin is significant due to the disease progression differential between lcSSc and dcSSc [60]. Additionally, mRSS has been shown to correlate with interstitial lung disease, ILD, [62], which is the most significant cause of death in SSc [63]. MRSS is also the only outcome measure for skin involvement that is fully validated and approved for clinical trials by the Outcome Measures in Rheumatology (OMERACT) research organisation [64]. However, its high inter-observer variability and importance of skin involvement as a prognostic biomarker is a major motivation for the development of non-invasive quantitative alternatives. One of which is OCT due to its high resolution and established use in medical imaging across multiple specialties [65].

The application of OCT in SSc skin fibrosis is relatively new, with the first study investigating its potential for disease assessment not being published until 2013. This study, by Abignano et al., compared 3D conventional OCT scans with histology of skin biopsies. They acknowledge the use of high frequency ultrasound, HFUS, as an established measurement technique for dermal thickness. However, its low resolution relative to OCT, despite its higher penetration depth, is a flaw in its application in SSc, where fine detail of structures can be clinically important [65].

A 2021 review of the application of HFUS in SSc by Ruaro et al. discussed the use of the technique in multiple evaluation assessment methods for the disease. They note that probes are primarily used between 18-32 MHz and are capable to reliably measuring dermal thickness with better inter- and intra-reliability than mRSS. The technique can identify thickening before a change in mRSS can be detected. However, dermal thickness measured by HFUS shows inconsistent correlation to global, or local, mRSS. HFUS can also be applied to the measurement of microvascular damage and perfusion, which has shown better correlation to mRSS [66]. There are currently few quantitative measures of skin thickness that can be reliably correlated to mRSS, which itself is only an observation-based measure of resistance to palpation. The increase in resistance is typically referred to as thickening, but is not a direct measure of it.

The study by Abignano et al. used 44 participants, consisting of 21 with SSc, 22 healthy controls and one with skin morphea [65], which is a similar skin condition described as, '*a rare inflammatory disease of the skin and subcutaneous tissue'* by Penmetsa et al. [67]. All participants were imaged on dorsal, top/backside, and volar, underside, of at least two fingers, dorsal hand, and dorsal and volar of the forearm using OCT. Images were taken with a SS-OCT system. These images were compared to three tissue biopsies, small tissue samples, taken from two dcSSc patients and one healthy control, as well as the mRSS of patients. From the OCT images the epidermis, dermal-epidermal junction, and papillary dermis, and in healthy controls the reticular dermis, could be identified. Figure 1.14 shows these dermal layers for reference. Overlay of the OCT average one-dimensional

scans of intensity as a function of depth, A-scans, on the histology images allowed for these structures to be identified from the intensity peaks, as seen in Figure 1.15. The intensity differential between the dermal-epidermal junction reflection peak and epidermal reflection minima showed significant change across the skin score groups with reduced intensity difference as mRSS increased. Though, it could not differentiate HC, mRSS 0 and 1. However, intensity at 300 µm did show significant difference between these groups. The authors identify OCTs ability to discriminate between skin groups as evidence of its potential as an alternative to mRSS. It is noted that its 1 mm penetration depth is a limitation, but it is suggested that in combination with HFUS a dual-modality assessment could be a viable alternative to mRSS [65]. Later studies corroborate the reduced intensity differential between epidermal and dermal-epidermal junction reflections in SSc patients in contrast to healthy controls [68] [69]. This characteristic was also shown to appear in other collagen deposition disorders by Ring et al. [68].

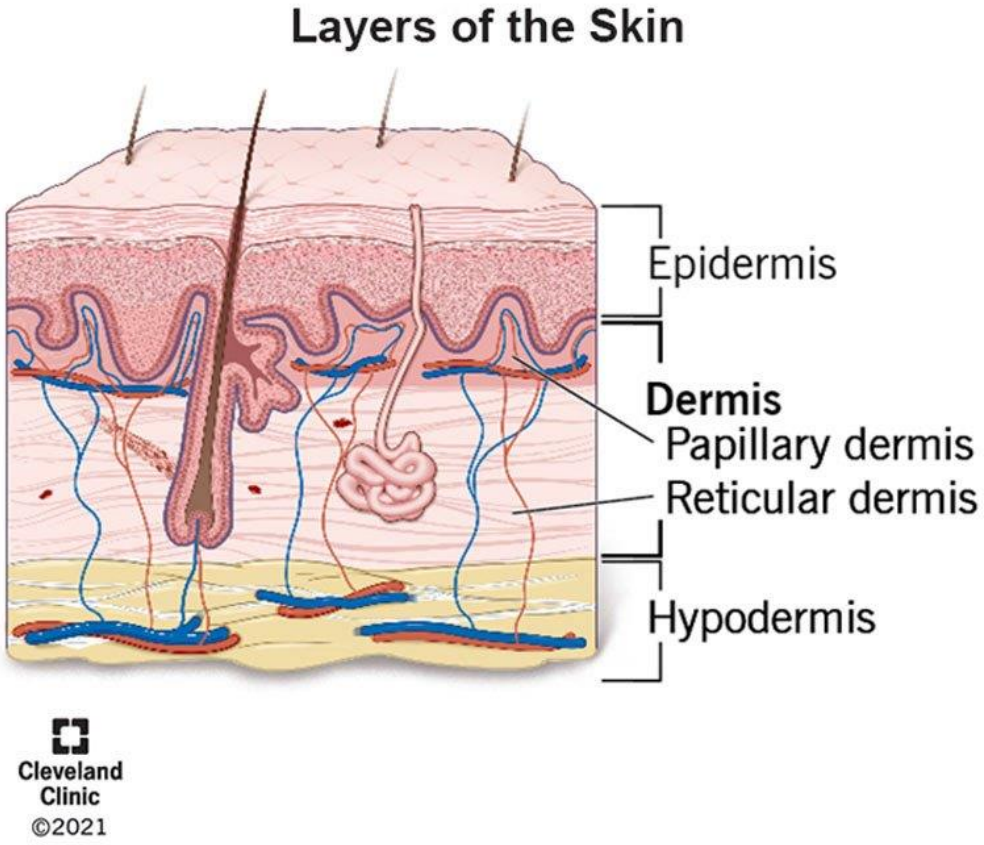

Figure 1.14: Skin layer diagram. For context, this diagram shows the skin layers and structures within it [70]. All layers vary in thickness due to factors including: site within an individual, ultra-violet light exposure, and ethnicity. The surface layer is the epidermis which is typically between 100 – 200 µm thick. The dermis follows this and is in order of a factor of ten thicker, between 1000 – 2000 µm. The base layer is the hypodermis which connects the skin to other tissue structures. It is not typically included in skin thickness measurements [67].

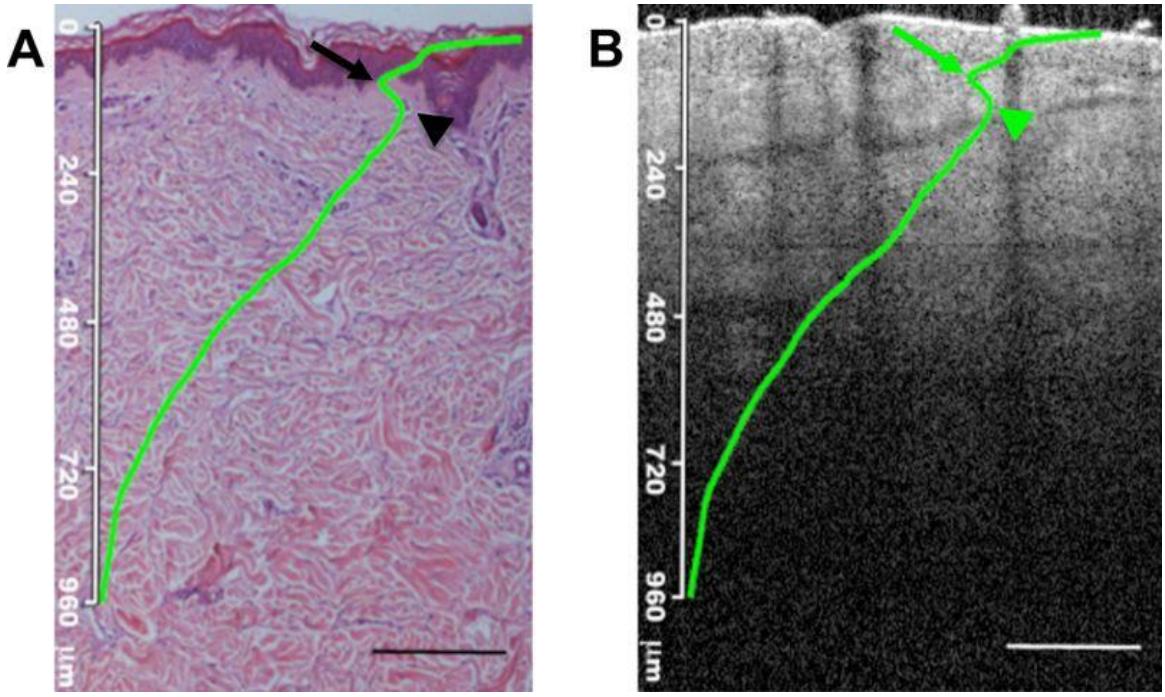

Figure 1.15: Healthy control biopsy with hematoxylin and eosin stain (A) and OCT two-dimensional scan of intensity as a function of depth, B-scan, (B). Both with full width averaged OCT A-scan overlay and first trough and second peak marked with arrows [65].

The enhanced modality of PS-OCT is also still relatively unknown for its functional capabilities in the application to SSc skin fibrosis. Polarisation imaging of fibrotic skin from SSc patients was first investigated as early as 1973 by McNeal et al.. This used a polarising microscope and was of interest due to the unknown mechanism responsible for the reduced compliance of SSc skin. Up to this point various imaging modalities investigated this problem, but few found evidence of any structural deviation from normal skin. Collagen was already known to be birefringent and the author notes that studies of scar tissue had shown reduced birefringence as well as a reduction in tensile strength. This was the motivation for the initial investigation [71].

The study by McNeal et al. used skin taken at autopsy from a patient with SSc and biopsies taken from 12 healthy controls. In addition to microscopy, strips of the skin were subjected to a stress test, and as expected the SSc skin shown significant reduction in compliance. Samples from all were prepared with traditionally histology strains, as well as viewed under polarised light, as shown in Figure 1.16. Sections were radially tensioned

and comparisons made of stress and unstressed tissue. The polarised light aided contrasting and allowed for easier collagen identification. They note that across the various tests SSc samples show rigid and compact collagen structure that only buckle and break under stress. This is in contrast to the loose weave of normal skin where collagen fibres straighten when stress is applied. However, the author does say that no non-normal birefringence was identified [71].

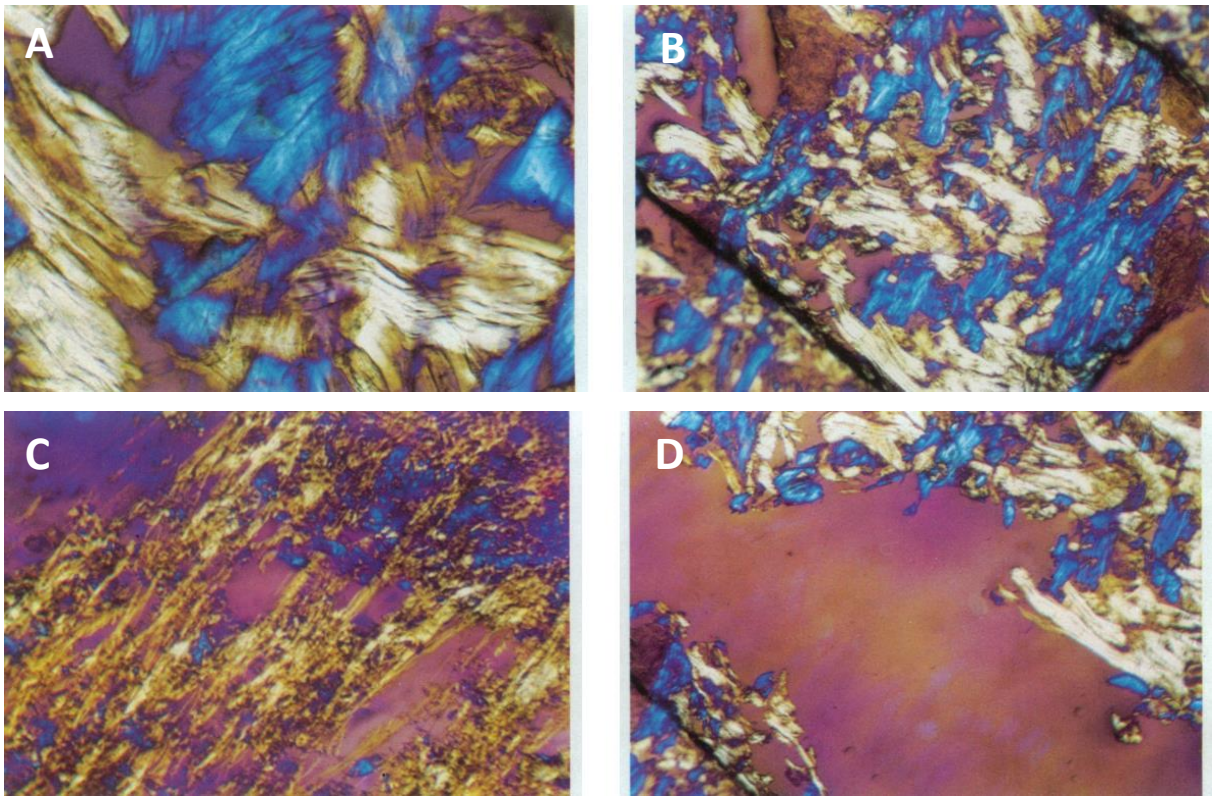

Figure 1.16: Polarising microscope images of horizontal polarisation applied to skin biopsies: Unstressed scleroderma skin (A), Scleroderma skin at breaking point with stress applied at top left corner (B), normal skin during tearing (C), scleroderma skin after tearing (D). B, C, and D are all taken at X11 magnification, and A was taken at X44. The samples are 1 cm wide by between 4 and 7 cm long. The starting thickness of the scleroderma skin was 7 µm and the normal skin started at 21 µm [71].

As of 2020, only one paper had been published on the application of PS-OCT in SSc skin fibrosis. This publication by Adams et al. investigated the potential of OA orientation as a metric of changing collagen structure within skin. It reasoned that retardation and DOP vary as a function of depth and hence a consistent measure across multiple sites cannot

be made with a fixed scale. However, OA orientation is consistent with depth and therefore is a superior metric for a multi-site assessment [72].

Adams et al. split 3D images into 2D layers and for each discrete depth OA entropy was calculated, as well as local retardation and DOP. However, only one healthy control with scar tissue and a mouse model with induced scleroderma were used. In the human study, comparison between data types confirm the postulation. All data type measurements showed significant difference between scar and normal tissue, however OA entropy was the only metric to do so independent of depth. The mouse study used induced fibrosis and images were taken over a 28 day longitudinal study. It found significant differences, $p<0.01$, in OA entropy between controls and mice with induced fibrosis at the end of the 28 day period. However, this was less significant than the human scar comparison for all data types which saw a $p<0.0001$ for OA entropy and DOP, and $p<0.003$ for retardation. Additionally, the induced fibrosis showed an inconsistent longitudinal trend and no data comparison was made for SSc [72].

It is evident that PS-OCT as a quantitative measurement method for biomarkers in SSc is a very underdeveloped area of research. Abignano et al, showed that OCT has the resolution and capability to take measurements that correlate with mRSS. However, the requirement for depth specific measurements is likely to be problematic in clinical applications [65]. PS-OCT has the potential for multiple measurable indicators of changes to collagen structure. The early polarisation microscopy study showed the fundamental structural deviation between normal and SSc fibrotic skin, laying the ground-work for polarisation imaging techniques. The publication by Adams et al. shows significant measurable differences in scar tissue compared to normal tissue in the most commonly used polarisation metrics [72]. However, the lack of SSc patient skin in the study leaves the question open as to its transferability and correlation to mRSS.

1.7 Context of Publications within Research Objective

The following three chapters report the work conducted during the course of study in the form of three publications. They cover three clinical studies focused on the application of PS-OCT as a clinical assessment method for SSc. As previously discussed, SSc is a debilitating chronic condition with the main assessment method for skin fibrosis being the relatively basic mRSS. Likewise, digital ulcers, DU, and pitting, DP, severely affect patient's quality of life [56] [57] and are almost only assessed by clinical observation. These investigations aim to establish quantitative alternatives to these methods.

Chapter 2 was published in Scientific Reports in February 2022. MRSS is the clinical gold standard for the skin thickness assessment, however it has poor inter-observer reliability. This study aimed to assess an objective quantitative alternative, PS-OCT retardation measurements, as a biomarker for SSc. The chapter presents data collected by non-circularly polarised PS-OCT comparing healthy controls and SSc cohorts at baseline and, one week and one month, post biopsy. This data showed broadly that polarisation-phase retardation correlated with mRSS; however, linear polarisation leads to the imaging being sensitive to optic axis orientation, limiting application.

Chapter 3 is a publication in the final draft stage before submission to Annals of the Rheumatic Diseases. Building on the relationship between retardation and mRSS observed in Chapter 2, this study aimed to validate PS-OCT depth measurements using HFUS. Additionally the reliability of PS-OCT was also investigated. This study used a depth calibrated system and circularly polarised light to increase the validity of the results. Data were collected, at volar and dorsal forearm sites in healthy controls and patients, with imaging replicated using both systems in order to establish convergence validity. Two observers imaged over two consecutive days to determine inter- and intra-observer reliability on same and consecutive days. Poor HFUS reliability resulted in correlation to

PS-OCT not being confirmed, however PS-OCT showed reliable inter- and intra-observer measurements.

Chapter 4 is a long form version of a letter that is in the draft stage for submission to Annals of the Rheumatic Diseases. Digital lesions severely detriment patient quality of life and the primary assessment method is clinical observation. This chapter presents a demonstration of a PS-OCT 3D scanning method for digital lesions, ulcers and pitting, in patients. This is an additional application of PS-OCT in SSc disease monitoring, where current methods cannot meet clinical requirements. The work establishes that high resolution 3D scans can provide detailed surface and sub-structural information for clinical assessment and longitudinal studies.

1.8 References

[1] P. Hariharan, Optical Interferometry, Sydney: Academic Press, 2003, pp. 1-8, 23-25.

[2] B. P. Abbott, "Observation of Gravitational Waves from a Binary Black Hole Merger," *Physical Review Letters,* vol. 116, no. 6, pp. 1-16, 2016.

[3] M. E. Brezinski, Optical Coherence Tomography Principles and Applications, Academic Press, 2006, pp. 98-106, 130-137.

[4] T.-H. Tsai, C. L. Leggett, A. J. Trindade, A. Sethi, A.-F. Swager, V. Joshi, J. J. Bergman, H. Mashimo, N. S. Nishioka and E. Namati, "Optical coherence tomography in gastroenterology: a review and future outlook," *Journal of Biomedical Optics,* vol. 22, no. 12, pp. 1-17, 2017.

[5] W. Drexler and J. G. Fujimoto, Optical Coherence Tomography Technology and Application, Springer International Publishing Switzerland, 2015, pp. 68, 70-76, 1057.

[6] J. F. Bille, High Resolution Imaging in Microscopy and Ophthalmology New Frontiers in Biomedical Optics, Cham: Springer Nature Switzerland AG, 2019, pp. 62, 67.

[7] D. S. Klinger, J. W. Lewis and C. E. Randall, Polarized Light in Optics and Spectroscopy, Academic Press, 1990, pp. 61-68.

[8] E. Collett, Field Guide to Polarisation, Bellingham: SPIE Press, 2005, pp. 57-58.

[9] G. Giusfredi, Physical Optics Concepts, Optical Elements, and Techniques, Cham: Springer Nature Switzerland, 2019, pp. 858-859, 868-869.

[10] A. K. Bain, Crystal Optics, Weinheim: Wiley-VCH, 2019, pp. 2-6, 27-28, 275.

[11] D. Clarke and J. Grainger, Polarized Light and Optical Measurements, Pergamon Press, 1971, p. 85.

[12] M. Kobayashi, H. Hanafusa, K. Takada and J. Noda, "Polarization-Independent Interferometric Optical-Time-Domain Reflectometer," *Journal of Lightwave Technology,* vol. 9, no. 5, pp. 623-628, 1991.

[13] M. R. Hee, D. Huang, E. A. Swanson and J. G. Fujimoto, "Polarization-sensitive low-coherence reflectometer for birefringence characterization and ranging," *Journal of the Optical Society of America B,* vol. 9, no. 6, pp. 903-908, 1992.

[14] J. F. De Boer, C. K. Hitzenberger and Y. Yasuno, "Polarization sensitive optical coherence tomography - a review," *Biomedical Optics Express,* vol. 8, no. 3, 2017.

[15] J. M. Schmitt and S. H. Xiang, "Cross-polarized backscatter in optical coherence tomography of biological tissue," *Optical Letters,* vol. 23, no. 13, pp. 1060-1062, 1998.

[16] J. F. de Boer, T. E. Milner and J. S. Nelson, "Determination of the depth-resolved Stokes parameters of light backscattered from turbid media by use of polarization-sensitive optical coherence tomography.," *Optics Letters,* vol. 24, no. 5, pp. 300-302, 1999.

[17] R. D. Allen, J. Brault and R. D. Moore, "A new method of polarization microscopic analysis," *The Journal of Cell Biology,* vol. 13, pp. 223-235, 1963.

[18] J. C. Ramella-Roman, I. Saytashev and M. Piccini, "A review of polarization-based imaging technologies for clinical and preclinical applications," *Journal of Optics,* vol. 22, no. 12, pp. 1-18, 2020.

[19] M. W. Kaplan, "Birefringence in biological materials," *Proceedings of SPIE,* vol. 112, pp. 112-119, 1977.

[20] A. Stanworth and E. J. Naylor, "The polarization optics of the isolated cornea," *British Journal of Ophthalmology,* vol. 34, no. 4, pp. 201-211, 1950.

[21] D. Post and J. E. Gurland, "Birefringence of the cat cornea," *Experimental Eye Research,* vol. 5, no. 4, pp. 286-295, 1966.

[22] V. Sankaran, J. T. Walsh Jr. and D. J. Maitland, "Comparative study of polarized light propagation in biologic tissues," *Journal of Biomedical Optics,* vol. 7, no. 3, pp. 300-306, 2002.

[23] J. F. de Boer, S. M. Srinivas, B. H. Park, T. H. Pham, Z. Chen, T. E. Milner and J. S. Nelson, "Polarization effects in optical coherence tomography of various biological tissues," *Journal of Selected Topics in Quantum Electronics,* vol. 5, no. 4, pp. 1200-1204, 1999.

[24] S. Alali and A. Vitkin, "Polarized light imaging in biomedicine: emerging Mueller matrix methodologies for bulk tissue assessment," *Journal of Biomedical Optics,* vol. 20, no. 6, pp. 1-9, 2015.

[25] N. Ghosh, A. Banerjee and J. Soni, “Turbid medium polarimetry in biomedical imaging and diagnosis,” *The European Physical Journal - Applied Physics,* vol. 54, no. 3, pp. 1-21, 2011.

[26] N. Ghosh and I. A. Vitkin, “Tissue polarimetry: concepts, challenges, applications, and outlook,” *Journal of Biomedical Optics,* vol. 16, no. 11, pp. 1-29, 2011.

[27] I. Ahmad, A. Khaliq, M. Iqbal and S. Khan, “Mueller Matrix polarimetry for characterization of skin tissue samples: A review,” *Photodiagnosis and Photodynamic Therapy,* vol. 30, pp. 1-7, 2020.

[28] R. J. Narayan, Monitoring and Evaluation of Biomaterials and Their Performance In Vivo, Elsevier, 2017, p. 154.

[29] K. Basak, M. Manjunatha and P. K. Dutta, “Review of laser speckle-based analysis in medical imaging,” *Medical & Biological Engineering & Computing,* vol. 50, no. 6, pp. 547-558, 2012.

[30] L. Tchvialeva, G. Dhadwal, H. Lui, S. Kalia, H. Zeng, D. I. Mclean and T. K. Lee, “Polarization speckle imaging as a potential technique for in vivo skin cancer detection,” *Journal of Biomedical Optics,* vol. 18, no. 6, pp. 1-7, 2013.

[31] Y. Wang, D. C. Louie, J. Cai, L. Tchvialeva, H. Lui, Z. J. Wang and T. K. Lee, “Deep learning enhances polarization speckle for in vivo skin cancer detection,” *Optics and Laser Technology,* vol. 140, pp. 1-11, 2021.

[32] J. M. Schmitt, “Optical Coherence Tomography (OCT): A Review,” *Journal of Selected Topics in Quantum Electronics,* vol. 5, no. 4, pp. 1205-1215, 1999.

[33] A. F. Fercher, K. Mengedoht and W. Werner, “Eye-length measurement by interferometry with partially coherent light,” *Optical Letters,* vol. 13, no. 3, pp. 186-188, 1988.

[34] D. Huang, J. Wang, C. P. Lin, C. Puliafito and J. G. Fujimoto, “Micron-resolution ranging of cornea anterior chamber by optical reflectometry,” *Lasers in Surgery and Medicine,* vol. 11, no. 5, pp. 419-425, 1991.

[35] D. Huang, E. A. Swanson, C. P. Lin, J. S. Schuman, W. G. Stinson, W. Chang, M. R. Hee, T. Flotte, K. Gregory, C. A. Puliafito and J. G. Fujimoto, “Optical Coherence Tomography,” *Science,* vol. 254, no. 5035, pp. 1178-1181, 1991.

[36] J. F. de Boer, T. E. Milner, M. J. C. van Gemert and J. S. Nelson, “Two-dimensional birefringence imaging in biological tissue by polarization-sensitive optical coherence tomography,” *Optics Letters,* vol. 22, no. 12, pp. 934-936, 1997.

[37] A. M. Zysk, F. T. Nguyen, A. L. Oldenburg, D. L. Marks and S. A. Boppart, “Optical coherence tomography: a review of clinical development from bench to bedside,” *Journal of Biomedical Optics,* vol. 12, no. 5, pp. 1-21, 2007.

[38] I.-K. Jang, Cardiovascular OCT Imaging, Cham: Springer Nature Switzerland, 2020, pp. 18-19.

[39] L. Fanea and A. J. Fagan, “Review: Magnetic resonance imaging techniques in ophthalmology,” *Molecular Vision,* vol. 18, p. 2538–2560, 2012.

[40] B. Cense, T. C. Chen, B. H. Park, M. C. Pierce and J. F. de Boer, “In vivo depth-resolved birefringence measurements of the human retinal nerve fiber layer by polarization-sensitive optical coherence tomography,” *Optics Letters,* vol. 27, no. 18, pp. 1610-1612, 2002.

[41] M. Pircher, C. K. Hitzenberger and U. Schmidt-Erfurth, “Polarization sensitive optical coherence tomography in the human eye,” *Progress in Retinal and Eye Research,* vol. 30, no. 6, pp. 431-451, 2011.

[42] E. Götzinger, M. Pircher, I. Dejaco-Rushswurm, S. Kaminski, C. Skorpik and C. K. Hitzenberger, “Imaging of birefringent properties of keratoconus corneas by polarization-sensitive optical coherence tomography,” *Investigative Ophthalmology & Visual Science,* vol. 48, no. 8, pp. 3551-3558, 2007.

[43] M. J. Gora, J. S. Sauk, R. W. Carruth, K. A. Gallagher, M. J. Suter, N. S. Nishioka, L. E. Kava, M. Rosenberg, B. E. Bouma and G. Tearney, “Tethered capsule endomicroscopy enables less invasive imaging of gastrointestinal tract microstructure,” *Nature Medicine,* vol. 19, no. 2, pp. 238-240, 2013.

[44] J. Payne-James, Encyclopedia of Forensic and Legal Medicine, London: Elsevier Ltd, 2005.

[45] J. M. Herrmann, C. Pitris, B. E. Bouma, S. A. Boppart, C. A. Jesser, D. L. Stamper, J. G. Fujimoto and M. E. Brezinski, “High resolution imaging of normal and osteoarthritic cartilage with optical coherence tomography,” *Journal of Rheumatology,* vol. 26, no. 3, pp. 627-635, 1999.

[46] Clarivate, “Web of Science,” Clarivate, [Online]. Available: https://www.webofscience.com/wos/woscc/basic-search. [Accessed 12 September 2022].

[47] C. R. Chu, A. A. Williams, C. H. Coyle and M. E. Bowers, “Early diagnosis to enable early treatment of pre-osteoarthritis,” *Arthritis Research & Therapy,* vol. 14, no. 3, pp. 1-10, 2012.

[48] E. Marjanovic, G. Dinsdale, M. Berks, T. Moore, J. Manning, V. Sharma, S. Leggett, M. Dickinson, A. Herrick, R. Watson and A. K. Murray, “PILOT STUDY OF POLARISATION SENSITIVE OPTICAL COHERENCE TOMOGRAPHY AS A BIOMARKER FOR FIBROSIS IN SYSTEMIC SCLEROSIS,” *Rheumatology,* vol. 57, no. 2, p. 102, 2018.

[49] Y. Allanore, R. Simms, O. Distler, M. Trojanowska, J. Pope, C. P. Denton and J. Varga, “Systemic sclerosis,” *Nature Reviews Disease Primers,* vol. 1, pp. 1-21, 2015.

[50] F. van den Hoogen, “2013 classification criteria for systemic sclerosis: an American college of rheumatology/European league against rheumatism collaborative initiative,” *Annals of the Rheumatic Diseases,* vol. 72, no. 11, pp. 1747-1755, 2013.

[51] “PubMed,” Federal Government of the United States, [Online]. Available: https://pubmed.ncbi.nlm.nih.gov/. [Accessed 23 September 2022].

[52] M. Hughes and A. L. Herrick, “Systemic sclerosis,” *British Journal of Hospital Medicine,* vol. 80, no. 9, 2019.

[53] A. L. Herrick and F. M. Wigley, “Raynaud's phenomenon,” *Best Practice & Research Clinical Rheumatology,* vol. 34, no. 1, pp. 1-21, 2020.

[54] Y. A. Suliman, C. Bruni, S. R. Johnson, E. Praino, M. Alemam, N. Borazan, L. Cometi, B. Myers, D. Khanna, Y. Allanore, M. Baron, T. Kreig, A. Herrick, A. Afonso and O. Distler, “Defining Skin Ulcers in Systemic Sclerosis: Systematic Literature Review and Proposed World Scleroderma Foundation (WSF) Definition,” *Journal of Scleroderma and Related Disorders,* vol. 2, no. 2, pp. 115-120, 2017.

[55] L. Amanzi, F. Braschi, G. Fiori, F. Galluccio, I. Miniati, S. Guiducci, M.-L. Conforti, O. Kaloudi, F. Nacci, O. Sacu, A. Candelieri, A. Pignone, L. Rasero and D. Conforti, “Digital ulcers in scleroderma: staging, characteristics and sub-setting through observation of 1614 digital lesions,” *Rheumatology,* vol. 49, no. 7, pp. 1374-1382, 2010.

[56] L. Mouthon, P. H. Carpentier, C. Lok, P. Clerson, V. Gressin, E. Hachulla, A. Bérezné, E. Diot, A. Khau Van Kien, P. Jego, C. Agard, A. B. Duval-Modeste, A. Sparsa and E. Puzenat, “Ischemic Digital Ulcers Affect Hand Disability and Pain in Systemic Sclerosis,” *The Journal of Rheumatology,* vol. 41, no. 7, pp. 1317-1323, 2014.

[57] E. Nolan, J. Manning, C. Heal, T. Moore and A. Herrick, “Impact and associates of digital pitting in patients with systemic sclerosis: a pilot study,” *Scandinavian Journal of Rheumatology,* vol. 49, no. 3, pp. 239-243, 2020.

[58] K. Strimbu and J. A. Tavel, “What are biomarkers?,” *Current Opinion in HIV and AIDS,* vol. 5, no. 6, pp. 463-466, 2010.

[59] R. L. Smeets, B. E. Kersten, I. Joosten, C. Kaffa, W. Alkema and H. J. V. M. C. Koenen, “Diagnostic profiles for precision medicine in systemic sclerosis; stepping forward from single biomarkers towards pathophysiological panels,” *Autoimmunity Reviews,* vol. 19, no. 5, pp. 1-7, 2020.

[60] A. Utsunomiya, N. Oyama and M. Hasegawa, “Potential biomarkers in systemic sclerosis: A literature review and update,” *Journal of Clinical Medicine,* vol. 9, pp. 1-26, 2020.

[61] D. Khanna, “Standardization of the modified Rodnan skin score for use in clinical trials of systemic sclerosis,” *Journal of Scleroderma and Related Disorders,* vol. 2, no. 1, pp. 11-18, 2017.

[62] K. M. Matsuda, A. Yoshizaki, A. Kuzumi, T. Fukasawa, S. Ebata, S. Miura, T. Toyama, A. Yoshuzaki, H. Sumida, Y. Asano, K. Oba and S. Sato, “Skin thickness score as a surrogate marker of organ involvements in systemic sclerosis: a retrospective observational study,” *Arthritis Research & Therapy,* vol. 21, no. 129, pp. 1-10, 2019.

[63] M. Elhai et al., “Mapping and predicting mortality from systemic sclerosis,” *Annals of Rheumatic Diseases,* vol. 76, no. 11, pp. 1897-1905, 2017.

[64] P. A. Merkel, P. J. Clements, J. D. Reveille, M. Suarez-Almazor, G. Valentini and D. Furst, “Current status of outcome measure development for clinical trials in systemic sclerosis. Report from OMERACT 6.,” *The Journal of Rheumatology,* vol. 30, no. 7, pp. 1630-1647, 2003.

[65] G. Abignano, S. Z. Aydin, C. Castillo-Gallego, V. Liakouli, D. Woods, A. Meekings, R. J. Wakefield, D. G. McGonagle, P. Emery and F. Del Galdo, “Virtual skin biopsy by optical coherence tomography: the first quantitative imaging biomarker for scleroderma,” *Annals of the Rheumatic Diseases,* vol. 72, no. 11, pp. 1845-1851, 2013.

[66] B. Ruaro, T. Santiago, M. Hughes, G. Lepri, G. Poillucci, E. Baratella, F. Salton and M. Confalonieri, “The Updated Role of Ultrasound in Assessing Dermatological Manifestations in Systemic Sclerosis,” *Open Access Rheumatology: Research and Reviews,* vol. 13, pp. 79-91, 2021.

[67] “StatPearls,” StatPearls Publishing, Treasure Island (FL), 2023.

[68] H. C. Ring, M. Mogensen, A. A. Hussain, N. Steadman, C. Banzhaf, L. Themstrup and G. B. Jemec, “Imaging of collagen deposition disorders using optical coherence tomography,” *Jourmal of the European Academy of Dermatology and Venereology,* vol. 29, pp. 890-898, 2015.

[69] N. S. M. Pires, A. T. Dantas, A. L. B. P. Duarte, M. M. Amaral, L. O. Fernandes, T. J. C. Dias, L. S. A. de Melo and A. S. L. Gomes, “Optical coherence tomography as a method for quantitative skin evaluation in systemic sclerosis,” *Annals of Rheumatic Diseases,* vol. 77, no. 3, pp. 465-466, 2018.

[70] “Dermis,” Cleveland Clinic, 2 7 2022. [Online]. Available: https://my.clevelandclinic.org/health/body/22357-dermis. [Accessed 28 9 2022].

[71] J. E. McNeal, “Scleroderma and the structural basis of skin compliance,” *Archives of Dermatological Research,* vol. 107, pp. 699-705, 1973.

[72] D. C. Adams, M. V. Szabari, D. Lagares, A. F. McCrossan, L. P. Hariri, A. M. Tager and M. J. Suter, “Assessing the progression of systemic sclerosis by monitoring the tissue optic axis using PS-OCT,” *Scientific Reports,* vol. 10, no. 1, 2020.

2. Polarisation-sensitive optical coherence tomography measurement of retardance in fibrosis, a non-invasive biomarker in patients with systemic sclerosis

E. J. Marjanovic, V. Sharma, L. Smith, C. Pinder, T. L. Moore, J. B. Manning, G. Dinsdale, M. Berks, V. L. Newton, S. Wilkinson, M. R. Dickinson, A. L. Herrick, R. E. B. Watson & A. K. Murray. Scientific Reports volume 12, Article number: 2893 (2022)

Context of contribution:

This chapter was published in February 2022 in Scientific Reports (Nature Group) jointly with thirteen other authors, of which I am third. At the time of joining the project the data had been collected, but no further steps taken. I handled the raw proprietary data format, converted it to readable data, and performed all, non-statistical, data processing. This required developing code in MATLAB for all steps.

Images of the depth profiles required the skin surface to be computationally flattened in order for analysis to be conducted. This needed to be consistently applied, accounting for artefacts, broken and irregular skin, and hairs, as well as folded images and noise. When this process had been completed for the intensity images the same realignments were applied to the paired retardation images. Intensity images were width averaged in order to create A-scans so that the dermal-epidermal boundary could be identified. Likewise, retardation images were width averaged in order to create a phase-angle depth relation, as would be later implemented in the following study analysis in Chapter 3.

However, due to high levels of noise in images the gradients varied significantly and as a result the decision was made to align the gradients around a known reference region, which was no birefringence in the epidermis. This should be seen as a zero gradient in this region and it was assumed that any deviation was not a real effect and so each data set was offset to match this. It should be noted that no depth calibration was possible and so all data is only appropriate for relative comparison. In the subsequent study in Chapter 3,

where matched thresholding significantly improved the data, these later steps were not required.

The following text, pages 59-82, are a direct reproduction of the article published in Scientific Reports in 2022 and as such has undergone peer review and proof checking. Within this publication I wrote the section which describes my work on data processing and analysis of the PS-OCT images, and I also advised on the writing of the results and discussion sections.

2.1 Abstract

Objective: Polarisation-sensitive optical coherence tomography (PS-OCT) offers a novel, non-invasive method of assessing skin fibrosis in the multisystem disease systemic sclerosis (SSc) by measuring collagen retardance. This study aimed to assess retardance as a biomarker in SSc.

Methods: Thirty-one patients with SSc and 27 healthy controls (HC) underwent PS-OCT imaging. 'Skin score' was assessed by clinical palpation (0-3 scale). A subset of ten patients and ten age/sex-matched HC had a biopsy and longitudinal imaging. Histological assessment included quantification of epidermal thickness, collagen content (to assess fibrosis) and matrix metalloproteinase (MMP) activity (in situ zymography). PS-OCT images were assessed for epidermal thickness (structure) and fibrosis (retardance).

Results: Positive correlation was observed between epidermal thickness as measured by histology and structural PS-OCT ($r=0.79$; $p<0.001$). Retardance was: HC mean 0.21 (SD 0.21) radian/pixel; SSc skin score 0, 0.30 (0.19); skin score 1, 0.11 (0.16); skin score 2, 0.06 (0.12); skin score 3, 0.36 (0.35). Longitudinal retardance decreased at one-week across

groups, increasing at one-month for HC/skin score 0-1; HC biopsy site retardance suggests scarring is akin to fibrosis.

Conclusion: Relationships identified between retardance with both biopsy and skin score data indicate that retardance warrants further investigation as a suitable biomarker for SSc-related fibrosis.

2.2 Introduction

Systemic sclerosis (SSc) is a rare autoimmune connective tissue disease that causes changes to microvascular architecture and function, in addition to fibrosis of soft tissue. Although rare (affecting around 6000 people in the UK), SSc carries a high mortality due to the fibrosis of internal organs, and has a huge impact on those affected in terms of pain and disability [1]. There is currently no proven effective disease-modifying therapy for SSc; clinical trials have been hampered by lack of both objective clinical outcome measures and lack of biomarkers to enable the evaluation of new therapies [2-3]. Skin changes reflect disease progression and the severity of internal organ involvement, and the degree of skin thickening is a predictor of mortality [4]. In clinical practice the standard method of assessing skin involvement in patients with SSc is by modified Rodnan skin score (mRSS) determined by clinical palpation [5-7]. Although quick and simple, the mRSS is subjective and affected by oedema; studies have shown that the repeatability of the measure - even by experienced investigators - can be poor [8]. More reliable measures that are sensitive to change are therefore required. High frequency ultrasound (measuring skin thickness and oedema) and other non-invasive imaging techniques such as durometry (measuring skin hardness), plicometry (measuring thickness of skin folds) and cutometry (measuring elasticity) have been trialled but have not met all of the validity criteria that would make them usable and reliable methods of assessment. Histology remains the gold standard to assess fibrosis but has the disadvantage of being invasive [8].

Optical coherence tomography (OCT) takes non-invasive, in vivo, 'optical biopsy' images of the skin, analogous to ultrasound, but using light to visualise skin structure [9]. This allows high resolution (<10 μm) measurement of epidermal thickness. The reviews by Olsen et al. and Guida et al. offer excellent overviews on the wider application of OCT in dermatology and the comparison of OCT and other optical imaging techniques in skin [10-11].

Polarisation-sensitive optical coherence tomography (PS-OCT) offers a novel non-invasive method of assessing skin fibrosis in SSc. The fibrillar collagens, a key component of the dermal extracellular matrix, cause skin to be anisotropic and thus to have birefringent properties (i.e. skin has different refractive indices depending on the polarisation state of the light, causing one light polarisation state to travel faster through the tissue than the other). Birefringence is measured as 'phase retardation' and can be assessed using polarised light. The retardance of a material is the change in the phase angle as the light travels through and is generally shown as cumulative colour maps of in-depth images.

Polarised light transmission microscopy has been shown to be sensitive to the spatial orientation pattern of collagen in histological sections. In skin with burn damage and scarring, changes to the birefringent properties of the skin can be observed [12-15]. Collagen fibrils are denatured by burn damage. This affects the structure of the fibrils (akin to unravelling), their orientation and density. Birefringence increases once tissue repairing/scarring begins. These changes in birefringence can be used as a measure of damage and potentially fibrosis. PS-OCT allows for measuring these changes and heterogeneity within the skin in addition to skin structure. In addition, recent advancements allow further understanding of skin structure [16, 17].

This study aimed to test the hypothesis that PS-OCT could measure differences in skin thickness and fibrosis, non-invasively, between patients with a range of clinical severities

of disease. The aim of this study was to gauge the potential of PS-OCT as a tool to quantify collagen retardance as a tractable biomarker of disease progression in SSc. Specific objectives were: 1) to obtain in vivo PS-OCT images of forearm skin in patients with SSc and in healthy controls, allowing comparison of structural (epidermal thickness) and retardance data (a measure of fibrosis), to the current clinically-validated method of assessment, mRSS (clinically accepted non-invasive measurement); 2) to validate in a matched subset, the PS-OCT images, comparing to biopsy tissue allowing assessment of epidermal thickness, fibrillary collagen content and potential involvement of matrix metalloproteinases (MMPs) in any observed tissue remodelling, and; 3) in a subset of those biopsied, carry out follow-up imaging to assess scarring, analogous to fibrosis.

2.3 Patients and Methods

Participants attended for a single imaging visit with the exception of a subset of ten HCs and ten patients with SSc who underwent a biopsy and were invited to attend for two follow-up visits to image the biopsy site. Participants were asked to refrain from caffeine and nicotine for four hours prior to the study and to attend without creams or make-up on the area to be imaged (the volar forearm). The study was approved by Greater Manchester West Research Ethics Committee (16/NW/0023). All research was performed in accordance with relevant guidelines and regulations. All participants gave informed, written consent for the study.

Participants: Fifty eight participants (31 patients with SSc and 27 HC) were recruited to the study; demographics (age, gender) of all participants and the biopsy subset (ten HCs and ten patients with SSc) are shown in Table 2.1. In addition, for patients, duration of Raynaud’s phenomenon, duration of SSc (from onset of first non-Raynaud's clinical manifestation) and SSc subtype were recorded. Raynaud’s phenomenon (cold hands with skin colour changes) is often the first symptom of SSc. SSc has two subtypes; limited cutaneous and diffuse cutaneous, dependent upon the extent of skin thickening [18].

Skin score: All participants with SSc underwent assessment of skin thickening at the site to be imaged. Skin is scored 0-3 via clinical palpation (0 [unaffected skin], 1 [thickened; can pinch], 2 [thickened; cannot pinch but can move], 3 [thickened cannot pinch or move] [5-7] (Table 2.1).

PS-OCT image collection: All participants were scanned using PS-OCT (Figure 2.1); a small optical scanning head (approx. 2 x 2 cm^2) was placed on the skin of the volar forearm. This held the imaging optics at the correct distance from the skin for the surface to be in focus. There was no cover glass used, to avoid compression of the tissue within the imaging area. The system was a Thorlabs OCS1310V1/PSOCT-1310V1 (Thorlabs Inc. NJ, US; central wavelength 1310 nm, tuning bandwidth 100 nm, 16 kHz acquisition rate, linearly polarised, pixel dimension of 3.91 µm width by 9.51 µm depth). The PS-OCT captured simultaneous structural and retardance images (512x2048 pixels). The subset of 20 participants (Table 1) undergoing biopsy were invited to return for imaging of the site at one-week (stitch removal, visit 2) and one-month (visit 3).

PS-OCT image analysis:

Images were extracted using ThorImage 4.3 acquisition software (part of the Thorlabs system). Structural (intensity) images were analysed using ImageJ (National Institutes of Health, MA, USA version 1.48). Retardance images were analysed using bespoke software (written by the authors) in MATLAB (version R2020a, Mathworks Inc, Mass, USA). The capture and processing pathway is shown in Figure 2.2.

	Full cohort		Biopsy subset	
	Patients (n=31)	**HC (n=27)**	**Patients (n=10)**	**HC (n=10)**
Age				
Mean (SD) yrs	62 (11)	50 (9)	53 (12)	53(12)
Gender				
Female, n (%)	21 (68)	17 (63)	7 (70)	7 (70)
SSc duration (years)				
Mean (SD)	16 (10)	N/A	11 (9)	N/A
Raynaud's phenomenon duration (years)*				
Mean (SD)	24 (16)	N/A	13 (11)	N/A
Skin score				
0	19	N/A	3	N/A
1	5		3	
2	4		3	
3	3		1	
SSc subtype				
Limited cutaneous SSc, n(%)	8 (26)	N/A	4 (40)	N/A
Diffuse cutaneous SSc, n(%) [Le Roy]	23 (74)		6 (60)	

Table 2.1: Demographic details of participants. *Raynaud's phenomenon, cold hands with colour changes is often the first symptom of SSc.

In ImageJ the structural images underwent post-capture processing, including 'flattening' the images by registering (aligning) the pixels of the surface of the skin horizontally. The greyscale values in the structural images represent the reflected amplitude of light from each boundary within the skin. As shown in Figure 2.2, measurements of epidermal thickness were performed on averaged 'A-scans' (amplitude of a single line of pixels into the skin) taken across the greyscale structural images' mean structural depth scan. Epidermal thickness was defined as the distance between the depth at which the

intensity of the first peak from the A-scan had reached half its maximum value (maximum signal occurs at the skin surface) and the depth at which the intensity of the second peak had reached half its maximum value (dermal-epidermal junction), as per previous studies [19-20]. It should be noted that the exact location of the dermal-epidermal junction in PS-OCT structural images was slightly ambiguous due to the boundary being neither thin, nor flat, but composed of rete ridges which could not be individually resolved by this PS-OCT system [21]. It has been shown previously that in patients with SSc the boundary becomes less identifiable with increasing skin score [22].

Retardance images (each pixel representing phase retardation) were further processed and analysed in MATLAB. Retardance images were registered (using the same process as for structural images, since the PS-OCT and structural images are intrinsically co-registered) to account for surface roughness. Phase retardation measurements above the assigned skin line were disregarded and the remaining data set was unwrapped. This produced an array of cumulative phase change. Images were then averaged across the width of the area of interest. It is commonly accepted that birefringence in the region between the epidermis and dermis layers is weak, not inducing local retardance [17]. Thus retardance was assessed from the epidermal-dermal junction to 100 pixels below (where the signal from the skin is lost). In order to ease comparison between images the minimum rate of change recorded for each image was used as a reference value to zero the minimum rate of cumulative phase change in this region of each image. Images were then averaged together within assigned groupings and plotted. The gradient of these curves was then calculated by least squares fit from the dermal peak to 30 lines below (approximately 285 μm; based upon observation of when the gradient started to become non-linear).

Biopsy collection: A 4 mm punch biopsy was obtained from a subset of the participants; ten patients with SSc (including different grades of skin score) and ten age- and sex-matched healthy controls. The biopsy was taken at the same location as the PS-OCT scan, the skin of the volar forearm. Biopsies were bisected. One half was embedded in optimal

cutting temperature compound (Miles; IN, USA) and flash-frozen in liquid nitrogen; the remaining half was fixed in buffered formalin and processed to wax (formalin-fixed, paraffin-embedded, [FFPE]).

Biopsy histology analysis: FFPE samples were cut to sections 5 µm thick. For standard histology samples were stained with haematoxylin and eosin (H&E) to identify epidermal thickness (under standard light microscopy). Picrosirius red (PSR) staining was performed to identify fibrillar collagen content (brightfield) and organisation (under polarised light). Percentage collagen was calculated in brightfield; the dermal tissue area was measured by image analysis (a free-drawing tool) prior to measuring the area positive for collagen; these data were used to calculate the percentage of dermal matrix occupied by fibrillar collagens.

To assess any potential collagen remodelling in the tissue, frozen sections were interrogated using in situ zymography to assess the activity of MMP-1 (collagenase) and MMPs-2 & -9 (72 kDa and 92 kDa gelatinases), essential enzymes for the remodelling of collagenous extracellular matrices (markers measuring synthesis/deposition and remodelling).

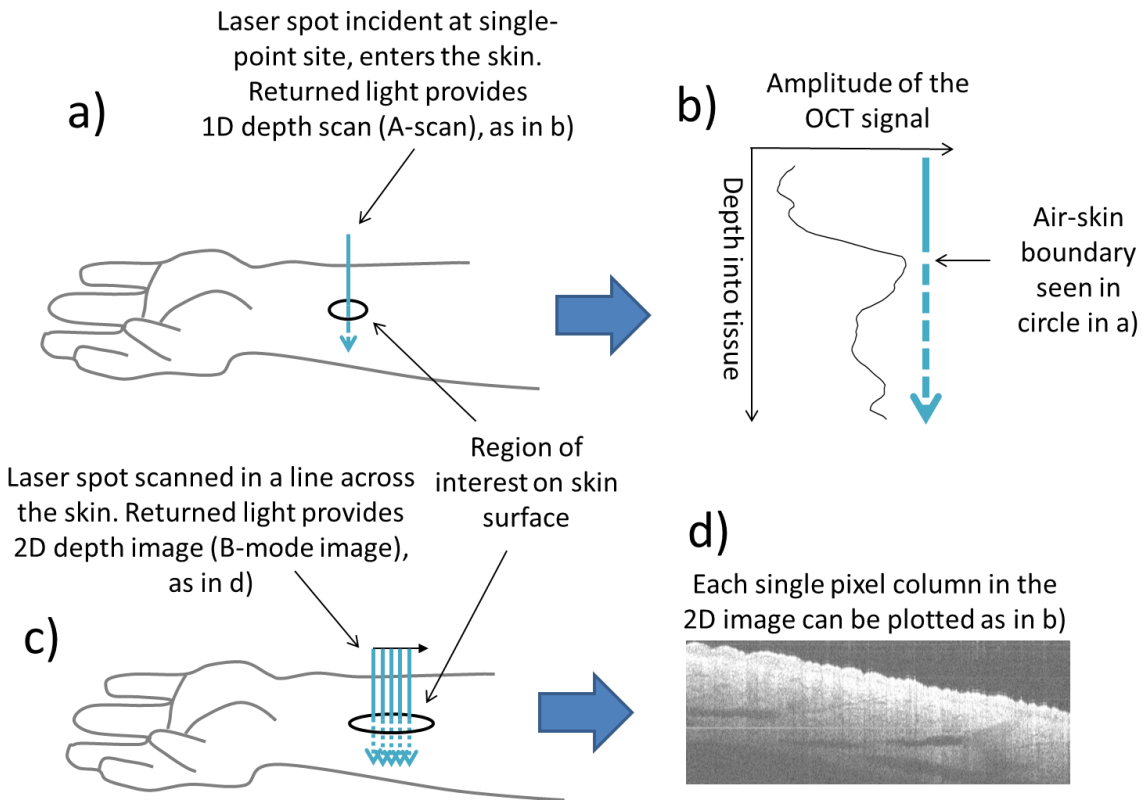

Figure 2.1: a-b) Generation of single depth scans (A-scans). At each point an A-scan (a one-dimensional, single pixel scan into the depth of the tissue) is generated for both images (structural and retardance, here shown as the greyscale structural image). In the structural image this represents the relative amplitude of returned light (analogous to echo location in ultrasound) from each boundary encountered where refractive index changes of the tissues occur (observed as hyper- or hypo-reflective structures, i.e. peaks or troughs in the A-scan). For the retardance image the A-scan shows the relative change in birefringence with depth (birefringence induced phase-retardation [i.e. the way the light is slowed in the tissue due to fibrotic changes which alter its path]) and as the laser line scanned over the surface of the skin multiple A scans (1D images) are obtained producing a B-Mode image (x-z plane [a 2D image along a line of the skin and into the depth into the skin); c-d) 2D depth images (B-mode scans) at the volar forearm. The black oval in a) and c) represent the site of imaging on the surface of the skin. The mean of the A-scans across the B-mode image was then calculated to produce a mean depth scan. The image in d) (8.00 x 4.87 mm) is made up of consecutive A-scans 4.87 mm deep. Image d was generated in ThorImage 4.3.

Relationships between epidermal thickness (from PS-OCT and histology), retardance gradient and percentage collagen and collagenase and gelatinase activity were assessed by Spearman's correlations (Stata v14.0, StataCorp, Tx, US). Despite sample size formal statistics comparing groups were carried out (Kruskal Wallis test); however, it is important to note that given the small sample size (when patients are in subgroups), absence of statistical significance cannot be interpreted to be due to the lack of relationships. Due to the small numbers in the SSc subsets, for plots comparing cumulative retardance with skin depth, patients with SSc were grouped in to skin score 0-1 and skin score 2-3 for comparison to the HC group.

2.4 Results

Comparison of epidermal thickness to the current clinical method of assessment, skin score, shows increased epidermal thickness with increasing skin score (Table 2.2). Phase retardation in patients with SSc is more variable and decreases in skin scores 1 and 2 before increasing in skin score 3. However, when grouped into HC, skin scores 0-1 and 2-3 there is a trend for increased retardance with increasing fibrosis (Figure 2.4a).

Imaging epidermal thickness: Epidermal thickness as measured by both classical histology and by structural PS-OCT and was found to be greater in the SSc cohort with skin scores 1-3 than the control group, regardless of the method of assessment (Table 2.2, examples shown in Figure 2.3a-d). There was a trend for increased epidermal thickness with increasing skin score in the patient group.

Retardance data: The gradient of the phase angle change with skin depth is shown in Table 2.2 and, for grouped data, in Figure 2.4a. Retardance images from one of the 27 controls could not be opened in the bespoke software. Gradient phase change did not differ significantly between healthy controls and patients (Kruskal Wallis; p=0.54), nor between groups of skin scores (Kruskal Wallis; p=0.10); although the small sample size must be taken into account when interpreting these data. When grouped (Fig 4a), the gradient was lower in HCs than those with skin score 0-1 (mild fibrosis) who had in turn a lower gradient than those with skin score 2-3 (moderate/severe fibrosis); i.e. retardance was higher in those with fibrosis.

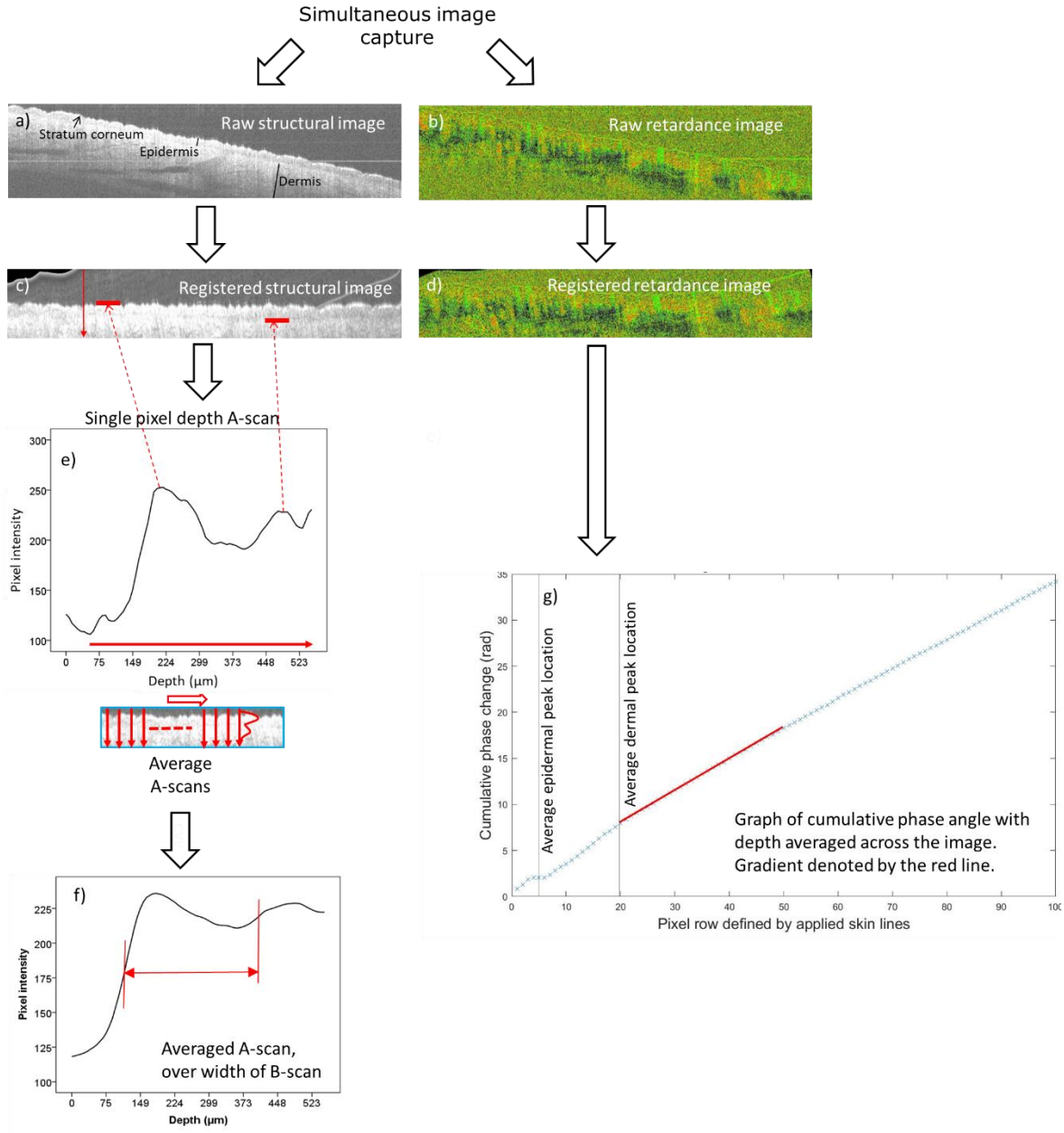

Figure 2.2: Image post-processing pathway. Examples of: raw PS-OCT B-scans for a) structural (showing the layers of the skin beneath the surface) and b) retardance images (birefringence manifests itself as observable skin heterogeneity and tissue organisation, heterogeneity here is due to the presence of structures such as sebaceous glands and hair follicles). Images a) and b) were generated in ThorImage 4.3; c-d) Scans are registered to align slices and provide a horizontal skin surface. Registration is performed by smoothing each A-scan in the structural image and selecting the first peak as the skin-air boundary. The vertical alignment of each A-scan in the structural and birefringence images are then adjusted so the skin-air boundary lies in a horizontal line across the image (using bespoke software (written by the authors) in MATLAB (version R2020a, Mathworks Inc, Mass, USA)). This makes birefringence (retardance) analysis easier as rows of pixels in the registered images correspond to tissue of consistent depth beneath the skin. e) A-scan [single pixel width depth profile] and f) averaged A-scan taken across the B-mode image [i.e. averaging all the A-scans over the width of the image to give an averaged measure of where peaks reflected from layers with in the skin occur]. Epidermal thickness was defined as the distance between the depth at which the intensity of the first peak had reached half its maximum value (skin surface) and the depth at which the intensity of the second peak had reached half its maximum value (dermal-epidermal junction); marked as a red horizontal arrow. g) shows the cumulative retardance (phase change [radians]) plotted for skin depth (pixels) from skin surface to 100 pixels (shown without errors). The epidermal and dermal peak locations are shown as blue vertical lines. The gradient at the first 30 pixels from the dermal line (used to measure the differences between the groups) is indicated by the red line.

Skin score for SSc group for whole cohort PS-OCT imaging [SSc n=31; HC n=27]		HC	SSc			
		NA	Skin score 0 [n=19]	Skin score 1 [n=5]	Skin score 2 [n=4]	Skin score 3 [n=3]
PS-OCT Structural image	Epidermal thickness (μm)	251.02 (25.08)	259.92 (28.31)	271.71 (34.64)	290.39 (60.59)	355.49 (65.98)
PS-OCT Retardance [SSc n=31; HC n=26]	Gradient of phase angle change (radian/pixel)	0.21 (0.21)	0.30 (0.19)	0.11 (0.16)	0.06 (0.12)	0.36 (0.35)
Skin score for SSc group for histology/zymography subset [SSc n=10; HC n=10]		**NA**	**Skin score 0 [n=3]**	**Skin score 1 [n=3]**	**Skin score 2 [n=3]**	**Skin score 3 [n=1]**
Histology	Epidermal thickness (μm)	33.87 (6.18)	30.98 (9.40)	45.29 (17.16)	53.14 (31.96)	67.18 No SD (n=1)
Histology	Percent collagen in dermis (%)	26.46 (6.47)	23.39 (4.82)	16.48 (8.38)	19.42 (9.97)	37.28 No SD (n=1)
Zymography	MMP-1 (collagenase, arb units)	467.25 (66.43)	506.93 (42.76)	424.22 (51.92)	391.25 (80.35)	458.91 No SD (n=1)
Zymography	MMPs-2, -9 (gelatinase, arb units)	799.46 (195.87)	1024.96 (114.71)	877.23 (167.34)	782.10 (393.41)	698.67 No SD (n=1)

Table 2.2: Mean (SD) values of PS-OCT and histology

Comparison, in a matched subset, of the PS-OCT to biopsy tissue identified relationships between epidermal thickness and matrix metalloproteinases (MMPs).

Imaging epidermal thickness: Statistically significant correlation was observed between epidermal thickness as measured by histology and structural PS-OCT ($r=0.79$, $p<0.001$; Figure 2.3e).

Biopsy data: In situ zymography showed a trend for MMP activity to be reduced in SSc biopsy tissue with increasing skin score, suggesting that skin-resident enzymes may have been utilised to facilitate remodelling in line with increasing skin score (Table 2.2). Percentage collagen, identified by PSR staining, decreased with increasing skin score = 0-2 but was increased in skin score = 3 (Table 2.2).

Retardance (phase retardation) data: No relationship was found between optical retardance gradients and percentage collagen identified by PSR (0.23, $p=0.340$), or MMP activity in the participants that underwent biopsy (gelatinase -0.14, $p=0.548$; collagenase -0.27, $p=0.257$). Images from biopsy and retardance PS-OCT are shown in Figure 2.4 b-g.

The impact of the biopsy on scarring is akin to fibrosis and relates to changes in retardance.

The data for longitudinal follow-up visits (biopsy-scar imaging) as compared to baseline data (non-scar tissue imaging) is shown in Figure 2.5 (eight HCs and seven patients attended for the one-week visit; five HCs and four patients attended for the one-month visit). Figure 2.5a shows all data on a single plot and 5b separates the date according to HC or SSc skin score group to allow the trends to be observed more clearly. The baseline data in the biopsy subset graph shows the same trend at baseline as in the wider group; retardance is higher with increasing skin score (comparing HC, 0-1, 2-3). For all groups retardance decreased at the one-week visit and for all but skin score 2-3 then increased at the one-month visit. For HC and groups 0-1 the increase in retardance at the one-

month visit is higher than baseline. For patients with skin score 2-3 the one-month retardance did not return to baseline values. The HC one-month retardance levels were the highest of all the groups.

2.5 Discussion

In this study we have, for the first time in SSc, utilised both structural and retardance images from PS-OCT *in vivo* imaging to assess the skin of patients with SSc. When grouped, the retardance gradient (radian/pixel) was higher for patients with skin score 2-3 than for those with skin score 0-1 and these were higher than in the HC group, indicating that despite our small sample size we are able, by grouping data, to detect a relationship between retardance and fibrosis.

The structural PS-OCT image data correlated with epidermal thickness identified from biopsy tissue, confirming data shown by previous studies [22, 23]. Taken together these studies, including this one, indicate that OCT can be used as a technique for measuring epidermal thickness reflective of histological samples. We did not identify a relationship between retardance and biopsy histology data. The activity of MMPs-1 (collagenase), -2 and -9 (gelatinase) in biopsies, relates to collagen remodelling and/or turnover. Collagenase was highest in HC and lower skin scores. Gelatinase was highest in skin scores 0 and 1. The full relationship between MMPs, fibrosis and retardance are yet to be fully understood.

The longitudinal retardance data decreased in all groups (HC and SSc groups 0-1 skin score and 2-3 skin score) from baseline to one-week. For HC and SSc groups 0-1 skin score retardance then increased between one-week to one-month. For HC and skin score 0-1 the one-month retardance values were higher than baseline; indicative that retardance increases with long term scarring. For 2-3 skin score (who have more severe fibrosis prior to biopsy), follow-up visits were close in value and did not return to baseline values. HC one-month retardance was higher than that of the 0-1 and 2-3 SSc skin score groups;

indicating that scarring in the HC groups is similar to fibrosis observed in patients (the next highest value was the 2-3 skin score baseline value).

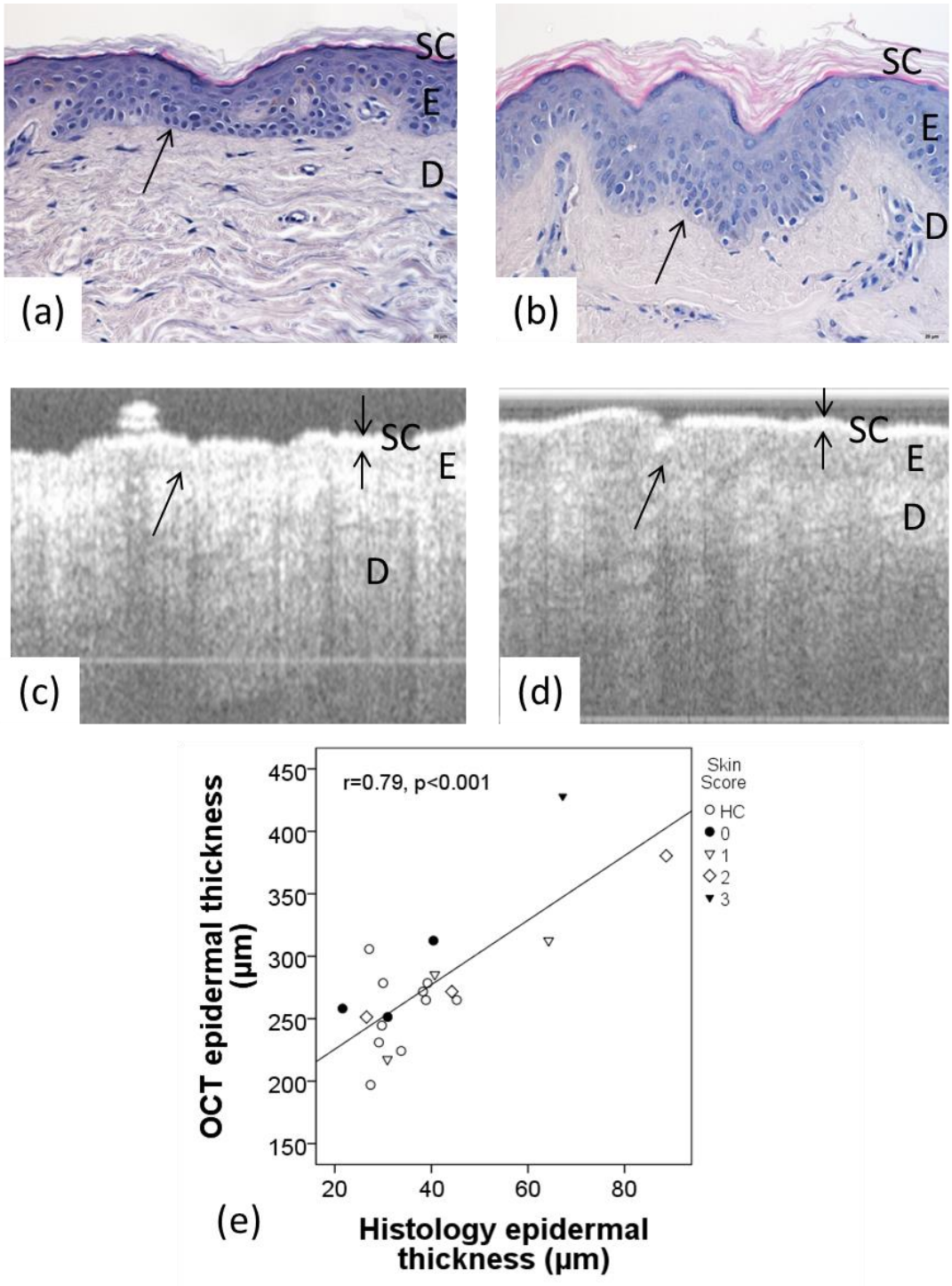

Figure 2.3: H&E stained histology showing skin thickness in: a) a HC and; b) a patient with SSc (skin score = 3). Structural PS-OCT in: c) the same HC and; d) same patient with SSc. Skin structure is labelled as stratum corneum (SC, indicated by double arrow in c and d), epidermis (E), dermis (D) and the single arrow shows the dermal-epidermal junction; scale bar 20 µm. e) displays the positive correlation between histology and PS-OCT (r = 0.79, p <0.001; n=20), for HC and patients, patient skin score shown on the legend as 0-3.

How these differences relate to changes in the skin needs to be further investigated. It is likely that in fibrotic tissue, the usual open basket weave arrangement of collagen fibres has been replaced with a more uniform alignment of the collagen, making the tissue less flexible; our data suggests that these changes can be directly related to the different birefringent properties of aligned bundles of collagen fibrils. Thus PS-OCT potentially provides a new non-invasive method for assessing fibrosis. These data indicate that there is no significant decrease in remodelling with SSc; but rather the balance is shifted towards greater accumulation of collagen that favours/equates to fibrosis.

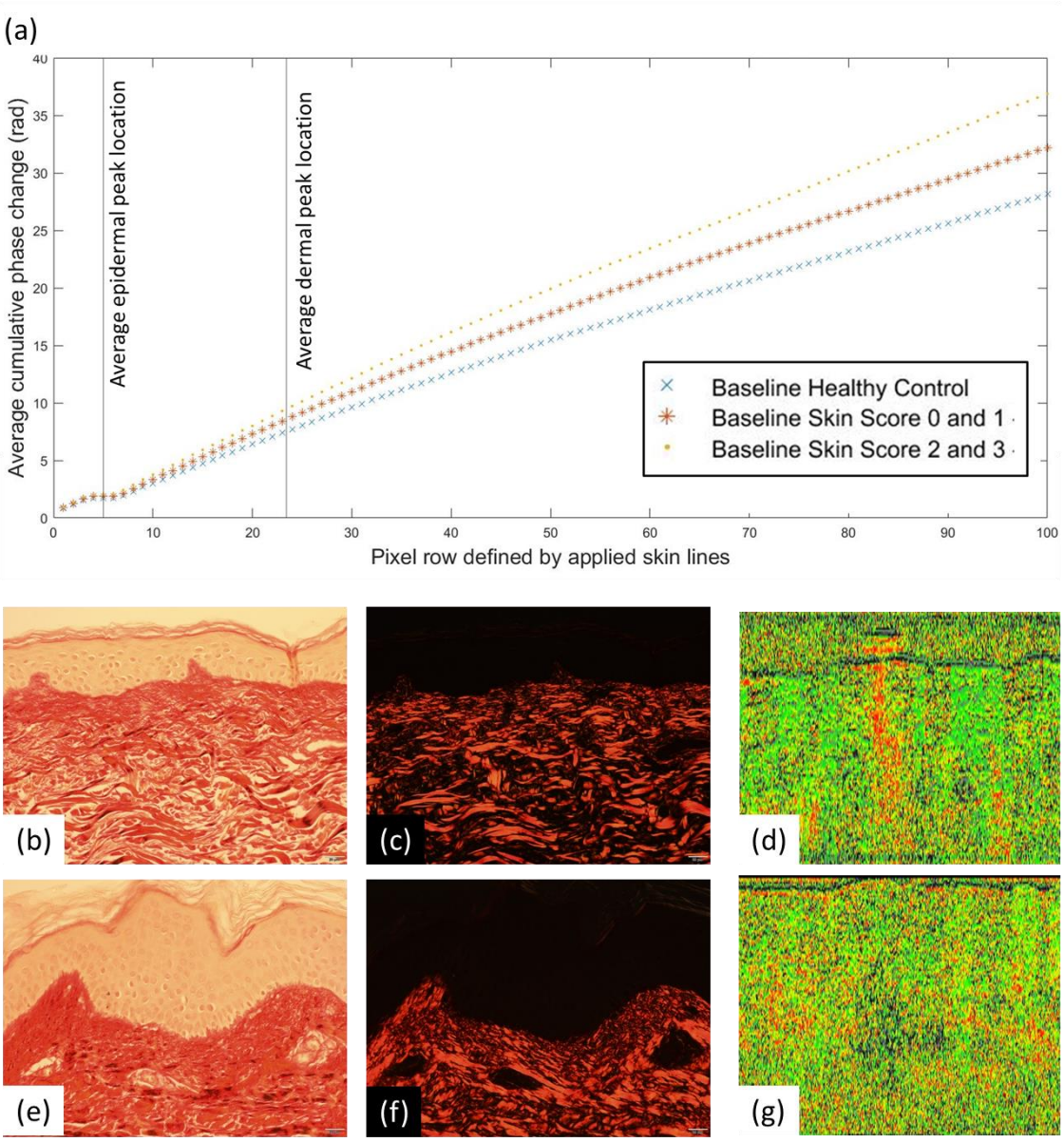

Figure 2.4: a) Plot of baseline cumulative retardance with depth for HCs (N=26) and patients with SSc grouped according to 0-1 (N=24) and 2-3 (N=7) skin score (shown without error bars, graphs with error bars provided in supplemental data). Averaged locations for the epidermal and dermal peaks are denoted by the vertical blue lines. The graph indicates a higher gradient for patients with skin score 2-3 as compared to those with 0-1 and HCs. b) PSR brightfield histology, skin score = 0-1; c) PSR polarised histology, patient skin score = 0-1; d) PS-OCT matching retardance images (arbitrary false colour); e-g) corresponding imaging techniques in a patient with SSc (skin score = 2-3). Images d) and g) were generated in ThorImage 4.3.

The skin changes in patients with SSc are due to a combination of epidermal thickening, fibrosis and oedema, thus making it difficult to assess any one independently; PS-OCT offers the opportunity to assess all three skin properties. Whilst cutaneous fibrosis is well-described, epidermal thickening [24] and oedema [25] have also been described in

systemic sclerosis; hence, the data presented here supports the concept that such imaging measures report these aspects of pathology in the skin of SSc patients. Here we have assessed epidermal thickness (in structural PS-OCT images) and fibrosis (in the retardance images). Oedema causes a reduction in the visibility of the boundaries by altering the refractive index of the tissue, leading to less reflection at boundaries. Previous studies have measured this as a change in optical density [22, 26]). We have not assessed optical density as part of this study as oedema may be transient and not be a maintained feature of the skin of SSc patients; instead, we have focussed on novel retardance measurements to assess fibrosis. The current standard clinical method for assessing changes in skin fibrosis is the mRSS, which is subjective. Gold standard histology is invasive and as such cannot be used longitudinally. Objective, non-invasive measures are therefore highly desirable for early phase clinical studies to assess efficacy of emerging therapies for SSc.

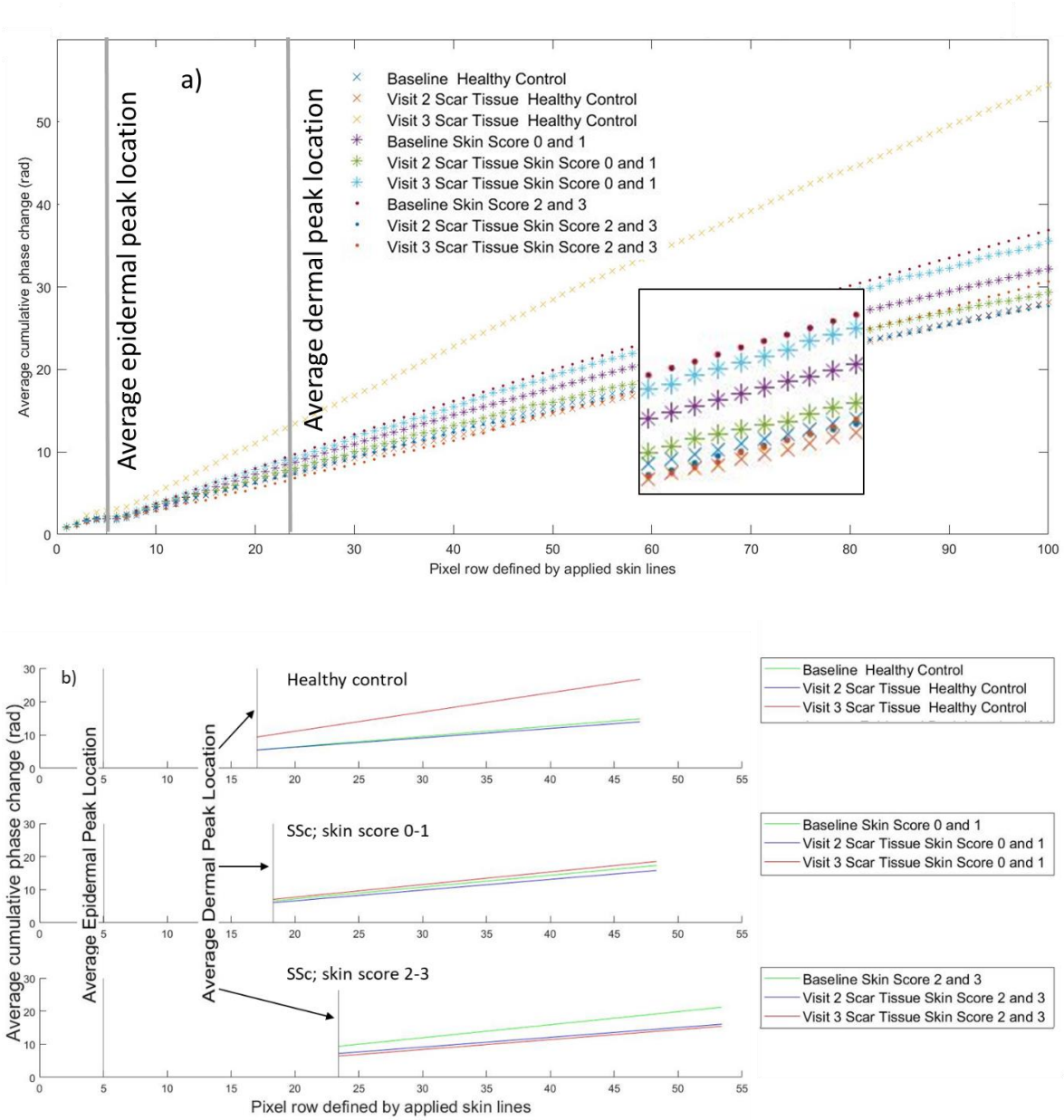

Figure 2.5: a) Cumulative retardance plotted with depth for the three visits grouped for HCs and patients with skin scores 0-1 and 2-3 (without error bars for clarity, a version with error bars is shown in the supplementary data). Averaged locations for the epidermal and dermal peaks over all groups are denoted by the vertical blue lines. Inset box is a higher magnification of the lines to enable clearer view of the trends. Baseline data shows the same trend as for Figure 2.4. The graph indicates that for both HCs and patients with skin scores of 0-1 (mild fibrosis) retardance decreases from baseline to one-week post biopsy visits but then increases by the one-month visit to above the baseline retardance value, with the HC one-month retardance being higher than SSc values. In contrast the patients with skin score 2-3 (moderate to severe) whilst also showing a show a decrease at the one-week visit show an increase at one-month that is still below the baseline retardance value. Baseline N=10 for both HC and SSc, one-week visit, N=8 for HCs and N= 7 patients, one-month N=5 for HCs and N= 4 for SSc; 5b) gradients of the data in 5a displayed grouped across the baseline, one-week and one-month visits for each group separately; average dermal is shown per group . Each gradient beginning at the individual group average for dermal peak location.

High frequency ultrasound has been used to measure skin thickness, including in the hands and the forearm [27, 28]. Forearm skin thickness has been found to be inversely

correlated to disease duration in patients with SSc and increased as compared to controls [29]. Assessments have showed good inter- and intra-observer reliability and correlation to mRSS [28-30]. It has further been used to identify increased skin thickness and oedema in early disease (less than two years) [31], including longitudinally [32].

Other techniques for measurement of skin fibrosis in SSc have included durometry, plicometry and cutometry. Durometry has shown good inter- and intra-observer reproducibility, and is more sensitive than mRSS [33] but, despite the change in durometry scores correlating well with the change in mRSS, there can be a wide range of durometry scores within each skin score [34]. Plicometry and cutometry have also been assessed at different anatomical sites but are not fully validated and the review by Merkel et al. notes that these techniques require further validation [33].

Structural OCT has been used in several studies of skin outside of SSc [12-14, 35-37]. PS-OCT has been used ex vivo and in vivo to compare normal skin with that of damage due to burns, hypertrophic and fibrotic scars [12, 14]. It has been noted that in thermally-damaged skin collagen retardance decreased because of protein denaturation; conversely as scars are formed the re-organized collagen exhibits increased retardance relative to normal skin [37]. There are a small number of structural OCT studies specific to SSc. Abignano et al. [22] found significant differences in the 'optical density' of tissue with depth in structural OCT images of 21 patients with SSc and 22 healthy controls and were able to discriminate between patients with different mRSS scores. However, OCT epidermal thickness was compared against only three biopsy samples (two patients and one healthy control). The dermal-epidermal junction could not easily be observed in the patient OCT images, indicative of optical density changes with increasing fibrosis and likely partly due to the index-matching effect of oedema in the tissue 'washing out' boundaries. Pires et al. [26] have confirmed a similar finding of a relationship between optical density and mRSS as measured by OCT in a cohort of 33 Brazilian patients and 35 controls where images were taken at the finger and forearm.

We acknowledge that this study was relatively small. It was designed to collect, analyse and compare PS-OCT to skin score and histology. Our structural PS-OCT epidermal thickness measurements obtained in the control cohort were larger in magnitude than measurements of epidermis made by other studies using confocal microscopy, histology and OCT [19, 35-36]. This is likely due to, in part, our choice of anatomical location (volar forearm), the choice of peaks in the A-scan used to calculate epidermal thickness and potentially the lack of visualisation of the rete ridges, due to the resolution of the system. Skin biopsies taken for histological analysis are further subject to shrinkage due to tissue contractility, fixation and processing [38].

The PS-OCT system had a single linearly polarised input. Thus image appearance and data extracted are more reliant on sample axis orientation than for circularly polarised light. Since the scanning head allowed perpendicular positioning of the probe on the surface of the skin, the effect should have been minimal. In addition, since skin does not have a well-defined optic axis (as opposed to striated tissue such as muscle), the sensitivity of data to sample alignment should also be minimal.

Epidermal thickness, as measured by structural PS-OCT and histology, showed strong correlation ($r=0.79$, $p<0.001$) as per previous studies in control groups, providing robust evidence that PS-OCT can be used to quantify this anatomical feature [23, 39]. The ungrouped (HC and individual skin scores 0-3) retardance gradient-skin score relationships were not statistically significant (possibly due to small sample size); however, the retardance data, when grouped, is indicative of increasing retardance with increasing skin score (fibrosis). Biopsy longitudinal data suggests that in HCs that as scarring occurs retardance increases to similar levels observed in those with more severe fibrosis.

This study therefore suggests that PS-OCT may be a useful non-invasive technique for simultaneously assessing both epidermal thickness and retardance of collagen in tissue

associated with fibrosis, and so may be a reliable clinical measure in longitudinal studies of patients and as an outcome measure in clinical trials. Larger studies now need to be carried out for robust validation.

2.6 References

[1] Mayes, M.D., et al. Prevalence, incidence, survival, and disease characteristics of systemic sclerosis in a large US population. *Arthritis Rheum.* 48, 2246-2255 (2003).

[2] Merkel P.A., et al. OMERACT 6; Current status of outcome measure development for clinical trials in systemic sclerosis. Report from OMERACT 6J. *Rheumatology.* 30, 1630-1647 (2003).

[3] Furst, D., et al. Systemic sclerosis - continuing progress in developing clinical measures of response. *Rheumatology.* 34, 1194-1200 (2007).

[4] Clements, P.J., et al. Skin thickness score as a predictor and correlate of outcome in systemic sclerosis: high dose versus low-dose penicillamine trial. *Arthritis Rheum.* 43, 2445- 2454 (2000).

[5] Clements, P.J., Lachenbruch, P.A., Ng, S.C., Simmons, M., Sterz, M., Furst, D.E. Skin score. A semiquantitative measure of cutaneous involvement that improves prediction of prognosis in systemic sclerosis. *Arthritis Rheum.* 33, 1256-1263 (1990).

[6] Clements, P., et al. Inter- and intraobserver variability of total skin thickness score (modified Rodnan TSS) in systemic sclerosis. *J Rheumatol.* 22, 1281-1285 (1995).

[7] Khanna, D., et al. Standardization of the modified Rodnan skin score for use in clinical trials of systemic sclerosis. *J Scleroderma Relat Disord.* 2, 11–18 (2017).

[8] Kumánovics, G. Assessment of skin involvement in systemic sclerosis. *Rheumatology.* 56(suppl_5), v53-v66 (2017). 19

[9] Fercher, A.F., Drexler, W., Hitzenberger, C., Lasser, L. Optical coherence tomography—principles and applications. *Rep Prog Phys.* 66, 239-303 (2003).

[10] Pierce, M.C., Sheridan, R.L., Hyle Park, B., Cense, B., de Boer, J.F. Collagen denaturation can be quantified in burned human skin using polarization-sensitive optical coherence tomography. *Burns.* 30, 511-517 (2004).

[11] Pierce, M.C., Strasswimmer, J., Hyle Park, B., Cense, B., De Boer, J.F. Birefringence measurements in human skin using polarization-sensitive optical coherence tomography. *Biomed Opt.* 9, 287-291 (2004).

[12] LeRoy, E.C., et al. Scleroderma (systemic sclerosis): classification, subsets and pathogenesis. *J Rheumatol.* 15, 202-205 (1988).

[13] Neerken, S., Lucassen, G.W., Bisschop, M.A., Lenderink, E., Nuijs, T. Characterization of age-related effects in human skin: A comparative study that applies confocal laser scanning microscopy and optical coherence tomography. *J Biomed Opt.* 9, 274-281 (2004).

[14] Welzel, J., Lankenau, E., Birngruber, R., Engelhardt, R. Optical coherence tomography of the human skin. *J Am Acad Dermatol.* 37, 958–963 (1997).

[15] Newton, V.L., Mcconnell, J.C., Hibbert, S.A., Graham, H.K., Watson, R.E. Skin aging: molecular pathology, dermal remodelling and the imaging revolution. *G Ital Dermatol Venereol.* 150, 665-674 (2015).

[16] Newton, V.L., et al. Novel approaches to characterize age-related remodelling of the dermal-epidermal junction in 2D, 3D and in vivo. *Skin Res Technol.* 23, 131–148 (2017). 20

[17] Abignano, G., et al. Virtual skin biopsy by optical coherence tomography: the first quantitative imaging biomarker for scleroderma. *Ann Rheum Dis.* 72, 1845–1851 (2013).

[18] Pires, N.S.M., et al. Optical coherence tomography as a method for quantitative skin evaluation in systemic sclerosis. *Ann Rheum Dis.* 77, 465-466 (2018).

[19] Santiago, T., et al. Utrasonography for the assessment of skin in systemic sclerosis: a systematic review. *Arthritis Care Res.* 71, 563–574 (2019).

[20] Moore, T.L., Lunt, M., McManus, B., Anderson, M.E., Herrick, A.L. Seventeen-point dermal ultrasound scoring system--a reliable measure of skin thickness in patients with systemic sclerosis. *Rheumatology.* 42, 1559–1563 (2003).

[21] Scheja, A., Akesson, A. Comparison of high frequency (20 MHz) ultrasound and palpation for the assessment of skin involvement in systemic sclerosis (scleroderma). *Clin Exp Rheumatol.* 15, 283-288 (1997).

[22] Kaloudi, O., et al. High frequency ultrasound measurement of digital dermal thickness in systemic sclerosis. *Ann Rheum Dis.* 69, 1140-1143 (2010).

[23] Hesselstrand, R., Scheja, A., Wildt, M., Akesson, A. High-frequency ultrasound of skin involvement in systemic sclerosis reflects oedema, extension and severity in early disease. *Rheumatology.* 47, 84-87 (2008).

[24] Akesson, A., Hesselstrand, R., Scheja, A., Wildt, M. Longitudinal development of skin involvement and reliability of high frequency ultrasound in systemic sclerosis. *Ann Rheum Dis.* 63, 791-796 (2004). 21

[25] Merkel, P.A., et al. Validity, reliability, and feasibility of durometer measurements of scleroderma skin disease in a multicenter treatment trial. *Arthritis Rheum.* 59, 699–705 (2008).

[26] Kissin, E.Y., et al. Durometry for the assessment of skin disease in systemic sclerosis. *Arthritis Rheum.* 55, 603-609 (2006).

[27] Mogensen, M., Morsy, H.A., Thrane, L., Jemec, G.B.E., Morphology and epidermal thickness of normal skin imaged by optical coherence tomography. *Dermatology.* 217, 14-20 (2008).

[28] Trojahn, C., Dobos, G., Richter, C., Blume-Peytavi, U., Kottner, J. Measuring skin aging using optical coherence tomography in vivo: a validation study. *J Biomed Opt.* 20, 045003 (2015).

[29] Pierce, M.C., Strasswimmer, J., Park, B.H., Cense, B., de Boer, J.F. Advances in optical coherence tomography imaging for dermatology. *J Invest Dermatol.* 123, 458-463 (2004).

[30] Kerns, M.J., et al. Shrinkage of cutaneous specimens: formalin or other factors involved*? J Cutan Pathol.* 35, 1093-1096 (2008).

[31] Gambichler, T., et al. Epidermal thickness assessed by optical coherence tomography and routine histology: preliminary results of method comparison*. J Eur Acad Dermatol Venereol.* 20, 791–795 (2006)

3. A comparative study of epidermal thickness measurements taken with polarisation-sensitive optical coherence tomography and high frequency ultrasound, for skin thickness assessment in systemic sclerosis

Context of contribution:

This chapter is a draft publication for Annals of the Rheumatic Diseases (British Medical Journal) for which I am lead author. At the time of joining the project the grant had been approved and an idea of the methodology had been conceived. I advised and oversaw the writing of the procedure, did initial testing and alignment of the equipment, was the lead observer meeting and imaging the participants with both PS-OCT and HFUS, converted and processed the data, performed all the statistical tests, and wrote the entirety of the paper.

The data processing broadly followed the same process as in the previous study (Chapter 2): conversion, flattening, filtering, registering, and averaging. However, the form of the data were different enough to require entirely new code to be written in MATLAB for every stage. The techniques used learnt from the limitations and achievements of the previous work. Additional filtering and processing steps where included to improve the quality of the resultant data set. In addition to this, the statistical tests undertaken were all manually coded as to ensure a clear understanding of the parameters being investigated.

The writing of the following chapter is entirely my own work with only minor modifications based on the oversight of the principle investigator and my supervisor. This body of work would not have been possible without the NHS staff who worked as my second observer during data collection and in the recruitment of participants.

3.1 Abstract

Objective: Polarisation-sensitive optical coherence tomography (PS-OCT) has demonstrated a relationship between tissue birefringence and modified Rodnan skin score (mRSS), in systemic sclerosis (SSc) patients. The primary objective of this study was to investigate PS-OCT's reliability at assessing epidermal thickness when compared to high frequency ultrasound (HFUS), to determine its validity. Additionally, inter- and intra-observer reliability was assessed for both systems on same and consecutive days. Correlation between tissue birefringence and epidermal thickness was also assessed.

Method: Healthy control (HC) and patients with SSc were recruited, with forearm mRSS assessed in patients by clinical palpation. Participants were imaged with PS-OCT and HFUS at forearm volar and dorsal. A subset of which were imaged on two consecutive days. The majority of participants were imaged by the same two observers, one of which imaged the remainder.

Results: 86 participants were recruited, of which 45 were HC and 41 were SSc patients. Of the patients, 22 were mRSS 0, 16 were mRSS 1, and three were mRSS 2. Comparison between PS-OCT and HFUS epidermal thickness using Spearman's correlation coefficient was statistically significant for volar sites (ρ=0.3211, p-value=0.003), but not for dorsal (p-value=0.872). HFUS had poor reliability for all comparisons, except dorsal intra-observer consecutive days (0.6213). Intra-class correlation coefficients found PS-OCT epidermal thickness to be moderately reliable (0.5-0.75) for same and consecutive days' site specific comparison of intra- and inter-observer variability. Retardation was found to have good reliability for same day observer variability comparisons. Correlation of PS-OCT epidermal thickness and retardation was highly significant (p-value$\ll$0.001).

Conclusions: HFUS and PS-OCT measurements of epidermal thickness have been demonstrated to correlate in volar tissue. However, poor reliability of HFUS

measurements has resulted in validation not being possible, and is likely the cause of no significant correlation found for dorsal sites. PS-OCT has been shown as a reliable high resolution assessment method for epidermal thickness and tissue birefringence. The statistically significant correlation found between epidermal thickness and birefringence shows potential for PS-OCT application in skin assessment.

3.2 Introduction

Systemic sclerosis (SSc) is a debilitating rheumatic autoimmune condition [1] with patients often suffering from chronic morbidity [2] and high mortality rates [3]. Genetic vulnerabilities are believed to be one potential explanation to pathogenesis by means of susceptibility to environmental triggering [4]. The first symptom is often secondary Raynaud's phenomenon [1, 4, 5], resulting from early microvascular damage [6], and is typically followed by fibrosis of skin (scleroderma) and internal organs [5]. Skin thickness is routinely used as a basis for clinical assessment of skin fibrosis [1]. *'Skin thickening in the fingers of both hands extending proximal to the metacarpophalangeal joints'*, as defined by the American College of Rheumatology and the European League against Rheumatism, is a significant indicator of the disease. It is the highest weighted criteria in their disease classification process, with more than double the score of any of the other indicators [7].

The importance of assessing and monitoring skin involvement is twofold. The extent and location of fibrotic skin defines the two subgroups of the disease. Limited cutaneous (lcSSc) only affects the fingers and face, whereas diffuse cutaneous (dcSSc) additionally affects the trunk and proximal extremities. The distinction between these groups is significant with dcSSc associated with rapid disease progression [1]. Additionally, the extent of skin involvement is also strongly correlated with the main cause of death in SSc, interstitial lung disease (ILD) [8]. As a result, the monitoring of the condition is of significant importance and hence clinicians perform a rudimentary assessment, the modified Rodnan skin score (mRSS), through skin palpation. This technique is the

standard clinical procedure, and gold standard, for skin involvement monitoring in SSc and produces a score between 0 and 3 depending on the compliance. The system defines a score of 0 as, '*normal skin where the examiner appreciates fine wrinkles but no skin thickness is present*' and a score of 3 as, '*Severe skin thickness with inability to make skin folds between 2 examining fingers'* [9]. The assessment requires specialist training and has a large inter-user variability [10].

Polarisation-sensitive optical coherence tomography (PS-OCT) is a development of OCT, which itself is an imaging modality that has only entered clinical use in the last two decades [11]. The system is an optical arrangement, based on the Michelson interferometer, which outputs two-dimensional depth scans through the creation of a low coherence interferogram [12]. PS-OCT additionally circularly polarises the light in order to measure polarising characteristics of the sample, including birefringence [11]. Previous work has shown correlation between measured polarisation phase retardation, which can be directly related to tissue birefringence, and grouped mRSS, showing PS-OCT's potential as a quantitative alternative to mRSS [13]. Hence, there is a need to validate this measurement technique's ability to accurately record relative depth measurements through the performance of a convergent validity assessment.

High-frequency ultrasound (HFUS) is an enhanced modality of medical ultrasound with output pressure-wave frequencies greater than 9 MHz. This enables increased resolution for tissue structure imaging, however with reduced depth penetration [14]. A transducer transmits the pulsed pressure-wave and the system uses time-of-flight to map reflected pulses relative to depth of acoustic boundaries. The transducer must be physically scanned across the lateral imaging range in order to create the 2D B-scan, formed of stacked amplitude, A, scans [15]. HFUS has been established as a means of measuring skin thickness *in vivo* with non-significant inter- [16] and intra-observer variabilities [17] in recent studies. As a result, it was proposed that measurements acquired using HFUS can be reliably used as reference for validation, of PS-OCT, when both systems image the same specified *in vivo* location.

This study aimed to validate depth measurements acquired using PS-OCT with reference to HFUS, through direct comparison of specified sites, in a cohort of patients with SSc and healthy controls. Additionally, the study investigated inter- and intra-observer variability and repeatability over two consecutive days for a subset of participants. Thickness of the epidermis layer as well as skin birefringence were also compared between healthy controls (HC) and patient skin score groups. In addition, comparison of both metrics were also conducted for younger, 18 – 30 years, (HC ≤30) and older, ≥70 years, (HC ≥70) in groups of participants to determine the influence of aging on these results.

3.3 Methods

Participants attended a single day, with a subset attending on two consecutive days. All potential healthy control participants were asked to report any historical skin problems, and participants with skin problems were excluded from the study. All participants were asked to be alcohol and caffeine free for at least 4 hours before their visits. This study was approved by West Midlands - Edgbaston Research Ethics Committee (21/WM/0212). All research was performed in accordance with relevant guidelines and regulations. All participants gave informed, written consent for the study.

86 total participants were recruited to the results, consisting of 41 SSc patients and 45 HC. Of which, 24 SSc patients and 26 HC returned for the second visit. 33 HC between 18 – 30 years and 22 ≥70 years were recruited. Demographics of recruitment are presented in Table 3.1. 44 total participants returned for a second day consecutively.

Patients provided their diagnosed sub-condition (lcSSc or dcSSc) and were asked several questions regarding their condition. They were asked: when they first experienced Raynaud's phenomenon, when they had their first non-Raynaud's symptom, how many attacks they experienced in the past seven days, what current medication they were

taking, and if they had any other medical history. Additionally they were also asked if they had been an inpatient for: IV Vasodilators, digital debridement, or digital amputation, and when that had taken place. Antibody status was also recorded from medical records. All patients had their forearm mRSS assessed by the same trained observer at the dorsal site of the arm being imaged.

All participants went through the same imaging procedure. The participant's non-dominant arm was imaged, where possible. Dominant arms were only imaged in a small subset of participants, seven healthy controls, who had unrelated biopsies taken on their non-dominant arm immediately prior to attending the scan. Each observer measured the distance between the wrist and elbow and marked the centre of the volar and dorsal with two adhesive markers either side of the measuring tape. This was conducted independently by each observer for each visit. Each imaging system was removed and relocated between repeats. One day they were seen by observers one and two, a joint visit, and the other day they were only seen by observer two, a solo visit. Both observers took all measurements independently of each other, without observation or discussion, in order to remove any potential influence on inter-observer variability.

		Patients with SSc (n=41)	**HC (n=45)**	
			≤30 (n=23)	**≥70 (n=22)**
Mean Age (SD) yrs		60 (11)	25 (3)	75 (5)
Female Gender, n (%)		34 (82.93)	20 (86.96)	11 (50)
mRSS	**0**	22		
	1	16		
	2	3		
Limited cutaneous SSc, n(%)		30 (73%)		
Diffuse cutaneous SSc, n(%)		11 (27%)		

Table 3.1: Demographic distribution for all participants, split into groupings, Patients with SSc, HC ≤30, and HC ≥70

PS-OCT imaging was conducted using a ThorLabs Polarization-Sensitive Spectral Domain OCT Telesto Series Imaging System (TEL220PSC2) with ThorLabs OCT-LK4 scan lens kit and Thorlabs ThorImage OCT 5.5.5 proprietary software. This system used a super luminescent diode with a 1300 nm central wavelength and a bandwidth of more than 170 nm. The axial resolution in skin can be approximated to be 3.9 µm based on the stated resolution in air and the refractive index in the medium. The scan lens kit provided a focal length of 54 mm and a lateral resolution of 20 µm. Light from the scan lens is left hand circularly polarised. The system was manually focused, by the observer, in reference to the software, onto the skin surface in the marked region of interest. Approximately twenty frames were recorded across a 2.00 x 2.61 mm² field of view. An example intensity scan is shown in Figure 3.1. This process was repeated twice by observer one for each imaging location, and once by observer two. Preliminary testing showed the system could achieve an imaging depth in region of 1 mm, although many factors such as skin surface condition can affect this.

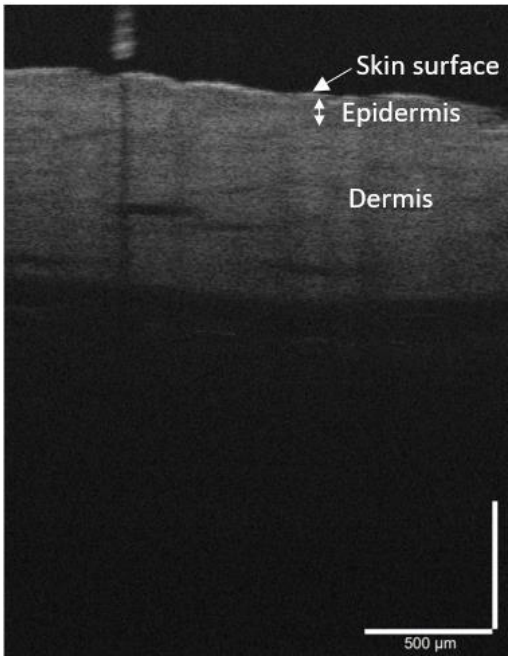

Figure 3.1: 2D total intensity PS-OCT image of volar forearm of patient with mRSS 0

HFUS imaging was performed with a Longport Episcan I-200 system. The system used a scanning transducer handheld probe of centre frequency of 34 ± 3 MHz, with a

– 3dB bandwidth of 37.0 ± 5.3 MHz and focal length of 10 mm. The system has a maximum theoretical axial resolution of 15 µm. Each scan created eight 2D image frames of 14.9 × 8.09 mm². Ultrasound gel was applied to the marked region of interest and the probe was manually positioned such that the observer could see a clear image of the dermis with the associated software. The system was able to achieve a penetration depth up to 2 mm, although as with PS-OCT this varied between scans. As with the PS-OCT imaging, this was repeated twice for each marked region of interest by observer one and once by observer two. Additionally, once the eight frames had been collected, the frame with the clearest dermal boundary was selected based on operator observation. The software was used to take three measurements across the image of the distance between the skin surface and the lower dermal boundary and the epidermal-dermal boundary, as shown in Figure 3.2.

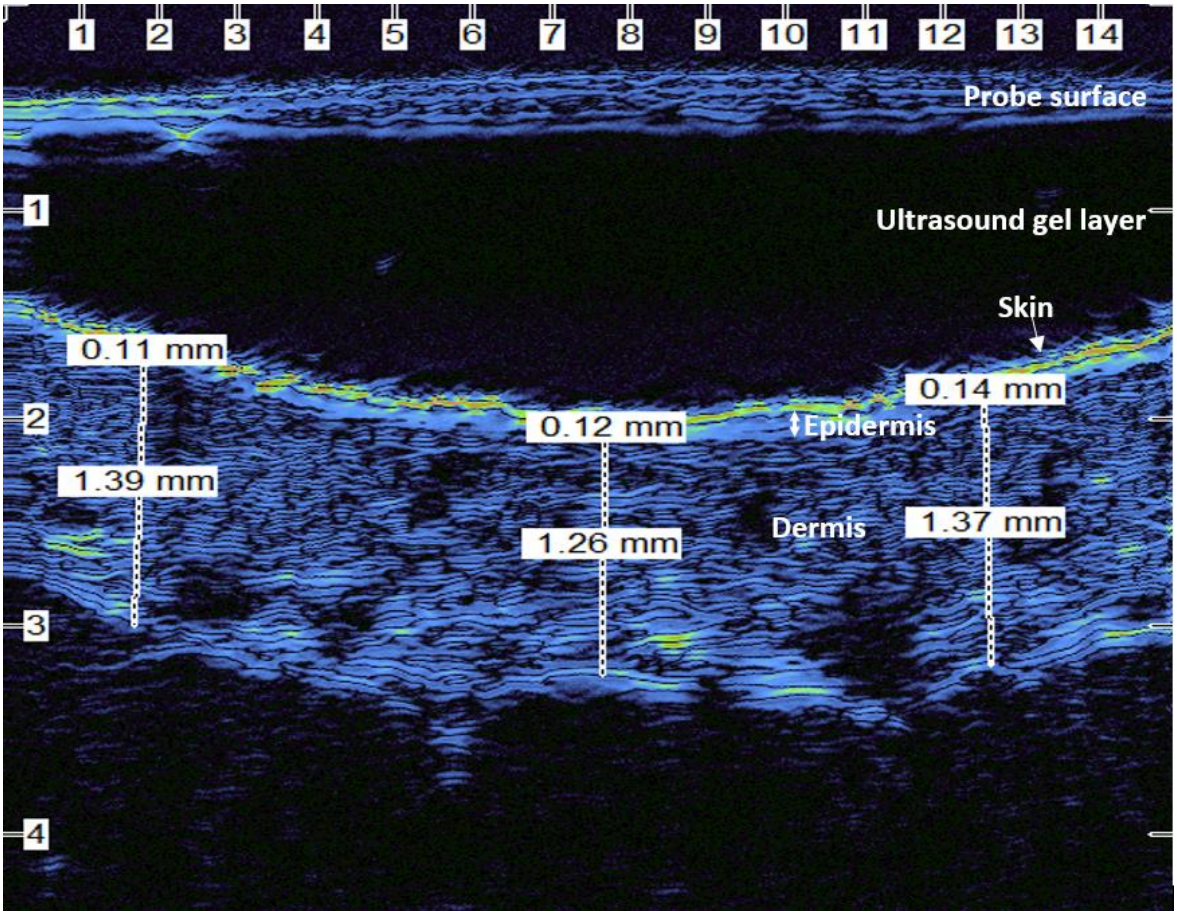

Figure 3.2: Annotated HFUS image. Axes in mm. The colour scale is black for low intensity reflections and orange for high intensity. Annotated measurements mark epidermal and dermal thicknesses at left, centre, and right side of the image.

For both modality's data sets, all processing and statistical analysis was conducted in bespoke software (written by the author) in MATLAB (version R2023a, Mathworks Inc, Mass, USA). For the OCT data, images were thresholded at 90 dB for noise reduction. They were then flattened along the skin line and width averaged to produce an intensity A-Scan. Peak finding was then used to identify the optical epidermal boundaries and hence determine the epidermal thickness. Polarisation images were thresholded and flattened using the same process. Width averaging was also implemented and the epidermal-dermal optical boundary, as found from the intensity images, was used to determine the start of the birefringent region. After this point, in the majority of cases, polarisation phase was observed to linearly change for approximately 200 µm. The rate of change in this region was chosen to be the characteristic of interest, as it is the most significant section of data. The values were calculated using a weighted linear least-squares fit. The form of this data is shown in Figure 3.3.

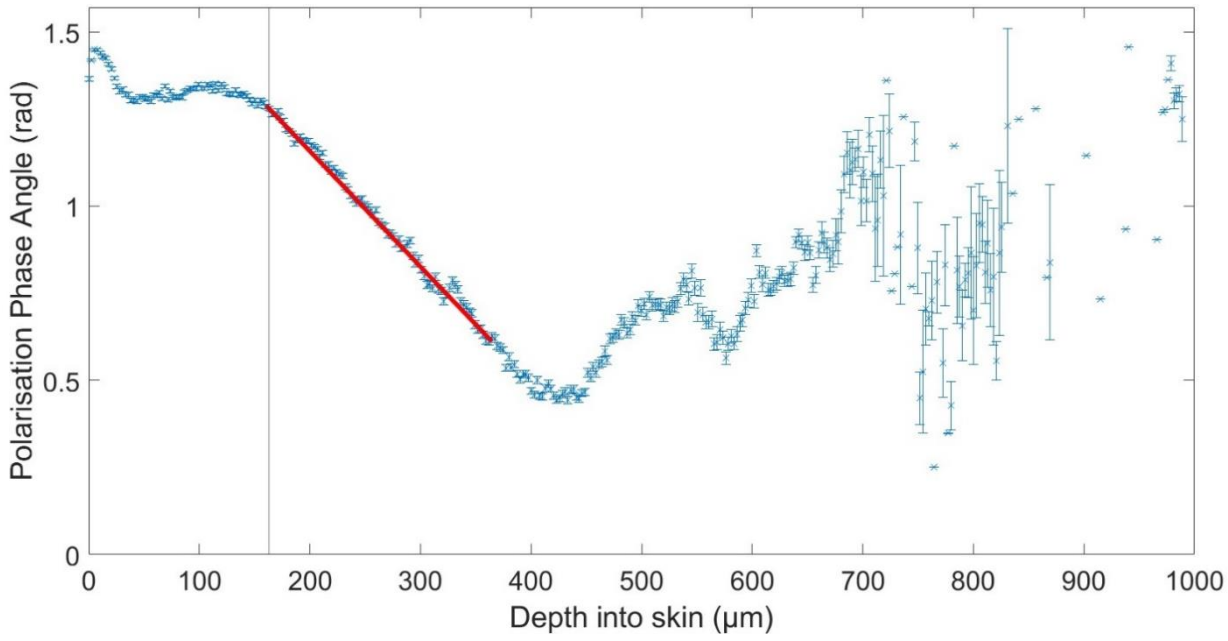

Figure 3.3: Example polarisation phase angle plot with linear least-squares fit marked in red. Black line marks epidermal-dermal boundary.

Ultrasound annotations were averaged across the width of each image. This allowed for a dermal and epidermal thickness value to be calculated for each image. For both the ultrasound and PS-OCT, data were grouped by site location, observer, and participant characteristic in order to produce comparative boxplots and calculate statistical significance of differential group averages.

Four different statistical tests were used for the analysis. Comparison between different data types, OCT and HFUS, and epidermal thickness and retardation, were made using Spearman's correlation. This identifies monotonic correlation between data sets enabling unknown relations to be found, such as measures of different data types. Assessments of reliability were conducted using intra-class correlation, ICC. This compares both correlation and agreement between data sets. There are multiple models for this assessment and the appropriate one in each case was selected based on the comprehensive review by Koo et al. [18]. Comparisons between volar and dorsal sites were conducted using paired T-tests. This assesses whether the data sets are statistically different. Two-way analysis of variance, ANOVA, was used to determine the existence and source of statistical deviation between multiple groups and sites.

3.4 Results

OCT - HFUS Correlation Coefficient

Epidermal thickness data from OCT and HFUS were averaged across repeats and observers. Spearman's correlation coefficient, ρ, and the associated p-value was calculated for data grouped by site. The results show a significant confidence in a correlation for volar measurements, but a high probability of no observable correlation for dorsal measurements. These results can be seen in Table 3.2.

	Volar	Dorsal
ρ	0.3211	0.0176
p-value	0.003	0.872

Table 3.2: Correlation coefficients between OCT and HFUS for epidermal thickness measurements

Inter- and Intra-Observer Correlation Coefficient

Intra- and inter-observer variability was assessed for all data types using ICC calculations. Both tests were done using site specific data sets, as shown in Table 3.3. PS-OCT epidermal thickness measurements were found to show moderate reliability (0.5-0.75) for all comparisons. PS-OCT retardation showed good reliability (0.75-0.9) for intra-CC of observer one (same day) at both sites and inter-CC for both sites, however observer two (consecutive days) was found to have poor (<0.5) intra-CC. HFUS epidermal thickness was found to have poor (<0.5) inter- and intra-CC for all comparisons, with the exception of dorsal observer two (consecutive days) intra-CC which had moderate reliability (0.6213).

Comparison	ICC by Modality		
	PS-OCT Thickness	PS-OCT Retardation	HFUS Thickness
Intra- Same day Volar	0.7311	0.8100	0.2459
Intra- Same day Dorsal	0.5722	0.8745	0.2594
Intra- Consecutive days Volar	0.6739	0.3918	0.3805
Intra- Consecutive days Dorsal	0.6454	0.3020	0.6213
Inter- Volar	0.6268	0.7865	0.4832
Inter- Dorsal	0.7133	0.8162	0.1019

Table 3.3: Inter- and Intra-Observer Variability Correlation Coefficients for OCT thickness and retardation, and HFUS thickness

Site Comparison T-test

For all data sets, data were averaged across repeats and observers, and compared between sites using a paired T-test. Comparisons were done for healthy control groupings, HC ≤30 years and HC ≥70 years, and patients, as seen in Table 3.4. Significant differences were seen between sub-grouped retardation data, as well as HC ≤30 years, and patient HFUS thickness measurements.

		Modality		
Comparison		**OCT Thickness**	**OCT Retardation**	**HFUS Thickness**
HC ≤30		0.747	0.003	0.022
HC ≥70		0.645	0.001	0.826
Patients		0.6450	0.006	0.082
Grouping	**Site**	**Median [IQR] (µm)**	**Median [IQR] (radmm^{-1})**	**Median [IQR] (µm)**
HC ≤30	Volar	149.7437 [27.5061]	-1.3000 [0.57169]	157.0833 [22.3333]
	Dorsal	158.8770 [24.3201]	-1.9000 [0.69187]	141.9167 [24.0417]
HC ≥70	Volar	108.3252 [18.0542]	-0.41517 [0.35204]	137.0833 [22.8333]
	Dorsal	107.3694 [16.5674]	-0.27056 [0.24369]	135.3333 [23.7500]
Patients	Volar	129.3530 [23.6829]	-1.00000 [0.62419]	137.5556 [20.8958]
	Dorsal	118.9453 [32.2321]	-0.66177 [0.92274]	130.8333 [22.3333]

Table 3.4: Site comparison by Paired T-test.

Site and Grouping Analysis of Variance (ANOVA)

For all data sets, data were averaged across repeats and observers in order to perform a two-way ANOVA for sites and groupings. Groupings used were both healthy control

groups, HC ≤30 years and HC ≥70 years, as well as patients. All ANOVA showed a very significant difference between groupings and a marginally non-significant difference between sites. The p-values for these tests can be seen in Table 3.5.

	Modality		
Comparison	**OCT Thickness**	**OCT Retardation**	**HFUS Thickness**
Groups	$\ll 0.001$	$\ll 0.001$	<0.001
Sites	0.525	0.420	0.031

Table 3.5: P-values for two ANOVA comparison for groups and sites

It was confirmed that significance of the grouping data is mostly due to the very significant difference seen between the HC ≤30 years and HC ≥70 years groups. This can be seen in box plots, as shown in Figures 3.4 and 3.5.

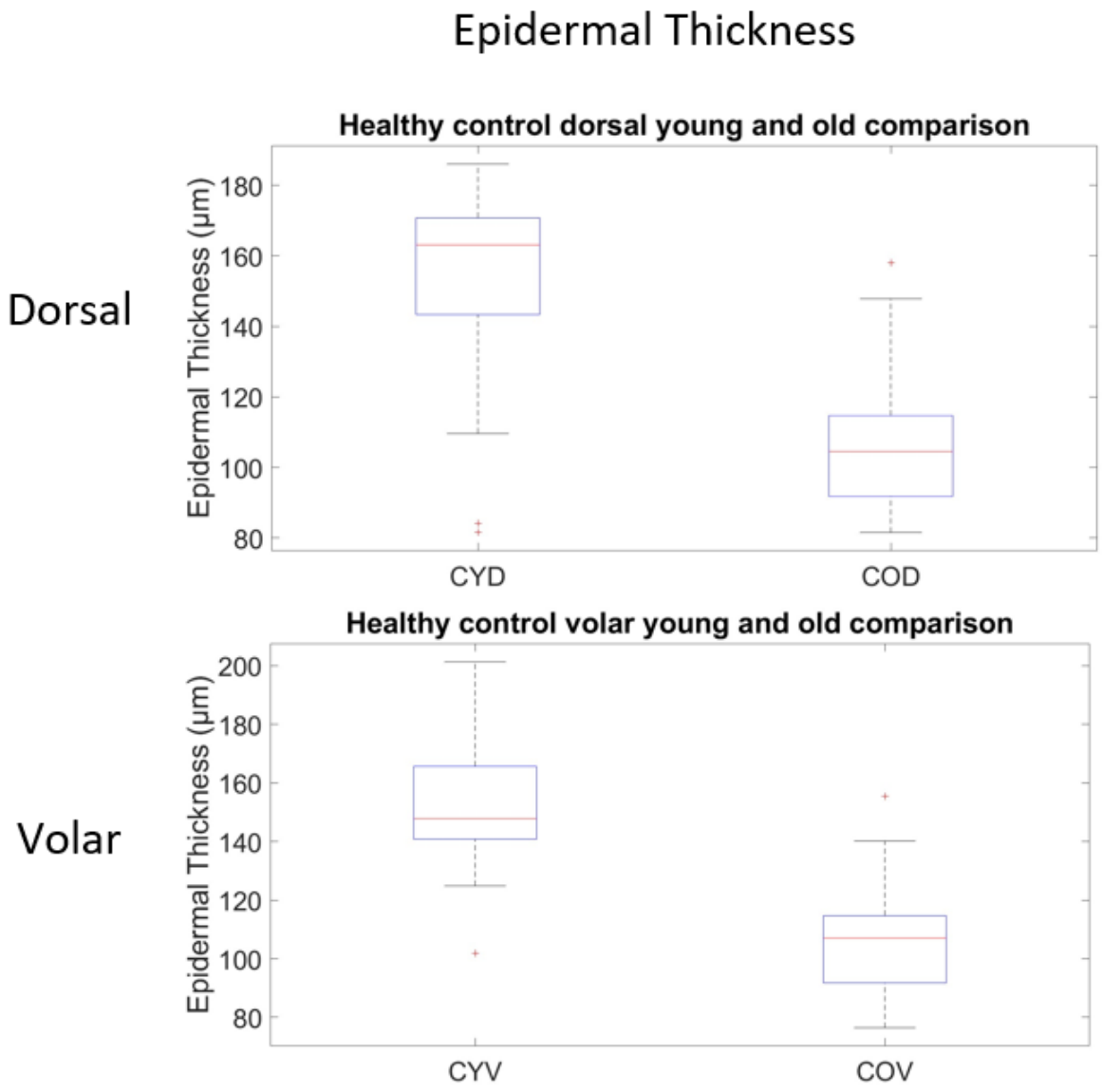

Figure 3.4: Boxplots of PS-OCT epidermal thickness data for comparisons between HC ≤30 years (Control Young: CY) and HC ≥70 years (Control Old: CO) groups for both sites, volar (V) and dorsal (D)

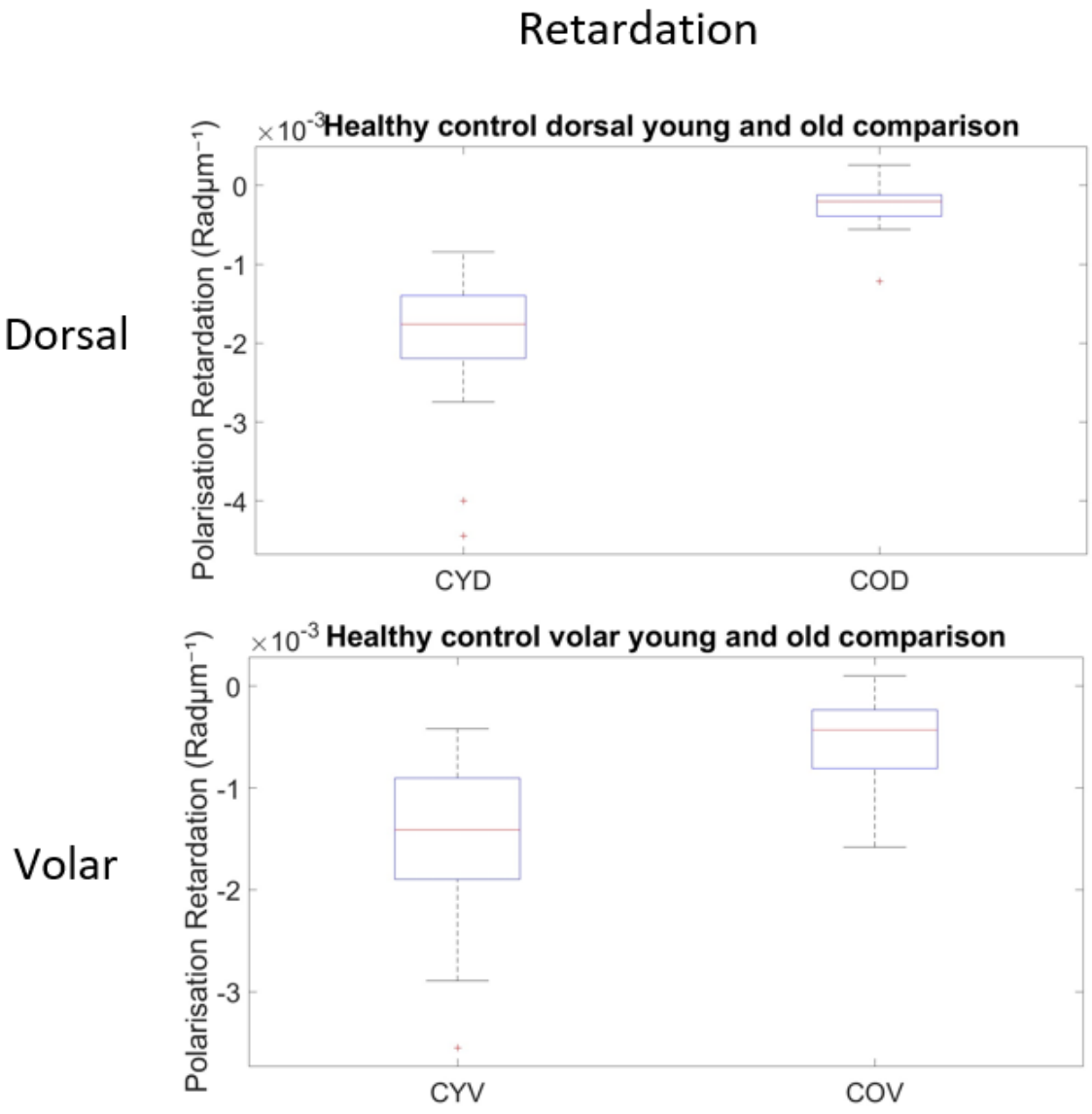

Figure 3.5: Boxplots of PS-OCT retardation data for comparisons between HC ≤30 years (CY) and HC ≥70 years (CO) groups for both sites, volar (V) and dorsal (D)

Retardation – Epidermal Thickness (OCT) Correlation

Likewise, for retardation data and OCT epidermal thickness data were averaged across observers and repeats. Spearman's correlation coefficients were calculated for site grouped data. Both sites showed a very significant confidence of a significant negative correlation. As shown in Table 3.6.

	Volar	Dorsal
ρ	-0.5679	-0.5267
p-value	$\ll$0.001	$\ll$0.001

Table 3.6: Correlation coefficients between retardation and OCT Epidermal Thickness

Heathy control – Patient mRSS comparison with PS-OCT

Observer two performed scans on all participants and therefore this allowed one measurement from each to be sorted into subgroupings. Data were collated into sets for site specific healthy controls, which were then subdivided into HC ≤30 years and HC ≥70 years, as well as patient mRSS. Mean for each were then calculated for OCT epidermal thickness and retardation. These results are presented in Table 3.7. As described previously, the significant difference between HC ≤30 years and HC ≥70 years groups is seen here, as well as the similarity between volar and dorsal values in the majority of groupings. Additionally, mRSS 1 were measured to have the largest patient epidermal thickness and retardance, with mRSS 0 and 2 having similar values. However, there is no statistically significant Spearman correlation between epidermal thickness and mRSS (ρ=0.0580, p-value=0.722).

Grouping		Epidermal Thickness [SD] (μm)	Retardation [SD] (Radmm^{-1})
All HC	Volar	131.520 [31.3365]	-1.0000 [0.7724]
	Dorsal	130.104 [33.8793]	-1.1000 [1.1000]
HC ≤30	Volar	154.149 [22.9892]	-1.5000 [0.7449]
	Dorsal	153.151 [28.2461]	-1.9000 [0.8621]
HC ≥70	Volar	107.862 [18.8844]	-0.5425 [0.3994]
	Dorsal	106.008 [19.4695]	-0.2566 [0.2932]
Patient mRSS 0	Volar	122.951 [17.7854]	-0.8866 [0.6581]
	Dorsal	121.858 [26.6547]	-0.7033 [0.6361]
Patient mRSS 1	Volar	126.167 [24.0005]	-1.2000 [0.6373]
	Dorsal	126.008 [33.9542]	-1.1000 [0.7948]
Patient mRSS 2	Volar	120.645 [23.5451]	-1.1000 [0.3184]
	Dorsal	96.856 [35.3176]	-0.4002 [0.2833]

Table 3.7: Mean observer 2 single measurements across subgroups for OCT epidermal thickness and Retardation

3.5 Discussion

This study has found correlation between epidermal thicknesses measured with PS-OCT and HFUS, and confirmed the reliability of PS-OCT for epidermal thickness measurements and retardation. It is also the first to confirm correlation between tissue birefringence and epidermal thickness. This data also confirms epidermal thinning with age, as established across multiple previous studies [19-22].

Two studies have previously assessed depth measurement correlation between HFUS and OCT. These investigated measurements of intradermal volumes and scar thickness in animal models and healthy controls respectively, and have shown strong, statistically-significant ($P<0.001$), correlations [23, 24].

Data from our study was also able to show statistically significant correlation ($\rho=0.3211$, p-value=0.003) between HFUS and OCT, for volar measurements. It is believed that the lack of reproducibility in the dorsal measurements ($\rho=0.0176$, p-value=0.872) is likely due to poor inter- and intra-observer correlation coefficients (<0.5) seen for HFUS measurements. This is believed to also be the cause of less significant correlation, compared to the previous studies, seen in volar measurements.

OCT epidermal thickness measurements were found to have strong inter- and intra-observer reliability for both same day and consecutive day comparisons. This is in agreement with several previous comparable studies [25-27]. Inter-observer reliability and same day intra-observer reliability were also found to be strong for tissue birefringence. However, consecutive day intra-observer reliability was found to have non-significant correlation. This may be because of variability across possible tissue imaging locations, or environmental effects between visits. It is notable that all of these results are true for both imaging sites.

As previously discussed, HFUS measurements showed poor inter- and intra-correlation across all comparisons, with the exception of intra-observer consecutive day dorsal measurements. The weakness of these results is in contrast to previous publications [28, 29]. The cause of this deviation is unclear, however it may be because the procedure used manual annotation of the images across a relatively wide cross-section. However, previous studies have shown poor reliability in epidermal measurements [30], which could also explain the findings. As a result of this poor reliability, comparisons using the HFUS data have not been considered viable.

Comparison between data found across the two imaging sites, volar and dorsal, were assessed using Paired t-tests. Across participant cohorts, HC ≤30 years and HC ≥70 years, and patients with SSc, no significant difference in epidermal thickness was found (p-value>0.05), however tissue birefringence differences were highly significant (p-value<0.05) in all comparisons. Volar and dorsal sites were chosen on the basis of ultraviolet light exposure differences and this is expected to be the cause of these differences.

Multiple studies have previously shown epidermal thinning occurs with age [19-22] and this study affirms those results. The highly significant statistical results (p-value<0.001) are seen in the two-way ANOVA. Furthermore, the differences are clearly evident between HC ≤30 years and HC ≥70 years groups from comparative boxplots. Notably these differences occur both in epidermal thickness and tissue birefringence.

Comparisons between tissue birefringence and epidermal thickness, by means of a Spearman's correlation coefficient, find highly significant correlation. This is believed to be the first evidence of such a relation and could allow for new and innovative skin assessment.

Neither OCT assessment, epidermal thickness nor retardation, showed correlation with mRSS. Previous studies have shown correlation between dermal thickness, assessed by HFUS, and mRSS [28, 29], however this relationship was not identified in this study. The low recruitment of patients with high mRSS to this study was likely a limiting factor, especially with only three with mRSS 2 and none of mRSS 3. Additionally, the use of epidermal thickness, rather than dermal thickness may be an explanation for this.

In addition to the novel demonstration of epidermal thickness – retardation correlation, this study is also believed to be the first use of circularly polarised light PS-OCT in imaging of SSc patients. Although correlation was not found with mRSS in this case, the study presented in Chapter 2 did find correlation with linear polarisation in grouped mRSS and hence it is believed that data from a cohort of higher mRSS may be able to establish a relationship. MRSS is typically higher in the hands and so an application looking at dorsal hands or digits may recruit a more even distribution of patients.

This study has considered a large number of variables in order to get the most accurate assessment of repeatability. It is likely that removing and relocating the scanners at the region of interest between repeats will have increased variability due to uncertainty in imaging the same location. However, this is an important determination as the existence of notable changes across small areas undermines the functional application of the data. Likewise, the weak ICC results for HFUS being attributed to the relatively large imaging width of 14 mm reaffirms this variability. Conversely these inconsistencies may be attributable to the methods used for data extraction. Manual annotation of HFUS images is likely to have introduced additional uncertainty, which could potentially be mitigated using an analytical method. Additionally, due to the variability of OCT images across their width some have less well defined epidermal – dermal boundaries after width averaging which may also reduce reliability to determination of this value.

3.6 Conclusion

This study has been able to find correlation between PS-OCT and HFUS epidermal thickness measurements. However, this was only possible in volar aspect. This may be due to low reliability of HFUS measurements, with most ICC values <0.5. Variability in epidermal thickness was also observed which is likely to have introduced additional uncertainty. However, PS-OCT was found to have moderate reliability (ICC=0.5-0.75) in all epidermal thickness measurements, as well as good reliability (ICC>0.75) in all retardation comparisons, except for consecutive days. This establishes PS-OCT as a functional clinical research tool in both modalities. Further investigation is required to determine the cause of longitudinal retardation changes. Additionally, this study is the first to demonstrate correlation between PS-OCT epidermal thickness and retardation increasing possible skin assessment applications. Future work should look to affirm the PS-OCT – HFUS correlation with improved HFUS reliability. Furthermore, better mRSS distribution using dorsal hand values should further investigate potential correlation to retardation. Confirming these relations is crucial in order to apply PS-OCT to SSc disease monitoring in clinical practise.

3.7 References

[1] Y. Allanore *et al.*, "Systemic sclerosis," *Nature Reviews Disease Primers,* vol. 1, pp. 1-21, 2015.

[2] M. Racine, M. Hudson, M. Baron, and W. R. Nielson, "The Impact of Pain and Itch on Functioning and Health-Related Quality of Life in Systemic Sclerosis: An Exploratory Study," (in eng), *J Pain Symptom Manage,* vol. 52, no. 1, pp. 43-53, Jul 2016, doi: 10.1016/j.jpainsymman.2015.12.314.

[3] M. D. Mayes *et al.*, "Prevalence, incidence, survival, and disease characteristics of systemic sclerosis in a large US population," (in eng), *Arthritis Rheum,* vol. 48, no. 8, pp. 2246-55, Aug 2003, doi: 10.1002/art.11073.

[4] T. R. Katsumoto, M. L. Whitfield, and M. K. Connolly, "The pathogenesis of systemic sclerosis," (in eng), *Annu Rev Pathol,* vol. 6, pp. 509-37, 2011, doi: 10.1146/annurev-pathol-011110-130312.

[5] M. Hughes and A. L. Herrick, "Systemic sclerosis," *British Journal of Hospital Medicine,* vol. 80, no. 9, 2019.

[6] M. Koenig *et al.*, "Autoantibodies and microvascular damage are independent predictive factors for the progression of Raynaud's phenomenon to systemic sclerosis: a twenty-year prospective study of 586 patients, with validation of proposed criteria for early systemic sclerosis," (in eng), *Arthritis Rheum,* vol. 58, no. 12, pp. 3902-12, Dec 2008, doi: 10.1002/art.24038.

[7] F. van den Hoogen, "2013 classification criteria for systemic sclerosis: an American college of rheumatology/European league against rheumatism collaborative initiative," *Annals of the Rheumatic Diseases,* vol. 72, no. 11, pp. 1747-1755, 2013.
[8] K. M. Matsuda *et al.*, "Skin thickness score as a surrogate marker of organ involvements in systemic sclerosis: a retrospective observational study," *Arthritis Research & Therapy,* vol. 21, no. 129, pp. 1-10, 2019.
[9] D. Khanna, "Standardization of the modified Rodnan skin score for use in clinical trials of systemic sclerosis," *Journal of Scleroderma and Related Disorders,* vol. 2, no. 1, pp. 11-18, 2017.
[10] P. Clements *et al.*, "Inter and intraobserver variability of total skin thickness score (modified Rodnan TSS) in systemic sclerosis," (in eng), *J Rheumatol,* vol. 22, no. 7, pp. 1281-5, Jul 1995.
[11] J. F. de Boer, T. E. Milner, M. J. C. van Gemert, and J. S. Nelson, "Two-dimensional birefringence imaging in biological tissue by polarization-sensitive optical coherence tomography," *Optics Letters,* vol. 22, no. 12, pp. 934-936, 1997.
[12] D. Huang *et al.*, "Optical Coherence Tomography," *Science,* vol. 254, no. 5035, pp. 1178-1181, 1991.
[13] E. J. Marjanovic *et al.*, "Polarisation-sensitive optical coherence tomography measurement of retardance in fibrosis, a non-invasive biomarker in patients with systemic sclerosis," *Scientific Reports,* vol. 12, no. 1, p. 2893, 2022/02/21 2022, doi: 10.1038/s41598-022-06783-7.
[14] H. Xu, L. Guo, and Q. Wang, *Diagnostic ultrasound in dermatology*. Singapore: Springer, 2022.
[15] P. R. Hoskins, K. Martin, and A. Thrush, Eds. *Diagnostic Ultrasound: Physics and Equipment*, 2 ed. Cambridge: Cambridge University Press, 2010.
[16] K. K. Alsing and J. Serup, "High-frequency ultrasound skin thickness: Comparison of manual reading and automatic border detection includes assessment of interobserver variation of measurement," (in eng), *Skin Res Technol,* vol. 26, no. 6, pp. 832-838, Nov 2020, doi: 10.1111/srt.12884.
[17] V. A. Flower *et al.*, "High-frequency Ultrasound Assessment of Systemic Sclerosis Skin Involvement: Intraobserver Repeatability and Relationship With Clinician Assessment and Dermal Collagen Content," *The Journal of Rheumatology,* vol. 48, no. 6, pp. 867-876, 2021, doi: 10.3899/jrheum.200234.
[18] T. K. Koo and M. Y. Li, "A Guideline of Selecting and Reporting Intraclass Correlation Coefficients for Reliability Research," (in eng), *J Chiropr Med,* vol. 15, no. 2, pp. 155-63, Jun 2016, doi: 10.1016/j.jcm.2016.02.012.
[19] M. Mogensen, H. A. Morsy, L. Thrane, and G. B. E. Jemec, "Morphology and Epidermal Thickness of Normal Skin Imaged by Optical Coherence Tomography," *Dermatology,* vol. 217, no. 1, pp. 14-20, 2008, doi: 10.1159/000118508.
[20] T. Gambichler, R. Matip, G. Moussa, P. Altmeyer, and K. Hoffmann, "In vivo data of epidermal thickness evaluated by optical coherence tomography: Effects of age, gender, skin type, and anatomic site," *Journal of Dermatological Science,* vol. 44, no. 3, pp. 145-152, 2006/12/01/ 2006, doi: https://doi.org/10.1016/j.jdermsci.2006.09.008.
[21] T. Tsugita, T. Nishijima, T. Kitahara, and Y. Takema, "Positional differences and aging changes in Japanese woman epidermal thickness and corneous thickness determined by OCT (optical coherence tomography)," (in eng), *Skin Res Technol,* vol. 19, no. 3, pp. 242-50, Aug 2013, doi: 10.1111/srt.12021.
[22] D. A. Lintzeri, N. Karimian, U. Blume-Peytavi, and J. Kottner, "Epidermal thickness in healthy humans: a systematic review and meta-analysis," (in eng), *J Eur Acad Dermatol Venereol,* vol. 36, no. 8, pp. 1191-1200, Aug 2022, doi: 10.1111/jdv.18123.

[23] K. Schuetzenberger *et al.*, "Comparison of optical coherence tomography and high frequency ultrasound imaging in mice for the assessment of skin morphology and intradermal volumes," *Scientific Reports,* vol. 9, no. 1, p. 13643, 2019/09/20 2019, doi: 10.1038/s41598-019-50104-4.

[24] S. Ud-Din *et al.*, "Objective assessment of dermal fibrosis in cutaneous scarring, using optical coherence tomography, high-frequency ultrasound and immunohistomorphometry of human skin," *British Journal of Dermatology,* vol. 181, no. 4, pp. 722-732, 2019, doi: https://doi.org/10.1111/bjd.17739.

[25] J. Monnier *et al.*, "In vivo characterization of healthy human skin with a novel, non-invasive imaging technique: line-field confocal optical coherence tomography," *Journal of the European Academy of Dermatology and Venereology,* vol. 34, no. 12, pp. 2914-2921, 2020, doi: https://doi.org/10.1111/jdv.16857.

[26] W. Jerjes, Z. Hamdoon, N. Al Rawi, and C. Hopper, "OCT in the diagnosis of head and neck pre-cancerous and cancerous cutaneous lesions: An immediate ex vivo study," *Photodiagnosis and Photodynamic Therapy,* vol. 27, pp. 481-486, 2019/09/01/ 2019, doi: https://doi.org/10.1016/j.pdpdt.2019.07.019.

[27] D. Rashed, D. Shah, A. Freeman, R. J. Cook, C. Hopper, and C. M. Perrett, "Rapid ex vivo examination of Mohs specimens using optical coherence tomography," *Photodiagnosis and Photodynamic Therapy,* vol. 19, pp. 243-248, 2017/09/01/ 2017, doi: https://doi.org/10.1016/j.pdpdt.2017.06.006.

[28] H. Li *et al.*, "High-frequency ultrasound of the skin in systemic sclerosis: an exploratory study to examine correlation with disease activity and to define the minimally detectable difference," (in eng), *Arthritis Res Ther,* vol. 20, no. 1, p. 181, Aug 16 2018, doi: 10.1186/s13075-018-1686-9.

[29] O. Kaloudi *et al.*, "High frequency ultrasound measurement of digital dermal thickness in systemic sclerosis," *Annals of the Rheumatic Diseases,* vol. 69, no. 6, pp. 1140-1143, 2010, doi: 10.1136/ard.2009.114843.

[30] T. L. Moore, M. Lunt, B. McManus, M. E. Anderson, and A. L. Herrick, "Seventeen-point dermal ultrasound scoring system--a reliable measure of skin thickness in patients with systemic sclerosis," (in eng), *Rheumatology (Oxford),* vol. 42, no. 12, pp. 1559-63, Dec 2003, doi: 10.1093/rheumatology/keg435.

4. Structural assessment of ulcers and digital pitting in patients with systemic sclerosis through the use of 3D polarisation-sensitive optical coherence tomography

Context of contribution:

This chapter is a draft publication for Annals of the Rheumatic Diseases (British Medical Journal) for which I am lead author. At the time of joining the project the grant had been approved. I developed the imaging procedure, was the sole observer meeting and imaging the participants, filtered and prepared the images using proprietary software, and wrote the entirety of the paper.

Image filtering and preparation was conducted using ThorLabs' proprietary software, ThorImageOCT 5.5.5. This process required a large amount of manual adjustment and visual interpretation in order to present the details of the scans in a clear and meaningful way.

The writing of the following chapter is entirely my own work with only minor modifications based on the oversight of the principle investigator and my supervisor. This body of work would not have been possible without the NHS staff who assisted during data collection in order to ensure patients were as comfortable as possible and in the recruitment of participants.

4.1 Abstract

Objective: Polarisation-sensitive optical coherence tomography (PS-OCT) is non-invasive optical imaging capable of micron scale resolution and high speed 3D scanning. Systemic sclerosis is a chronic autoimmune disease that can cause the formation of lesions on distal digits, such as ulcerations and pitting, resulting in pain and poor quality of life. This study aimed to investigate its potential of imaging both types of digital lesions in systemic sclerosis patients, using PS-OCT, to establish feasibility for longitudinal treatment studies.

Method: Participants were imaged by a single observer and were positioned and supported under the scanner due to low mobility in the hands. 3D polarisation-sensitive images were captured, and thresholding and surface identification was conducted in proprietary software.

Results: Four participants were recruited. One had only digital pitting (DP), one had DP and a digital ulcer (DU), and two had only DUs. Eight 3D scans were collected in total. They showed large and small pitting, as well as tissue adjacent to pitting in three separate images. One unscabbed and four scabbed ulcers were scanned across all participants. Images were cross-sectioned through structural features, where applicable. B-scans were also extracted for intensity and retardance.

Conclusions: Structural surface and subsurface features were clearly visible in scans, demonstrating feasibility for clinical annotation and assessment for monitoring and longitudinal study. Low mobility made positioning challenging and further work is required in this area to improve patient comfort.

4.2 Introduction

Systemic sclerosis (SSc) is a rheumatic autoimmune disease which is characterised by organ fibrosis, microvascular deterioration, and immune dysfunction [1]. Vasculopathy, observed as Raynaud's phenomena [2, 3], is often the first sign of the condition [3] and results in tissue hypoxia [1], leading to fibrosis [4]. It also causes ischaemia, which in distal digits has been shown to be associated with lesions: ulcerations in the majority of cases [5] and pitting [6]. A large study, conducted by Amanzi et al., on the characterisation of digital lesions in systemic sclerosis defines pitting as, '*small-sized hyperkeratosis'* [7]. There is disagreement on the definition of digital ulcers, but a systematic review by Suliman et al. proposed and tested the definition as, '*Loss of epidermal covering with a break in the basement membrane (which separates dermis from epidermis). It appears clinically as visible blood vessels, fibrin, granulation tissue and/or underlying deeper structures (e.g., muscle, ligament, fat) or as it would appear on debridement'.* This description has the best inter- and intra-rater reliability of any tested definition [8].

Pain and function studies have underlined the importance of further focused investigation into the pathophysiology and monitoring of ulcers [9] and pitting [10]. Half of patients report a history of ulceration [3] and a large 100 patient study has shown similar rates (44.1%) for digital pitting [7]. Mouthon et al. showed the significant impact ulcerations have on hand disability, patient quality of life and mental health [9]. Additionally, digital pitting has also been shown to correlate with increased pain and reduced function [10]. Currently, the standard assessment method for digital ulcerations is done purely on the observation of the attending clinician based on experience [11]. However, inter-observer variability has been shown to be poor and hence limiting the feasibility of multi-centre studies [12]. Clinical studies have also implemented clinical observation as a means to determine the presence of pitting [10], although little information is available on the variability of such metrics.

Polarisation-sensitive optical coherence tomography (PS-OCT) is a non-invasive optical imaging modality capable of creating 3D [13] polarisation-optical-biopsies [14]. It has been widely applied across clinical specialities due to its high resolution, relative to alternative techniques [15-17] which has allowed for substructure analysis previously not possible [17]. The systems are based on a Michelson interferometer and use a light source of broadband width, for high axial-resolution, in the near-infrared, for low-attenuation in skin [18]. Spectral domain imaging can be used for maximum time resolution in order to produce high speed depth scans [19]. Scanning mirrors then allow construction of 3D images [20].

As previously discussed, current ulceration assessments are very limited. In 2019, Bruni et al. proposed a more rigorous assessment scheme termed the digital ulcer clinical assessment score (DUCAS). This criteria consisted of seven metrics to better represent the extent DU caused clinical affliction experienced by the patients. However, this scoring system only looks at numeracy of ulcerations and how that changes longitudinally, observation of clinical complications, and the need for drug or surgical intervention. They propose that additional techniques, including laser imaging could be used for longitudinal ulcer tracking in clinical trials [8]. A small number of studies have tried a variety of techniques to create quantitative tracking of DU. This includes patients self-tracking DU with smartphone cameras [21], professional medical photography, with free-hand boundary identification and software ellipse overlay [22], and high-frequency ultrasound (HFUS) [23, 24].

The main aim of this study was to investigate the feasibility of PS-OCT as an assessment method for DU and DP. Additionally, post imaging analysis would then determine what quantitative measures could be recorded as metrics for disease monitoring. Importantly this would include investigation into the effects DU and DP have on tissue birefringence as this is yet to be studied.

4.3 Methods

All data was collected from patients with SSc in a single visit. All participants were asked to be alcohol and caffeine free for at least 4 hours before their visits. This study was approved by West Midlands - Edgbaston Research Ethics Committee (21/WM/0212). All research was performed in accordance with relevant guidelines and regulations. All participants gave informed, written consent for the study. Participants recruited had current DU or DP on the finger tips.

All participants were imaged by a single observer on a single visit. All imaging was completed using a consistent setup whereby finger-tips were scanned while participants' hands were gently held in place. However, alignment of the region of interest within the imaging area was challenging due to patient's limited mobility in the hands, even with the assistance of the clinical staff.

The three-dimensional scans were taken using a Thorlabs Polarization-Sensitive Spectral Domain OCT Telesto Series Imaging System (TEL220PSC2) with ThorLabs OCT-LK4 scan lens kit and Thorlabs ThorImage OCT 5.5.5 proprietary software. The scan lens kit provides and lateral resolution of 20 µm. The axial resolution in skin can be approximated to be 3.9 µm based on the stated resolution in air and the refractive index in the medium. The central wavelength is 1300 nm in order to reduce absorption in tissue. Positioning and focusing were conducted manually. Scans were taken of a 4 x 4 mm^2 surface area, to a scan depth of 2.61 mm. An example 3D intensity scan of an ulcer can be seen in Figure 4.1. All images are presented using ThorImage and as a result are limited in their display of axis, colour scales, and positioning.

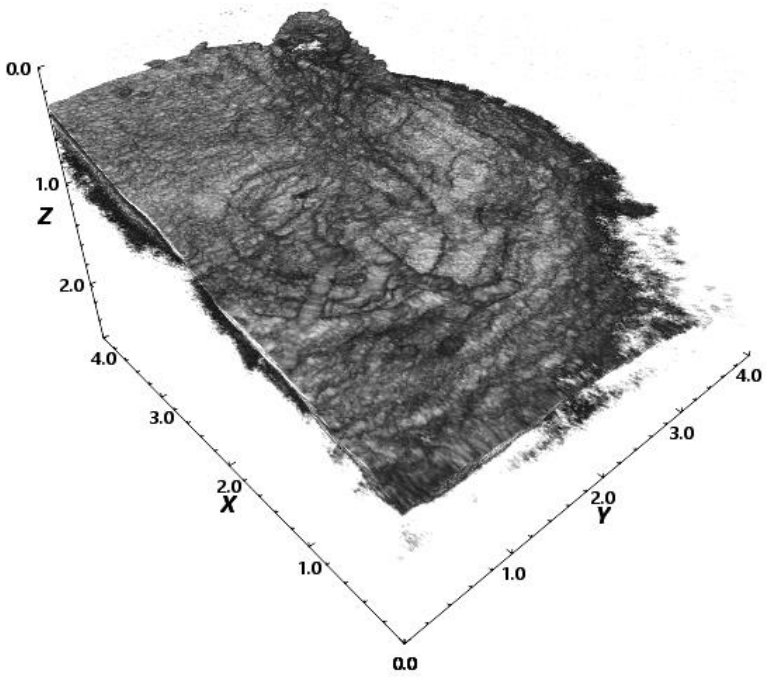

Figure 4.1: 3D OCT unscabbed digital ulcer intensity scan, at least one year old, on left index finger, forearm mRSS 1 at time of imaging. Axes in mm. Image contrast enhanced in post processing.

4.4 Results

Four participants met the criteria and were willing to partake. Three participants had DU and two DP.

Images cover digital pitting and tissue adjacent to pitting, as well as scabbed and unscabbed ulcerations. Structural features were clearly visible at the equipment resolution, as seen in Figure 4.1. Surface structures can be seen to vary in size but are typically equal to or less than 4 x 4 mm^2. They are easily identified and images allow for the possibility of longitudinal assessment by annotation. Substructure observation and depth measurements are also possible using image cross-sectioning.

In the following figures (4.2 – 4.8) the imaging region is marked with a red square. Where applicable the author has marked the boundary between the structure of interest being imaged and healthy tissue with a red curved line. The approximate location of the B-scan

is marked in green and the surface cross-section is marked with a blue a line. Retardation images are matched to B-scans.

Figures 4.2 and 4.3 show two contrasting pitting structures. Pitting in Figure 4.2 shows extensive tissue loss and the image captures the boundary between pitting and healthy tissue. Figure 4.3 shows localised pitting, where the entire pit is observed within the imaging range.

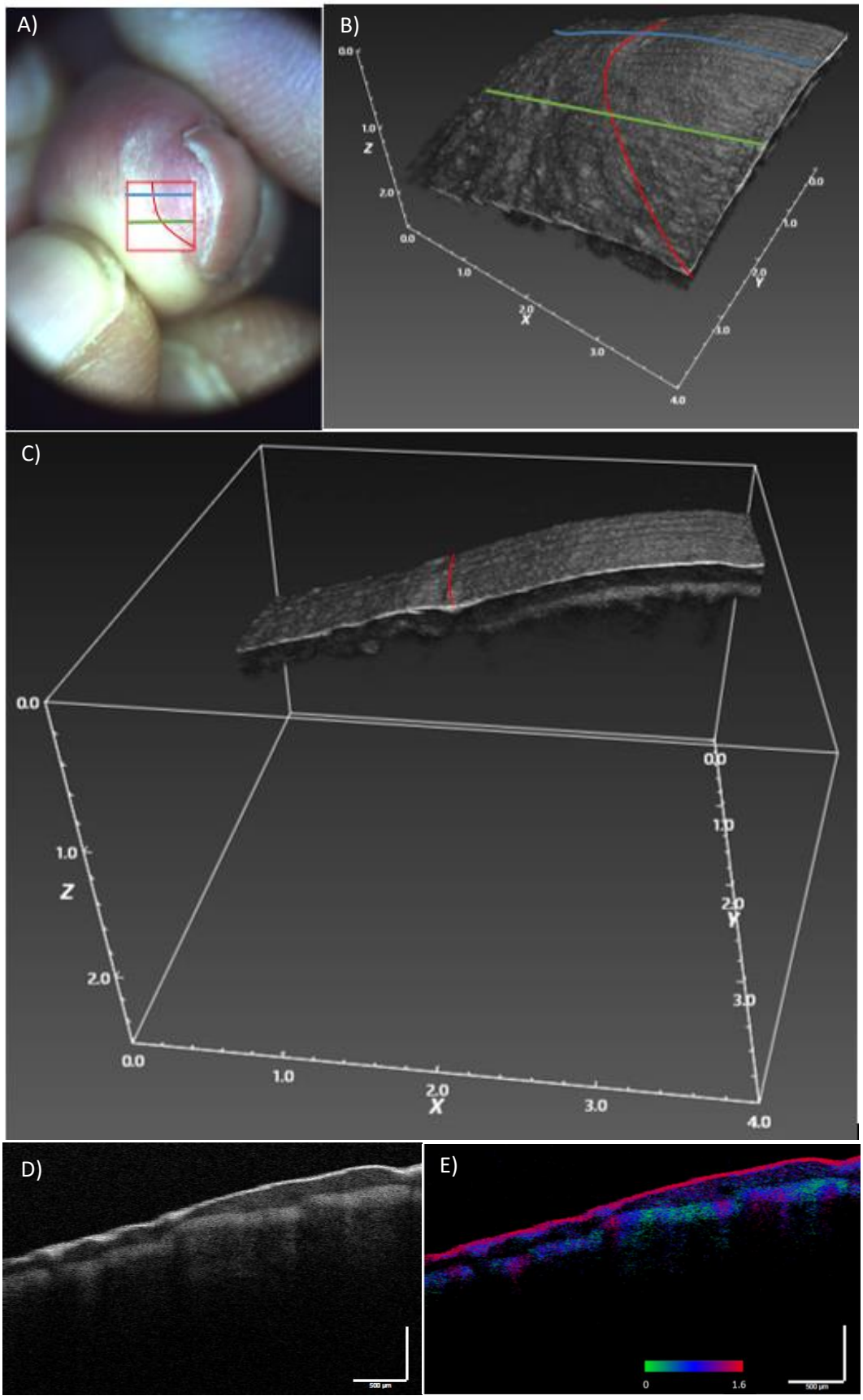

Figure 4.2: Digital pitting on left middle finger of patient with forearm mRSS 1 at time of visit. All axes are in mm A) Photograph of imaging area B) 3D scan of region of interest C) Surface cross-section D) B-scan across pitting and healthy tissue transition E) Retardation image of B-scan with a colour scale for reference, between 0 and 1.6 radians.

In Figure 4.2 A) the boundary between pitting and healthy tissue is clearly visible. The difference between these areas in B) can still be seen although less clearly. In both B) and C) the surface texture is notably different between pitted and healthy tissue, with the pitting area more uniform. This allows for identification of the region, assisted by A) as photo reference. Additionally, C) also shows a region of more significant reflection at the boundary, which may indicate hyperkeratosis. This is also visible in D) and to a lesser extent E). Skin layers are clearly visible in D), with possible epidermal thickening seen in the pitting region. E) demonstrates the possibility of additional functionality in retardation measurements within a volume of tissue, although no significant change is seen in this case.

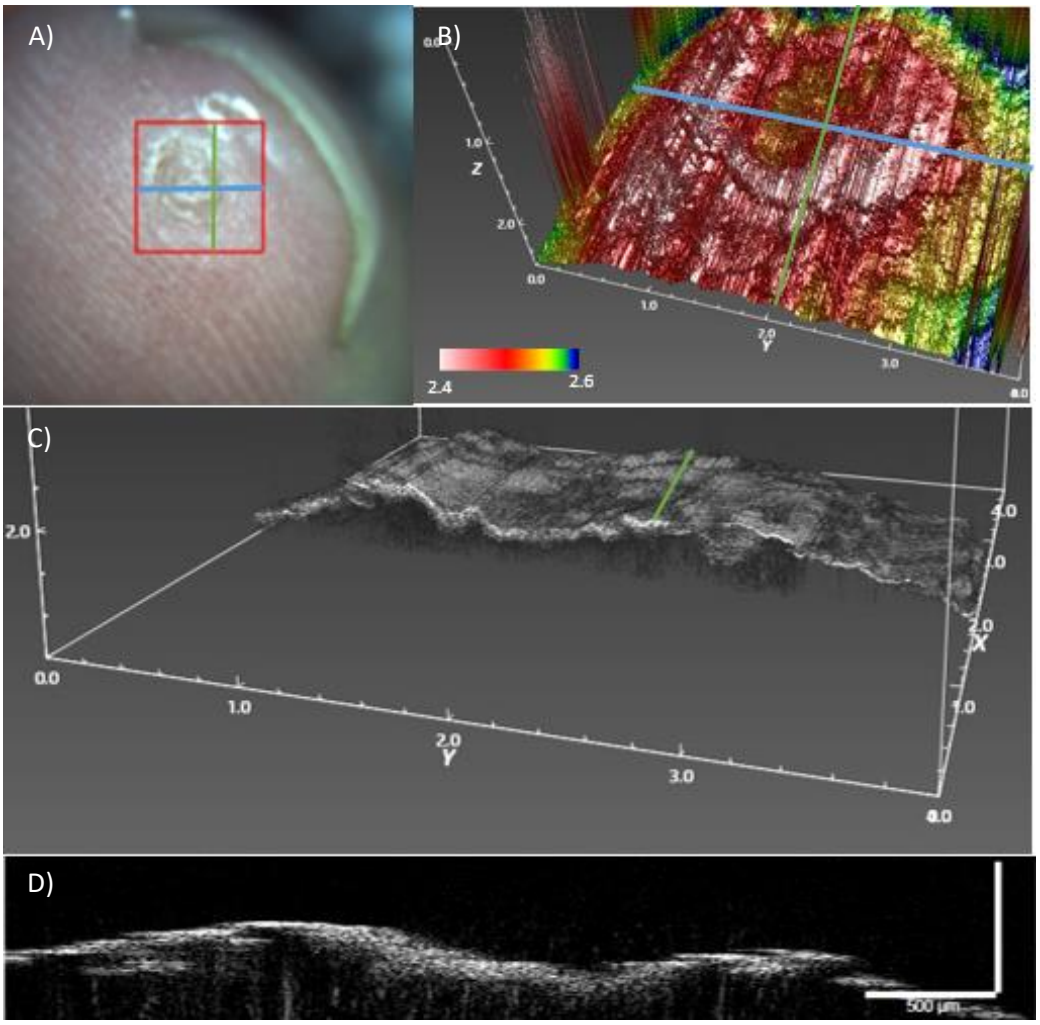

Figure 4.3: 3 month old digital pitting on the left middle finger of patient with forearm mRSS 0 at time of visit. All axes are in mm A) Photograph of pitting area within imaging region B) Depth coloured pitting surface with a colour scale for reference, between 2.4 and 2.6 mm C) Surface cross-section D) B-scan.

Figure 4.3 A) shows an entire pitting area captured within the imaging range, including surrounding healthy tissue. The surface has then been coloured by depth in order to highlight less significant structures as seen in B). With structural features easily identified, and hence annotated, longitudinal investigations and monitoring of structures is possible. In C) the surface depth change is clearly visible, with a higher intensity surface reflection possibly due to hyperkeratosis, adding to a possible range of investigations, such as the extent of pitting depth. The B-scan of the area is also presented in D), however due to the surface being close to the limit of the imaging depth of 2.61 mm, due to the difficulty of positioning patients, very little can be seen beyond the surface.

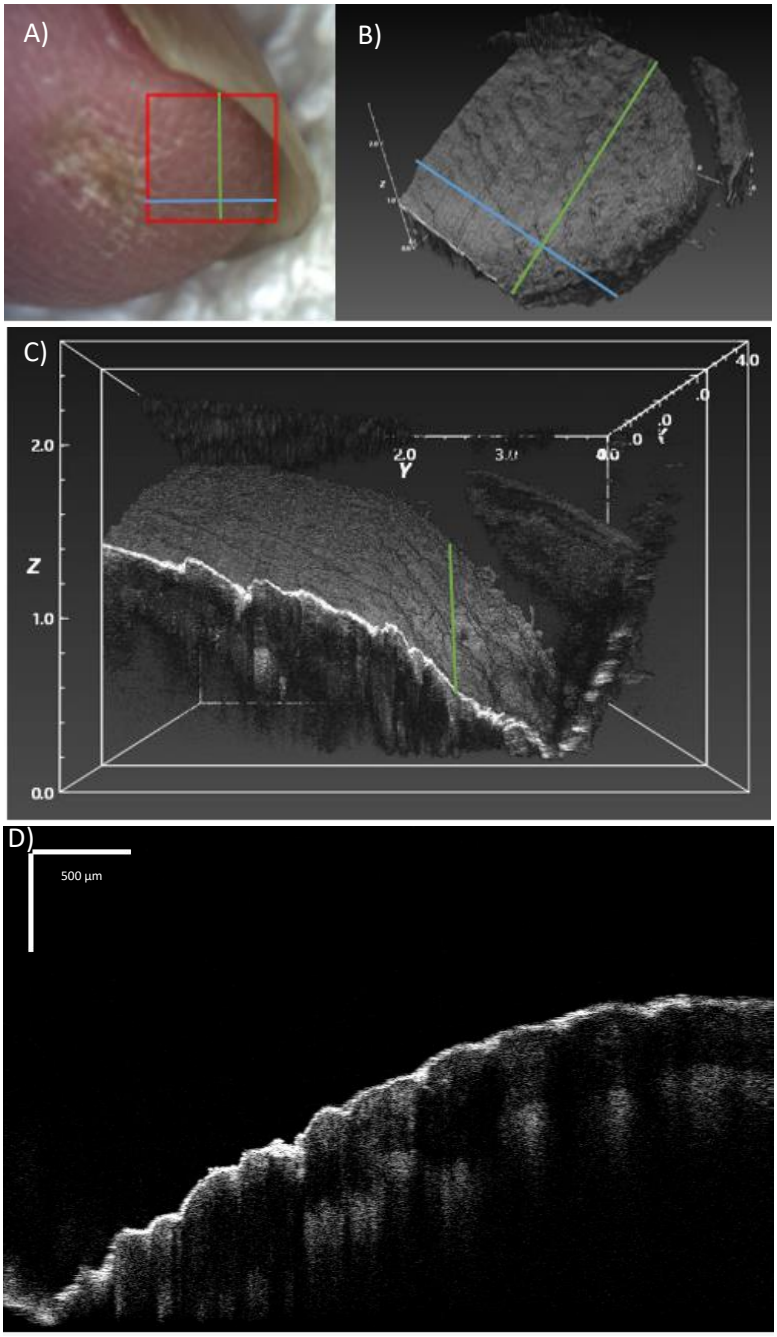

Figure 4.4: Pitting adjacent tissue from left thumb of patient with forearm mRSS 0 at time of visit. All axes are in mm. A) Photograph of imaging region adjacent to pitting B) 3D scan of region surface including nail C) Cross-section of scan D) B-scan of tissue.

As previously discussed, positioning the imaging region on small features when patients have limited mobility is challenging. This resulted in Figure 4.4 which has captured tissue adjacent to pitting. In A) the pitting region can be seen by the discoloured area, notably not in the imaging region. Due to the positioning a section of nail is also captured and in one area the surface is outside of the imaging range. These features appear in B) and C)

creating unwanted structures within the images. However, the nail does demonstrate the imaging capability of the system and its ability to scan multiple materials with differing optical properties within a single frame without distortion. As can be shown with scabbed ulcers, this uniformity and consistency is useful within clinical applications. As in Figure 4.2 D), the B-scan in Figure 4.4 D) clearly shows skin layers.

Digital ulcerations imaged were mostly scabbed, with one exception as seen in figure 4.5. With these images the surface structure can be seen to be notably more complex, but captured accurately. Within some scans where surfaces are folded, or contain large structures relative to other surface features, shadowing can occur resulting in gaps in the image. This is mostly seen as a non-significant effect relative to the total image integrity, but could be problematic in some applications.

Figure 4.5 captures an unscabbed ulceration that is at least one year old. A) shows a clearly visible structure, despite the overexposure. The detailed ring structure in B), as in Figure 4.1, is easily identifiable and shows the full structure of the ulcer. The surface cross-section in C) shows a clear symmetrical substructure that aligns with the surface rings. D) and E) are in the perpendicular direction to C), and although the substructure appears changed in the region under the ulcer any symmetry is less clear and no notable difference in birefringence can be seen.

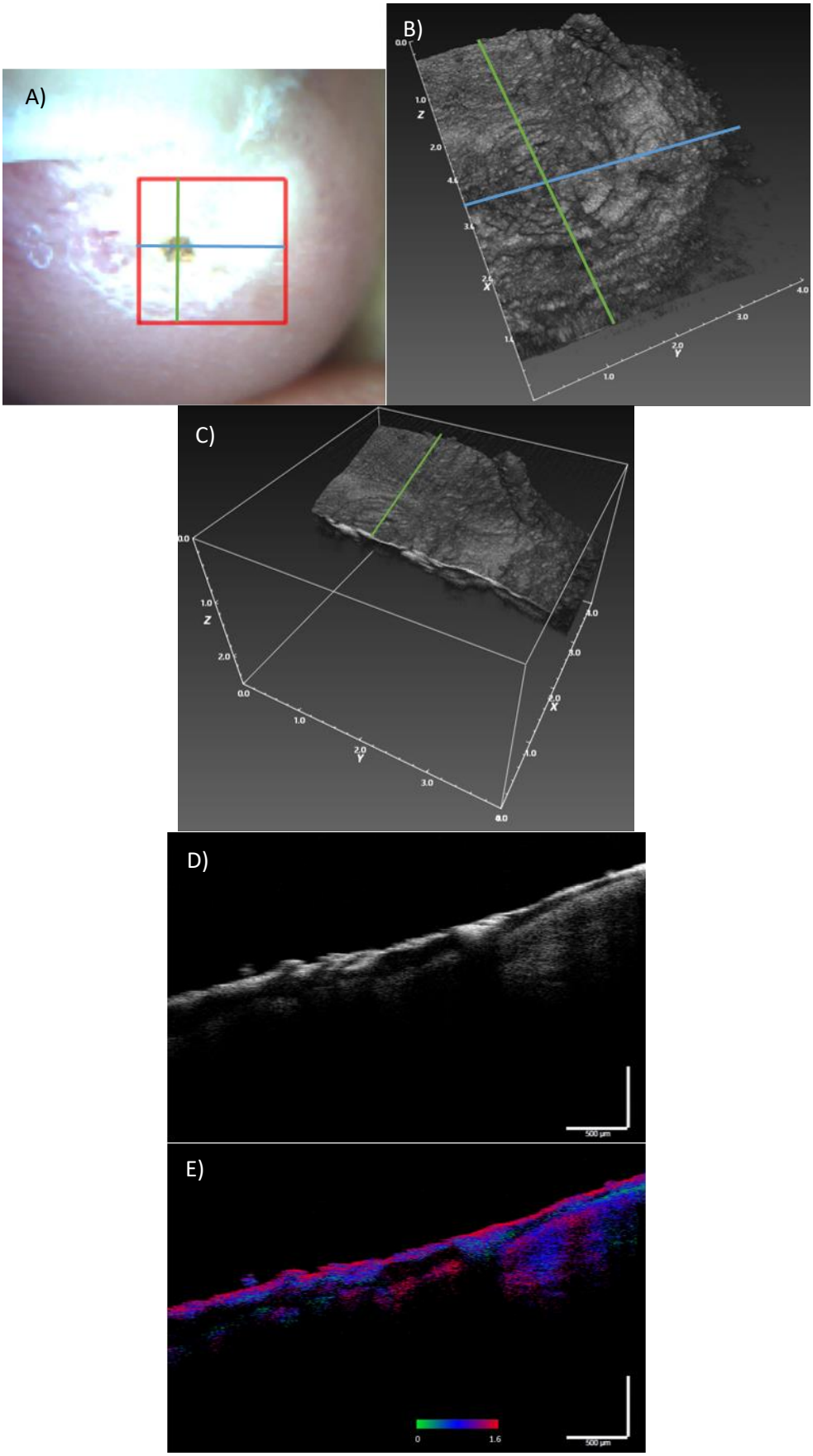

Figure 4.5: Unscabbed digital ulceration, at least one year old, on left index finger, forearm mRSS 1 at time of imaging. All axes in mm. A) Photograph of imaging region B) 3D surface scan C) Surface cross-section of ulceration D) B-scan of ulcer E) Retardance B-scan of ulceration with a colour scale for reference, between 0 and 1.6 radians.

Figures 4.6, 4.7, and 4.8 are images of three scabbed ulcers from a single patient who has a forearm mRSS of 0 at time of imaging. They are located at left and right index, and right middle finger respectively and are 5-6 months, 2 years and recurring, and 1 month old. Scabs were found to produce large surface reflections, however faint outlines of skin surface are visible below the structures. All figures capture both healthy skin and scabbed ulcers for comparison. This allows for substructure tracking and scab thickness assessment. Retardation images (E) were captured for all images, however in contrast to the earlier images they have had less thresholding applied in order to maintain faint substructure features. Figure 4.6 E) shows banding within the scab suggesting high birefringence in that region. However, its abrupt discontinuation and lack of recurrence suggests that it may not be a real feature. Figures 4.7 D) & E) show a clear substructure boundary that follows a continuous curve below the scab. Likewise, in Figure 4.8 D) the dermis can be seen in the healthy skin region and transitioning below the scab. As with pitting images, ulcer scans allow for the potential of longitudinal monitoring and annotation, or computational assessment.

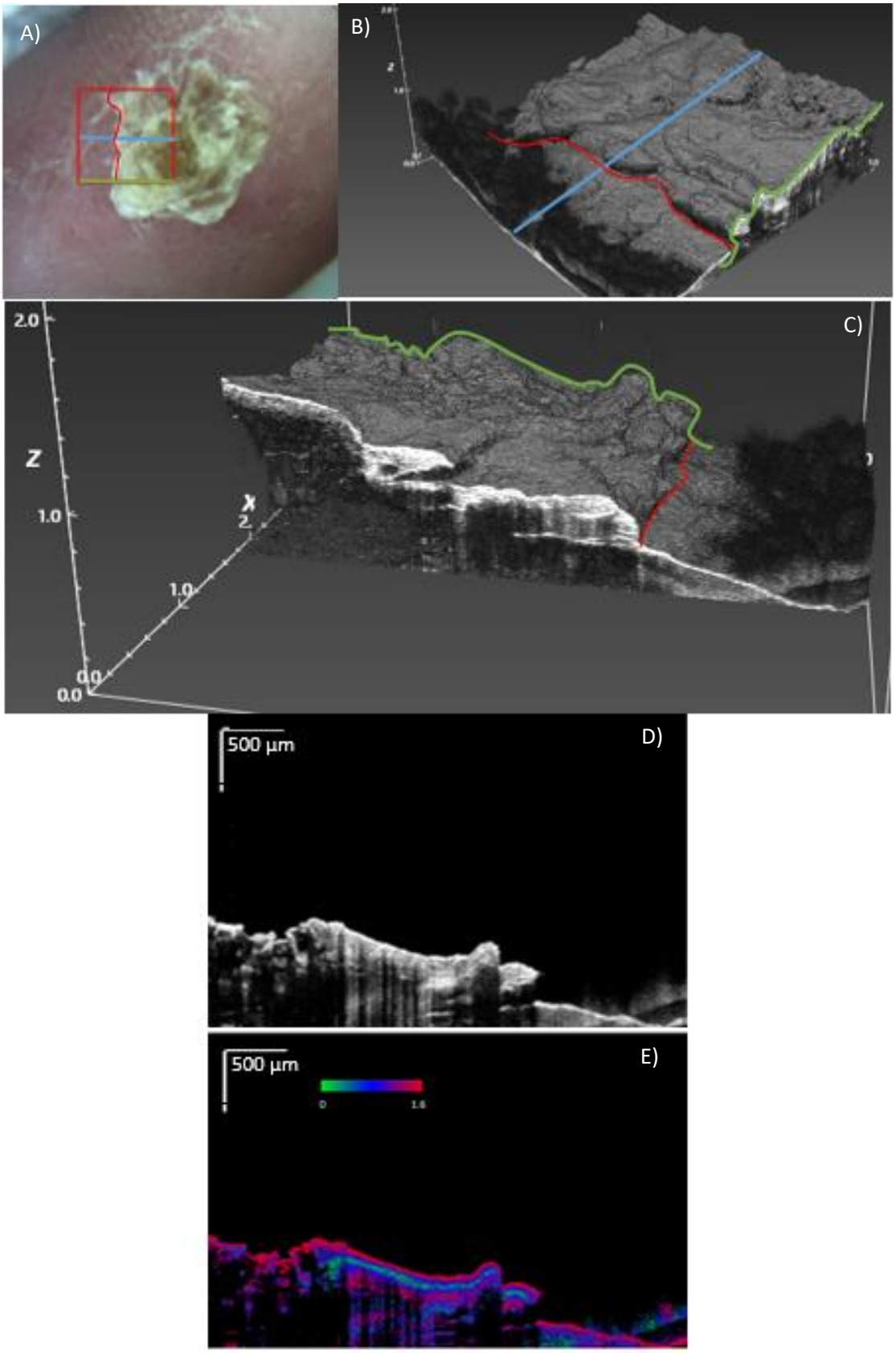

Figure 4.6: All axes in mm. A) Photograph of imaging region showing section of large scabbed ulceration and healthy skin transition B) 3D surface scan of imaging region, note dark region over skin is caused by inverted image section due to the surface being outside of imaging range C) Surface cross-section with clear continuation of stratum corneum from healthy skin under scab D) B-scan with some visible continuation of stratum corneum E) Retardation B-scan with banding in centre of image with a colour scale for reference, between 0 and 1.6 radians.

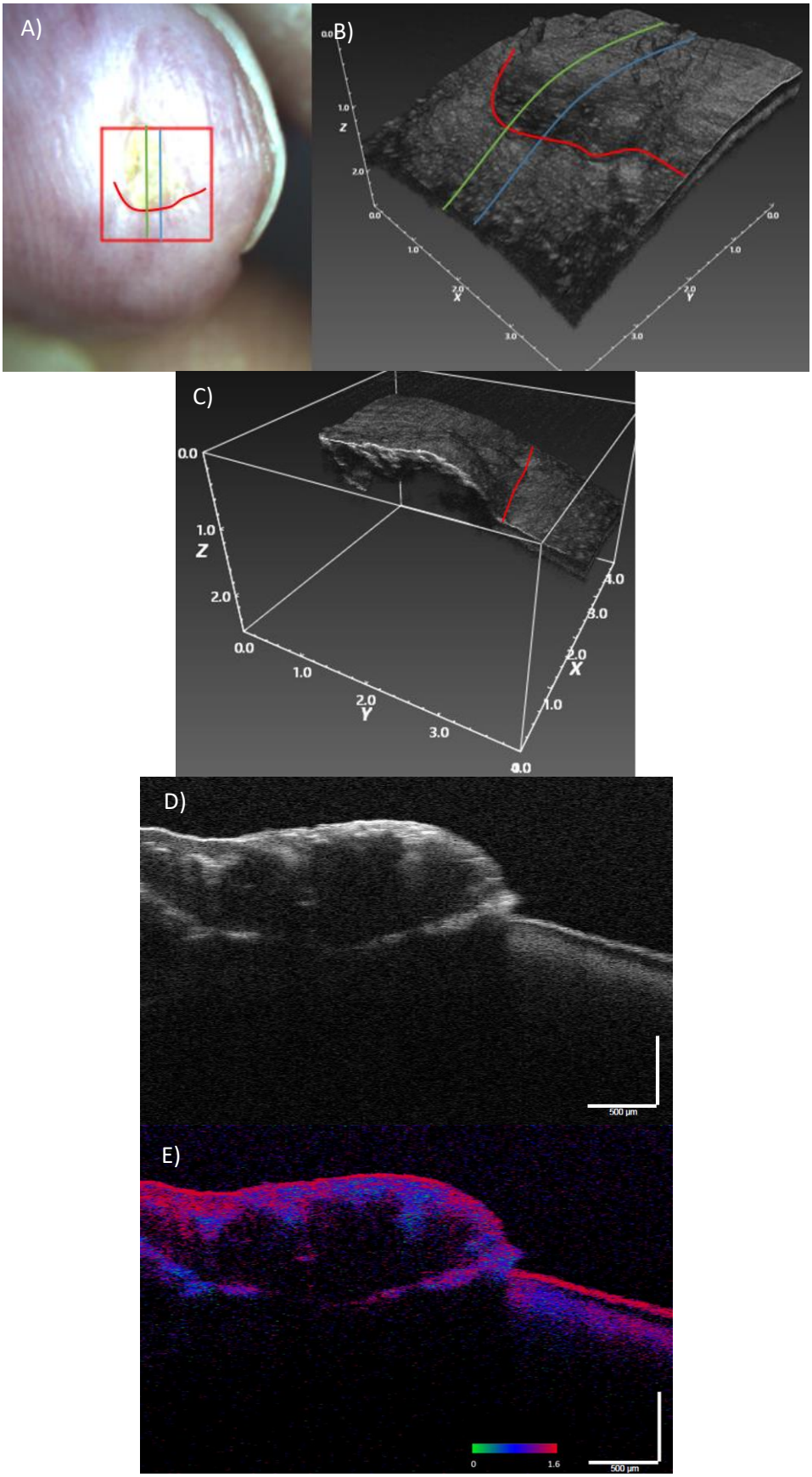

Figure 4.7: All axes in mm. A) Photograph of the imaging region with large proportion of scab within range B) 3D surface scan C) Surface cross-section scan D) B-scan with distinctive substructure visible E) Retardation image with subsurface reflection matching with a colour scale for reference, between 0 and 1.6 radians.

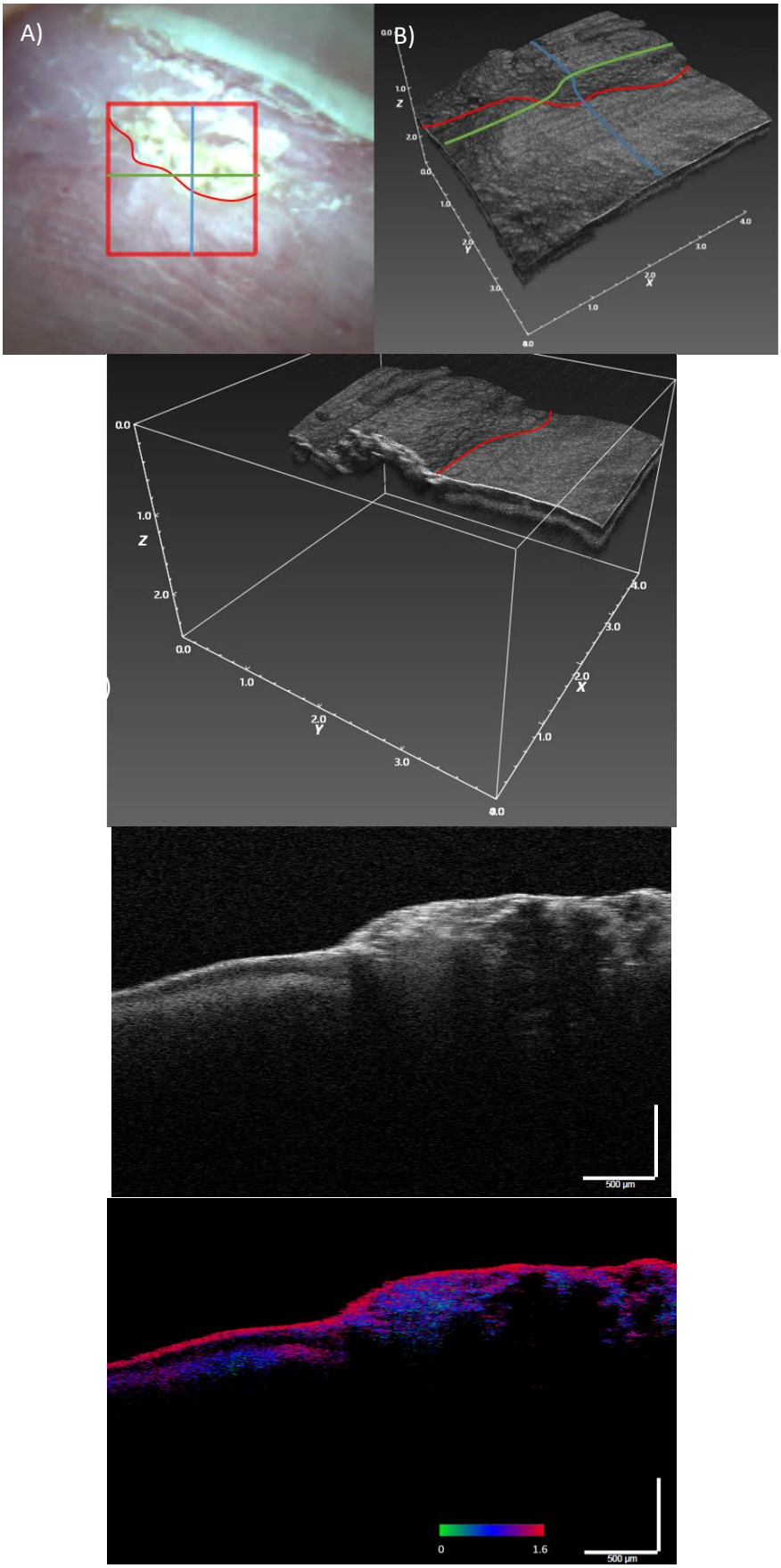

Figure 4.8: All axes are in mm. A) Photograph of imaging region B) 3D surface scan C) Surface cross-section D) B-scan with visible continuation of dermis under scabbed region E) Retardation image with a colour scale for reference, between 0 and 1.6 radians.

4.5 Discussion

This study is the first to demonstrate the application of 3D PS-OCT scanning in the assessment of digital pitting and ulcerations in systemic sclerosis. Images were able to clearly show pitting and ulceration surface structures, as well as substructure features and their transition into healthy tissue. Additionally, 3D retardation images demonstrate the potential of more detailed analysis of these imaged sites.

Multiple clinical fields are starting to investigate the possibility of *in-vivo* 3D OCT scanning as a means of wound assessment and monitoring [25-27]. Park et al. specifically applied swept source PS-OCT to clinically applied puncher wounds in mice over a 6 week period and demonstrated trackable changes in birefringence and tissue structure during recovery. Notably, surrounding tissue was found to also change over this period [25]. This is a significant practical demonstration of the feasibility of identifying changes and tracking recovery using PS-OCT 3D scanning.

The morphological assessment of digital lesions in this study builds on the work by Suliman et al. in their investigation into structural 2D analysis of ulcers using high-frequency ultrasound. They demonstrated that over larger depths structural tissue layers and tissue lose could be identified [24]. Our study has collected images that are visibly sharper and more detailed, although with only a fraction of the depth penetration, laying the ground for a clinical longitudinal study. Unfortunately, a quantitative comparison between the systems' functional abilities is not possible as Suliman does not provide specifics of their system's functionality.

Images taken during this study, of both pitting and ulcerations, were able to clearly resolve detailed structural surface components of the features. Substructures were also identified and changes between healthy tissue and wounds could be seen. This enables the possibility of clinical assessment of these features, such as multidimensional

measurements by annotation or computation. This is especially important for potential longitudinal studies. Additionally, the birefringence measurements enable additional metrics for measurement of severity and recovery, as previously demonstrated by Park [25]. All such quantitative assessments will need to be done with clinical oversight that could be aided by a biopsy study in order to ensure measurements are meaningful and representative.

However, the author would encourage the use of additional support for patient's hands during any further studies, as initial positioning and maintaining location was challenging for low mobility patients. Additionally, penetration depth, especially through scabbing, is a limiting factor, however good positioning at the top of the imaging region would improve this. The system used in this case was a class 1m, penetration depth can be reasonably assumed to improve with output power and an increase to class 2, with appropriate safety precautions, could be one way to improve this. Assuming the attenuation coefficient does not change with depth, penetration will increase as a function of the natural log of the incident intensity.

4.6 References

[1] Y. Allanore *et al.*, "Systemic sclerosis," *Nature Reviews Disease Primers,* vol. 1, pp. 1-21, 2015.

[2] M. Koenig *et al.*, "Autoantibodies and microvascular damage are independent predictive factors for the progression of Raynaud's phenomenon to systemic sclerosis: a twenty-year prospective study of 586 patients, with validation of proposed criteria for early systemic sclerosis," (in eng), *Arthritis Rheum,* vol. 58, no. 12, pp. 3902-12, Dec 2008, doi: 10.1002/art.24038.

[3] M. Hughes and A. L. Herrick, "Systemic sclerosis," *British Journal of Hospital Medicine,* vol. 80, no. 9, 2019.

[4] C. Beyer, G. Schett, S. Gay, O. Distler, and J. H. Distler, "Hypoxia. Hypoxia in the pathogenesis of systemic sclerosis," (in eng), *Arthritis Res Ther,* vol. 11, no. 2, p. 220, 2009, doi: 10.1186/ar2598.

[5] A. K. Murray *et al.*, "Pilot study assessing pathophysiology and healing of digital ulcers in patients with systemic sclerosis using laser Doppler imaging and thermography," (in eng), *Clin Exp Rheumatol,* vol. 34 Suppl 100, no. 5, pp. 100-105, Sep-Oct 2016.

[6] S. Friedrich *et al.*, "Disturbed microcirculation in the hands of patients with systemic sclerosis detected by fluorescence optical imaging: a pilot study," *Arthritis Research & Therapy,* vol. 19, no. 1, p. 87, 2017/05/08 2017, doi: 10.1186/s13075-017-1300-6.

[7] L. Amanzi *et al.*, "Digital ulcers in scleroderma: staging, characteristics and sub-setting through observation of 1614 digital lesions," *Rheumatology,* vol. 49, no. 7, pp. 1374-1382, 2010, doi: 10.1093/rheumatology/keq097.
[8] C. Bruni *et al.*, "Preliminary Validation of the Digital Ulcer Clinical Assessment Score in Systemic Sclerosis," *The Journal of Rheumatology,* vol. 46, no. 6, pp. 603-608, 2019, doi: 10.3899/jrheum.171486.
[9] L. Mouthon *et al.*, "Ischemic digital ulcers affect hand disability and pain in systemic sclerosis," (in eng), *J Rheumatol,* vol. 41, no. 7, pp. 1317-23, Jul 2014, doi: 10.3899/jrheum.130900.
[10] E. Nolan, J. Manning, C. Heal, T. Moore, and A. L. Herrick, "Impact and associates of digital pitting in patients with systemic sclerosis: a pilot study," (in eng), *Scand J Rheumatol,* vol. 49, no. 3, pp. 239-243, May 2020, doi: 10.1080/03009742.2019.1683888.
[11] M. Hughes, Y. Allanore, L. Chung, J. D. Pauling, C. P. Denton, and M. Matucci-Cerinic, "Raynaud phenomenon and digital ulcers in systemic sclerosis," *Nature Reviews Rheumatology,* vol. 16, no. 4, pp. 208-221, 2020/04/01 2020, doi: 10.1038/s41584-020-0386-4.
[12] A. L. Herrick *et al.*, "Lack of agreement between rheumatologists in defining digital ulceration in systemic sclerosis," (in eng), *Arthritis Rheum,* vol. 60, no. 3, pp. 878-82, Mar 2009, doi: 10.1002/art.24333.
[13] M. Pircher, E. Goetzinger, R. Leitgeb, and C. K. Hitzenberger, "Three dimensional polarization sensitive OCT of human skin in vivo," *Opt. Express,* vol. 12, no. 14, pp. 3236-3244, 2004/07/12 2004, doi: 10.1364/OPEX.12.003236.
[14] S. Srinivas *et al.*, *Determination of burn depth by polarization-sensitive optical coherence tomography* (BiOS '99 International Biomedical Optics Symposium). SPIE, 1999.
[15] A. M. Zysk, F. T. Nguyen, A. L. Oldenburg, D. L. Marks, and S. A. Boppart, "Optical coherence tomography: a review of clinical development from bench to bedside," *Journal of Biomedical Optics,* vol. 12, no. 5, pp. 1-21, 2007.
[16] T.-H. Tsai *et al.*, "Optical coherence tomography in gastroenterology: a review and future outlook," *Journal of Biomedical Optics,* vol. 22, no. 12, pp. 1-17, 2017.
[17] C. R. Chu, A. A. Williams, C. H. Coyle, and M. E. Bowers, "Early diagnosis to enable early treatment of pre-osteoarthritis," *Arthritis Research & Therapy,* vol. 14, no. 3, pp. 1-10, 2012.
[18] A. Sainter, T. King, and M. Dickinson, "Effect of target biological tissue and choice of light source on penetration depth and resolution in optical coherence tomography," *Journal of Biomedical Optics,* vol. 9, no. 1, 2004. [Online]. Available: https://doi.org/10.1117/1.1628243.
[19] T. Yuichi, S. Masayuki, and K. Fumihiko, "Two-dimensional optical coherence tomography using spectral domain interferometry," *Journal of Optics A: Pure and Applied Optics,* vol. 2, no. 1, p. 21, 2000/01/01 2000, doi: 10.1088/1464-4258/2/1/304.
[20] E. Götzinger, M. Pircher, and C. K. Hitzenberger, "High speed spectral domain polarization sensitive optical coherence tomography of the human retina," *Opt. Express,* vol. 13, no. 25, pp. 10217-10229, 2005/12/12 2005, doi: 10.1364/OPEX.13.010217.
[21] G. Dinsdale *et al.*, "Tracking digital ulcers in systemic sclerosis: a feasibility study assessing lesion area in patient-recorded smartphone photographs," *Annals of the Rheumatic Diseases,* vol. 77, no. 9, pp. 1382-1384, 2018, doi: 10.1136/annrheumdis-2017-212829.
[22] V. Simpson, M. Hughes, J. Wilkinson, A. L. Herrick, and G. Dinsdale, "Quantifying Digital Ulcers in Systemic Sclerosis: Reliability of Computer-Assisted Planimetry in Measuring Lesion Size," (in eng), *Arthritis Care Res (Hoboken),* vol. 70, no. 3, pp. 486-490, Mar 2018, doi: 10.1002/acr.23300.
[23] M. Hughes, T. Moore, J. Manning, G. Dinsdale, A. Murray, and A. Herrick, "247 A Pilot Study Using High-Frequency Ultrasound to Measure Digital Ulcers as an Outcome

Measure in Systemic Sclerosis Clinical Trials," *Rheumatology,* vol. 55, no. suppl_1, pp. i161-i162, 2016, doi: 10.1093/rheumatology/kew185.002.

[24] Y. A. Suliman *et al.*, "Ultrasound characterization of cutaneous ulcers in systemic sclerosis," *Clinical Rheumatology,* vol. 37, no. 6, pp. 1555-1561, 2018/06/01 2018, doi: 10.1007/s10067-018-3986-5.

[25] K. S. Park, W. J. Choi, S. Song, J. Xu, and R. K. Wang, "Multifunctional in vivo imaging for monitoring wound healing using swept-source polarization-sensitive optical coherence tomography," (in eng), *Lasers Surg Med,* vol. 50, no. 3, pp. 213-221, Mar 2018, doi: 10.1002/lsm.22767.

[26] H. Liu *et al.*, "Carbon Dots with Intrinsic Bioactivities for Photothermal Optical Coherence Tomography, Tumor-Specific Therapy and Postoperative Wound Management," (in eng), *Adv Healthc Mater,* vol. 11, no. 6, p. e2101448, Mar 2022, doi: 10.1002/adhm.202101448.

[27] S. Parsa, C. Wamsley, P. Kim, J. Kenkel, and Y. Akgul, "Use of Optical Coherence Tomography (OCT) in Assessment of Diabetic Skin Wound Characteristics and Blood Flow," *The Journal of Foot and Ankle Surgery,* vol. 62, no. 3, pp. 407-412, 2023/05/01/ 2023, doi: https://doi.org/10.1053/j.jfas.2022.10.001.

Conclusions

This body of work has investigated alternative means of clinical assessment and disease monitoring for systemic sclerosis using PS-OCT. Three clinical studies have been undertaken using three different imaging systems, two PS-OCT and one HFUS, collecting data on both healthy controls and patients at various stages of disease. Two and three dimensional PS-OCT scans were taken of healthy and diseased skin, as well as lesions.

The first study established that epidermal thickness measurements taken with PS-OCT correlate with measurements taken of biopsy tissue demonstrating that they are metrics of real structures. Additionally, retardation values for participant groupings, Healthy Controls, mRSS 0-1, and mRSS 2-3, identified an increase in line with fibrosis. This data provided motivation for the second study that investigated the reliability of PS-OCT. Inter- and intra-observer reliability on same and consecutive days was found to be strong for both epidermal thickness and birefringence. Moreover, this secondary study was able to establish a highly significant correlation between tissue birefringence and epidermal thickness. The increased functionality of the equipment used in this study also enabled 3D scans of lesions. In the third study this application demonstrated the high resolution imaging capabilities of the equipment and the potential for longitudinal assessment of these structures.

Initial investigations focused on establishing a relationship between skin structure observed in biopsies and PS-OCT measurements. The resulting scarring from biopsy extraction was longitudinally assessed and compared to fibrosis seen in patients. Structural measurements taken from biopsies were shown to correlate with PS-OCT epidermal thickness measurements, demonstrating that the technique can be used as a metric for these measurements. However, retardation was not found to correlate with the activity of collagen remodelling proteins. Nevertheless, it was found to increase with participant groupings in line with fibrosis. This shows the technique's potential for fibrosis extent quantification and hence disease monitoring. The longitudinal assessments

showed minimal change in retardation of scar tissue over the period for patients, but did find a significant change in healthy controls. The retardation of healthy control scar tissue was similar to higher mRSS patients showing that structural changes are comparable.

The second study built on the work established in the first, with improvements to the equipment, particularly the use of circularly polarised light. The main focus was to validate its measurements with HFUS and establish the reliability of PS-OCT. However, validation with HFUS was not possible. This is proposed to be because of the low reliability found in its measurements. This is in contrast to previous studies and is believed to be due to local variations across the relatively large area scanned, in comparison to PS-OCT, and potential inconsistent relocation between repeats. Additionally, the use of manual annotation is likely to have increased uncertainty in measurements. In the assessment of PS-OCT reliability, two observers imaged participants on same and consecutive days. Strong inter- and intra-observer reliability was found in structural assessment, but retardation measurements were only strong for same day comparisons. The strength of reliability of structural and same day retardation measurements is a significant finding as it demonstrates PS-OCT as a viable assessment technique. Additionally, a very significant correlation was found between epidermal thickness and retardation, directly linking thickening with increased birefringence.

The improved equipment also enables 3D image capture and this was applied to digital lesions. Scans were taken of both pitting and ulcerations and clearly demonstrated the equipment's ability to resolve detailed structural components. Images collected were able to show both surface and sub-surface features, as well as tissue birefringence. This is a significant functional development and opens up the possibility of longitudinal studies as these features are currently only assessed by observation.

Future Work

The next stage of work to build on what has been done in this body of work can be split into two distinct areas: further clinical studies and instrumentation review. The former can be split into unknowns resulting from each investigation and the later data types and ranges of interest.

The first study was not able to establish a relationship between retardance and collagen remodelling protein. However, Jaspers et al. found a correlation between birefringence and collagen density in scar tissue [1], and a recent study has shown collagen density increasing in line with mRSS [2]. It has been established that mRSS has poor inter-observer reliability and so using a quantitative alternative, that has shown correlation, would aid the development of PS-OCT as an alternative. Hence, a study taking *in*- and *ex vivo* retardation measurements as well as collagen density assessment via biopsy, in addition to a mRSS assessment would be valuable. Both local forearm and global mRSS has also been shown in multiple studies to correlate with hyalinised collagen [3-5], and there is historic data to support that unstained hyalinised collagen is strongly birefringent [6], although no recent studies have investigated this. Due to the strong correlation with mRSS this would also be valuable to include in the same study.

The validation of PS-OCT depth measurements with HFUS in the second study is also an area that needs review, specifically the reliability of the US system used. It's unclear precisely what the cause of the uncertainty was, but there are a number of areas that are likely to have led to increased variability. Manual annotation of HFUS is not a standard practise with many studies using an approach more similar to that used for the PS-OCT depth images. Re-treatment of this data using a computational approach would be a relatively straightforward method of determining if this was the route cause. A review of the calibration of the equipment may also be insightful before undertaking any further clinical work with it. If these two approaches show no significant differences, comparison

to another HFUS device and one of higher frequency, and hence resolution, may be a useful.

The 3D imaging of lesions, within the third study, has shown the great potential in imaging of high resolution surface and subsurface structures. In consultation with clinicians in the specialty, the next stage of works in this area should be an investigation into the clinical assessment potential within a longitudinal study. As previously discussed, assessment methods are currently very limited, being mainly observation, but lesions severely affect mental health and quality of life of patients. This highlights the importance of work in this area and the development of computational assessment of these images.

In addition to these continuation studies, work is needed in the assessment of the equipment itself. In particular, confirmation of lateral and axial resolutions at the refractive index of skin, optic axis insensitivity, and polarisation phase sensitivity and linearity across a range of relevant refractive indices, birefringences, and turbidities. Shortfalls in any of these areas undermine the validity and reliability of the data. The review by Chue-Sang et al. of polarising phantoms developed for a similar range of test shows the large variation in approach and quality [7]. Developing a set of standards for the field would be an extremely valuable asset in itself. Microspheres have been used in previous studies to act as scatters in the assessment of imaging systems [7] and would work well for resolution assessment. This could be customised for differing applications through induced birefringence in polymers through stressing. The various assessments of polarisation measurement functionality would be best investigated by high grade variable retarders. Turbidity would need a more novel approach but could either use varying distributions of microspheres, or a similar effect could be achieved using controlled freezing rates in ice to vary air pocket size and distribution.

[1] M. Jaspers, F. Feroldi, M. Vlig, J. de Boer, and P. P. van Zuijlen, "In vivo polarization-sensitive optical coherence tomography of human burn scars: birefringence quantification and correspondence with histologically determined collagen density," *Journal of*

Biomedical Optics, vol. 22, no. 12, p. 121712, 2017. [Online]. Available: https://doi.org/10.1117/1.JBO.22.12.121712.

[2] K. Showalter *et al.*, "Machine learning integration of scleroderma histology and gene expression identifies fibroblast polarisation as a hallmark of clinical severity and improvement," *Annals of the Rheumatic Diseases,* vol. 80, no. 2, pp. 228-237, 2021, doi: 10.1136/annrheumdis-2020-217840.

[3] E. Y. Kissin, P. A. Merkel, and R. Lafyatis, "Myofibroblasts and hyalinized collagen as markers of skin disease in systemic sclerosis," *Arthritis & Rheumatism,* vol. 54, no. 11, pp. 3655-3660, 2006, doi: https://doi.org/10.1002/art.22186.

[4] J. T. Van Praet, V. Smith, M. Haspeslagh, N. Degryse, D. Elewaut, and F. De Keyser, "Histopathological cutaneous alterations in systemic sclerosis: a clinicopathological study," *Arthritis Research & Therapy,* vol. 13, no. 1, p. R35, 2011/02/28 2011, doi: 10.1186/ar3267.

[5] J. Ziemek, A. Man, M. Hinchcliff, J. Varga, R. W. Simms, and R. Lafyatis, "The relationship between skin symptoms and the scleroderma modification of the health assessment questionnaire, the modified Rodnan skin score, and skin pathology in patients with systemic sclerosis," *Rheumatology,* vol. 55, no. 5, pp. 911-917, 2016, doi: 10.1093/rheumatology/kew003.

[6] J. C. McAlpine and J. D. Bancroft, "A histological study of hyaline deposits in laryngeal, aural, and nasal polyps and their differentiation from amyloid," *Journal of Clinical Pathology,* vol. 17, no. 3, pp. 213-219, 1964, doi: 10.1136/jcp.17.3.213.

[7] J. Chue-Sang *et al.*, "Optical phantoms for biomedical polarimetry: a review," *Journal of Biomedical Optics,* vol. 24, no. 3, p. 030901, 2019. [Online]. Available: https://doi.org/10.1117/1.JBO.24.3.030901.